UNIVERSITY OF CALIFORNIA SAN DIEGO

Investigating promoter-driven mRNA localization and translational control during stress

A dissertation submitted in partial satisfaction of the
requirements for the degree Doctor of Philosophy

in

Biology

by

Yang S. Chen

Committee in charge:

Professor Brian M. Zid, Chair
Professor Jens Lykke-Andersen, Co-Chair
Professor Xiang-Dong Fu
Professor James T. Kadonaga
Professor Lorraine Pillus

2021

The Dissertation of Yang S. Chen is approved, and it is acceptable in quality and form for publication on microfilm and electronically.

University of California San Diego
2021

DEDICATION

To my beloved family

(My parents, grandparents, and husband)

Thank for your perpetual support, trust, and love

EPIGRAPH

A Journey of a thousand miles must begin with a single step.

— Laozi

quoted from *Tao Te Ching*

TABLE OF CONTENTS

LIST OF FIGURES

LIST OF SUPPLEMENTAL FILES

Supplementary_1_strains_and_plasmids.xlsx

Supplementary_2_oligos.xlsx

Supplementary_3_strains_and_plasmids.xlsx

Supplementary_4_oligos.xlsx

ACKNOWLEDGEMENTS

I would like to thank my PhD advisor Professor Brian M. Zid for his extensive mentorship in scientific research and communication. His great passion and motivation for science has inspired me in my PhD. He is an extremely supportive, kind, encouraging and empathetic advisor who allows me to explore and has been very generous to provide me with all the opportunities, including scientific projects, conferences, career advice etc. I sincerely appreciate for his support and help.

I would like to thank my committee members: Professor Jens Lykke-Andersen, Professor James T. Kadonaga, Professor Lorraine Pillus, Professor Xiang-Dong Fu, for their helpful suggestions and advice. I really appreciate for Jim's generous help and advice from science to life.

I would like to thank my colleagues, Dr. Tatsuhisa Tsuboi, Dr. Anna R. Guzikowski, Fan Xu, Dr. Sharon Tracy, Vince Harjono, Shuhao Wang, Alexander T. Harvey and my collaborators Professor James Moresco, Professor John R. Yates III, for their close collaborations, helpful suggestions on the projects and generous help when I started my PhD. I would like to thank all past and present members of the Brian Zid lab.

I would like to thank the neighbor labs including the Kees Murre lab, the Wei Wang lab, the Ulrich Muller lab, the Simpson Joseph lab, the Elina Zuniga lab, the Yishi Jin lab, the Alexis Komor lab, the Colleen McHugh lab, the Navtej Toor lab for their generous help on sharing instruments and reagents.

I would like to thank my undergraduate thesis lab, Shuqun Zhang lab, for inspiring me to pursue a journey in the graduate school.

I would like to thank my family for their forever love, trust, and support. I would like to thank my parents for providing me with the best education and resources they could. I would like to thank my grandparents for always caring about me. Without them, I would not be able to finish my thesis and be where I am at.

I would like to thank my best friend and husband, Zhaoren He, for his overflowing love, encouragement, companion, support, and suggestions as I went through ups and downs in the PhD journey. I believe he was the major factor that made me stay positive, calm, persistent even in the toughest time. I would like to thank Zhaoren's parents for their encouragement and support.

I would like to thank my dear friends from UCSD, including Xiangyu Ren, Professor Emeritus Immo Scheffler, Hanqing Liu, Bili Dong, Shijia Liu, Jiayi Dong, Yue Sun, Wenhao Jin, Xinzhu Zhou, Rongxin Fang, Shu Zhang, Yuwenbin Li, Sifeng Gu, Zhaoning Wang, Yingcong Li, Jiaxi Wang, Liyang Xiong, Jingqiang Ye, Anzhi Yao, and so many other San Diego friends for sharing happiness and struggles together. I would like to thank my best girlfriends Chaofan Zhang and Weiwei Han for their love, caring and support since college. I would like to thank my close friends from the management consulting communities, college, teenagerhood and childhood. Their friendships have inspired me to chase the dreams and value the life.

Chatper 2, in full, is prepared for publication: Chen, Yang S.; Tracy, Sharon; Harjono, Vince; Xu, Fan; Moresco, James J.; Yates III, John R.; Zid, Brian M. 2021. "Rvb1/Rvb2 proteins couple transcription and translation during glucose starvation". The dissertation author was the first author of this paper.

Chapter 3, in full, is a reformatted published material as it appears as: Guzikowski, Anna R.*; Chen, Yang S.*; Zid, Brian M. 2019. Stress-induced mRNP granules: form and function of processing bodies and stress granules. Wiley Interdisciplinary Reviews: RNA, 10(3), e1524. The dissertation author was the co-first author of this paper.

VITA

EDUCATION

2016 Bachelor of Science, Zhejiang University
Biology (Hons)

2021 Doctor of Philosophy, University of California San Diego
Biology

PUBLICATIONS

Chen, Yang S.; Tracy, Sharon; Harjono, Vince; Xu, Fan; Moresco, James J.; Yates III, John R.; Zid, Brian M. 2021. "Rvb1/Rvb2 proteins couple transcription and translation during glucose starvation". *In preparation.*

Guzikowski, Anna R.*; **Chen, Yang S.***; Zid, Brian M. 2019. Stress-induced mRNP granules: form and function of processing bodies and stress granules. Wiley Interdisciplinary Reviews: RNA, 10(3), e1524.

Tsuboi, Tatsuhisa; Viana, Matheus P.; Xu, Fan; Yu, Jingwen; Chanchani, Raghav; Arceo, Ximena G.; Tutucci, Evelina; Choi, Joonhyuk; **Chen, Yang S.**; Singer, Robert H.; Rafelski, Susanne M.; Zid, Brian M. 2020. Mitochondrial volume fraction and translation duration impact mitochondrial mRNA localization and protein synthesis. Elife, 9, e57814.

*co-first author

ABSTRACT OF THE DISSERTATION

Investigating promoter-driven mRNA localization and translational control during stress

by

Yang S. Chen

Doctor of Philosophy in Biology

University of California San Diego, 2021

Professor Brian M. Zid, Chair
Professor Jens Lykke-Andersen, Co-Chair

During times of unpredictable stress, organisms must adapt their gene expression to maximize survival. Along with changes in transcription, one conserved means of gene

regulation during conditions that quickly represses translation is the formation of cytoplasmic phase-separated mRNP (messenger ribonucleoprotein) granules. Two well-known stress-induced mRNP granules are processing bodies (P-bodies) and stress granules. Previously, we identified that distinct steps in gene expression can be coupled during glucose starvation stress as promoter sequences in the nucleus are able to direct the subcellular localization to or excluded from the phase-separated granules and translatability of mRNAs in the cytosol. During my Ph.D., I have been investigating the underlying mechanisms of how promoter dictates the cytoplasmic fate of mRNAs during glucose starvation. Chapter 1 is a background introduction of the questions I asked. In chapter 2, I led a discovery of a promoter-directed mechanism mediated by AAA+ proteins Rvb1/Rvb2 that couple the transcription, mRNA cytoplasmic localization and translation of select genes during glucose starvation. In chapter 3, colleagues and I reviewed recent findings regarding stress-related phase-separated granules and shared our insights. Chapter 4 describes 3 projects that aimed to answer the promoter-dictation question from other perspectives, such as expression timing and promoter motifs. Finally, Chapter 5 discusses insights and future directions for my thesis work. I anticipate that these studies will provide us more insights into complex gene regulation during stressful and pathological conditions.

Chapter 1: Introduction

1.1 Stress responses

Cells do not always live in stable and optimal conditions, instead they are faced with various stressful conditions. The typical types of stresses include nutrient starvation, heat shock, toxins, pathogens, UV irradiation, and osmotic stresses (Majmundar et al., 2010; Richter et al., 2010).

In dynamic environmental conditions, to survive adverse changes, cells must balance disparate responses in gene expression as they quickly transition between homeostatic states. The cellular reprogramming that occurs in response to a disruptive or inimical external fluctuation is broadly termed as stress response. During stress, the control of gene expression is tightly regulated. Cellular stress response typically includes slowing or ceasing growth that is concomitant with repression of overall gene expression, although certain genes important for survival and repair such as heat shock genes are highly induced (De Nadal et al., 2011; Morimoto, 1998). Across the central dogma of gene expression, stress response was found in changes in regulation on chromatin remodeling and modification, transcription, mRNA stability and localization, translation, and post-translational modifications etc. The stress response is also highly reversible. When stressor is removed, cells and organisms have the tendency to quicky readjust the expression network for a fast recovery.

For *Saccharomyces cerevisiae* cells, the capability to sense and respond to a nutritional change in the environment is crucial for a robust and flexible growth. Among

the variable nutrition, glucose plays a key role as both a source metabolite and a signaling molecule. Glucose starvation refers to an acute type of stress that glucose is depleted from the cell environment. It is known that cells respond to glucose starvation by depressing the expression of most genes. Especially glucose starvation leads to a rapid inhibition on the translation (Ashe et al., 2000). The translational inhibition caused by glucose starvation is highly reversible that replenishment of glucose would reactivate the translation without requiring new transcription. What's more, besides regulations on gene expression, glucose starvation can lead to the reduction of the intracellular diffusion rates by a reduction in cell volume and an increase in molecular crowding subsequently (Joyner et al., 2016). Besides response within the cell, glucose starvation can also induce events on the cell membrane such as endocytic trafficking and entosis, which is a process that involves neighbor cell ingestion (Hamann et al., 2017; Laidlaw et al., 2021).

1.2 Stress-induced phase-separated granules

During stressful conditions one proposed means of post-transcriptional control is the phase separation of select mRNA transcripts and post-transcriptional regulatory proteins into phase-dense, concentrated, and membrane-less cytoplasmic structures generally described as phase-separated (Franzmann, Alberti, Morimoto, Hartl, & Kelly, 2019; Guzikowski, Chen, & Zid, 2019; Zid & O'Shea, 2014). Two well-known stress-induced phase-separated messenger ribonucleoprotein (mRNP) granules are processing bodies (P-bodies) and stress granules (Protter & Parker, 2016; Youn et al., 2019). The formation of these mRNP granules, which occurs on the scale of minutes after exposure to stress stimuli, is mediated by a physical process called liquid–liquid phase separation (LLPS) (Li, Chavali, Pancsa, Chavali, & Babu, 2018).

There are common biophysical characteristics and some shared components between stress granules and P-bodies as well as granule-specific features. It should be noted that, while the aptly named stress granules are broadly induced during stress, P-bodies are a bit more organismal-specific. *Saccharomyces cerevisiae* induces visible P-bodies primarily during stress response while, in mammalian cells, small, microscopically visible P-bodies are constitutive, but they become much larger and more abundant during stress. It should also be noted that the majority of research into these stress-induced granules is performed with yeast and mammalian cell culture systems. Ultimately, we posit stress granules and P-bodies should be considered as distinct yet closely related mRNP granules.

During stress, the direct connection between the formation of these granules coincident with an overall translational reduction suggests that the localization of mRNAs to these cytoplasmic granules might sequester the mRNAs away from the translational machineries, thus repressing the translation of the mRNAs (Attwood et al., 2020; Ivanov, Kedersha, & Anderson, 2019; Kedersha & Anderson, 2002; Sahoo et al., 2018). Although much progress has been made recently to identify the proteins and mRNAs that reside in these granules and the physical characteristics that underlie their formation, there is little known about the phenotypic or functional consequences of their formation during stress and therefore how significantly they contribute to stress response.

1.3 Coupling of gene expression steps

To date, it is generally thought that mRNA localization is predominantly dictated by *cis*-acting sequence elements within the RNA, which is recognized by associated *trans*-acting RBPs. Also, in eukaryotic cells, transcription and translation are separated in both space and time and are considered to be discrete processes. However, recent research has demonstrated that transcription can affect processes outside the nucleus by directing the cytoplasmic localization, translatability, and stability of mRNA. Also, our lab's past research found that the promoter in nucleus could direct the localization or exclusion of mRNAs to membrane-less compartments in cytoplasm and determine their translational rates (Zid and O'Shea, 2014). In our previous findings, upon glucose starvation in yeast, there were three different cytoplasmic fates for mRNA localization: exclusively P-body localization, P-body and stress granule localization, and diffuse cytoplasmic localization. During glucose starvation, Class 3 mRNAs whose transcription is active pre-starvation but deactivated during starvation become sequestered to P-bodies (e.g., *PGK1* and *PAB1*), while transcriptionally up-regulated mRNAs during starvation can be dissected into two classes: the Class 1 mRNAs that are preferentially translated and are diffuse in the cytoplasm (e.g., *HSP30*, *HSP26*), and the Class 2 mRNAs that are poorly translated during glucose limitation and are concentrated in P-bodies and stress granules (e.g., *GLC3*, *GSY1*). In each case, the localization was independent of *cis*-acting mRNA sequence elements (5' UTR, ORF or 3'UTR) but was instead controlled by non-transcribed promoter elements. In addition, the artificial synthesized promoter-directed mRNA localization experiment showed that three or more occurrences of Hsf1 binding

elements (HSEs) in the promoter were sufficient for specifying the diffuse mRNA localization and robust translation of the transcripts with uniform mRNA sequence.

In eukaryotes, transcription and translation are usually considered to be discrete processes, both spatially and regarding regulatory factors. However, close coordination of transcription and translation for subsets of cellular mRNAs would be advantageous when an organism needs to rapidly alter its cellular composition, such as during environmental stress. As the promoter exclusively resides in the nucleus, we hypothesize that factors exist that interact with promoters and are co-transcriptionally loaded onto mRNA prior to nuclear export. Later chapters describe the attempts of testing the hypothesis and investigating the potential mechanism of how promoter in the nucleus leave an impact on the mRNAs in the cytosol.

1.4 References

Ashe, M.P., De Long, S.K., Sachs, A.B., 2000. Glucose depletion rapidly inhibits translation initiation in yeast. Mol. Biol. Cell 11, 833–848.

Attwood, K.M., Robichaud, A., Westhaver, L.P., Castle, E.L., Brandman, D.M., Balgi, A.D., Roberge, M., Colp, P., Croul, S., Kim, I., McCormick, C., Corcoran, J.A., Weeks, A., 2020. Raloxifene prevents stress granule dissolution, impairs translational control and promotes cell death during hypoxia in glioblastoma cells. Cell Death Dis. 11, 1–18.

De Nadal, E., Ammerer, G., Posas, F., 2011. Controlling gene expression in response to stress. Nat. Rev. Genet.

Franzmann, T.M., Alberti, S., Morimoto, R.I., Hartl, F.U., Kelly, J.W., 2019. Protein Phase Separation as a Stress Survival Strategy.

Guzikowski, A.R., Chen, Y.S., Zid, B.M., 2019. Stress-induced mRNP granules: Form and function of processing bodies and stress granules. Wiley Interdiscip. Rev. RNA 10, e1524.

Hamann, J.C., Surcel, A., Chen, R., Teragawa, C., Albeck, J.G., Robinson, D.N., Overholtzer, M., 2017. Entosis Is Induced by Glucose Starvation. Cell Rep. 20, 201–210.

Ivanov, P., Kedersha, N., Anderson, P., 2019. Stress granules and processing bodies in translational control. Cold Spring Harb. Perspect. Biol. 11, a032813.

Joyner, R.P., Tang, J.H., Helenius, J., Dultz, E., Brune, C., Holt, L.J., Huet, S., Müller, D.J., Weis, K., 2016. A glucose-starvation response regulates the diffusion of macromolecules. Elife 5.

Kedersha, N., Anderson, P., 2002. Stress granules: sites of mRNA triage that regulate mRNA stability and translatability. Biochem. Soc. Trans.

Laidlaw, K.M.E., Bisinski, D.D., Shashkova, S., Paine, K.M., Veillon, M.A., Leake, M.C., MacDonald, C., 2021. A glucose-starvation response governs endocytic trafficking and eisosomal retention of surface cargoes in budding yeast. J. Cell Sci. 134.

Li, X.H., Chavali, P.L., Pancsa, R., Chavali, S., Babu, M.M., 2018. Function and Regulation of Phase-Separated Biological Condensates. Biochemistry.

Majmundar, A.J., Wong, W.J., Simon, M.C., 2010. Hypoxia-Inducible Factors and the Response to Hypoxic Stress. Mol. Cell.

Morimoto, R.I., 1998. Regulation of the heat shock transcriptional response: Cross talk between a family of heat shock factors, molecular chaperones, and negative regulators. Genes Dev.

Protter, D.S.W., Parker, R., 2016. Principles and Properties of Stress Granules. Trends Cell Biol.

Richter, K., Haslbeck, M., Buchner, J., 2010. The Heat Shock Response: Life on the Verge of Death. Mol. Cell.

Sahoo, P.K., Lee, S.J., Jaiswal, P.B., Alber, S., Kar, A.N., Miller-Randolph, S., Taylor, E.E., Smith, T., Singh, B., Ho, T.S.Y., Urisman, A., Chand, S., Pena, E.A., Burlingame, A.L., Woolf, C.J., Fainzilber, M., English, A.W., Twiss, J.L., 2018. Axonal G3BP1 stress granule protein limits axonal mRNA translation and nerve regeneration. Nat. Commun. 9, 1–14.

Youn, J.Y., Dyakov, B.J.A., Zhang, J., Knight, J.D.R., Vernon, R.M., Forman-Kay, J.D., Gingras, A.C., 2019. Properties of Stress Granule and P-Body Proteomes. Mol. Cell.

Zid, B.M., O'Shea, E.K., 2014. Promoter sequences direct cytoplasmic localization and translation of mRNAs during starvation in yeast. Nature 514, 117–121.

Chapter 2: Rvb1/Rvb2 proteins couple transcription and translation during glucose starvation

2.1 Abstract

During times of unpredictable stress, organisms must adapt their gene expression to maximize survival. Along with changes in transcription, one conserved means of gene regulation during conditions that quickly represses translation is the formation of cytoplasmic phase-separated mRNP (messenger ribonucleoprotein) granules such as processing bodies (P-bodies) and stress granules. Previously, we identified that distinct steps in gene expression can be coupled during glucose starvation as promoter sequences in the nucleus are able to direct the subcellular localization and translatability of mRNAs in the cytosol. Here, in chapter 2, we report that Rvb1 and Rvb2, conserved ATPase proteins implicated as protein assembly chaperones and chromatin remodelers, were enriched at the promoters and mRNAs of genes involved in alternative glucose metabolism pathways that we previously found to be transcriptionally upregulated but translationally downregulated during glucose starvation in yeast. Microscopy revealed that Rvb1/Rvb2-containing cytoplasmic granules were colocalized with the enriched mRNAs upon starvation. Engineered Rvb1/Rvb2-binding on mRNAs was sufficient to sequester the mRNAs into phase-separated granules and repress their translation. Additionally, this Rvb-tethering to the mRNA drove further transcriptional upregulation of the target genes. Overall, our results point to Rvb1/Rvb2 coupling transcription, mRNA granular localization, and translatability of mRNAs during glucose starvation. This Rvb-

mediated rapid gene regulation could potentially serve as an efficient recovery plan for cells after the stress removal.

2.2 Background

Gene expression encompasses many steps across discrete cellular boundaries including transcription, mRNA processing and export, translation, and decay. Cells do not always live in stable and optimal conditions, instead they are faced with various types of stresses, such as nutrient starvation, heat shock, toxins, pathogens and osmotic stresses (Majmundar, Wong, & Simon, 2010; Richter, Haslbeck, & Buchner, 2010). In dynamic environmental conditions, cells must balance disparate responses in gene expression as they quickly transition between homeostatic states. This can present challenges such as when cells repress overall translation while needing to upregulate the protein expression of stress response genes (De Nadal, Ammerer, & Posas, 2011). To date, it is generally thought that mRNA cytoplasmic activities are predominantly dictated by *cis*-acting sequence elements within the RNA; however, coupling steps in gene expression presents an attractive strategy to overcome the challenges by creating regulons of mRNAs that are similarly controlled at the transcriptional level and can be coordinately tuned at the post-transcriptional level as well.

In recent years “imprinting” by co-transcriptional loading has been implicated as an alternative mechanism to *cis*-acting RNA sequence elements in determining cytoplasmic mRNA fate. For instance, it was found that promoters determined mRNA decay rates through the co-transcriptional loading of RNA-binding proteins (RBPs) to the nascent RNA (Bregman et al., 2011; Trcek, Larson, Moldón, Query, & Singer, 2011). Similarly, Vera *et al*. showed that the translation elongation factor eEF1A coupled the transcription and translation of *HSP70* mRNAs through co-transcriptional loading during

heat shock in mammalian cells (Vera et al., 2014). Zander *et al*. showed that transcription factor Hsf1 might be functioning in loading the nuclear mRNA export protein Mex67 on stress-related mRNAs during heat shock in yeast (Zander et al., 2016).

During stressful conditions one proposed means of post-transcriptional control is the phase separation of select mRNA transcripts and post-transcriptional regulatory proteins into phase-dense, concentrated, and membrane-less cytoplasmic structures generally described as phase-separated granules (Guzikowski, Chen, & Zid, 2019; Zid & O'Shea, 2014). Two well-known stress-induced phase-separated messenger ribonucleoprotein (mRNP) granules are processing bodies (P-bodies) and stress granules (Protter & Parker, 2016; Youn et al., 2019). During stress, the direct connection between the formation of these granules coincident with an overall translational reduction suggests that the localization of mRNAs to these cytoplasmic granules might sequester the mRNAs away from the translational machineries, thus repressing the translation of the mRNAs (Attwood et al., 2020; Ivanov, Kedersha, & Anderson, 2019; Kedersha & Anderson, 2002; Sahoo et al., 2018). Yet how mRNAs are partitioned to or excluded from stress-induced granules remains unclear.

Previously we found that during glucose starvation in yeast, promoter sequences play an important role in determining the cytoplasmic fate of mRNAs (Zid & O'Shea, 2014). mRNAs transcribed by active promoters in unstressed cells (Class III, e.g., *PGK1*, *PAB1*) were directed to P-bodies. Meanwhile, stress-induced mRNAs showed two distinct responses: mRNAs of most heat shock genes (Class I, e.g., *HSP30, HSP26*) are transcriptionally induced, actively translated, and remain diffuse in the cytoplasm; however, Class II mRNAs are transcriptionally induced but become sequestered in both

P-bodies and stress granules and are associated with inactive translation. Class II mRNAs are enriched for alternative glucose metabolic function such as glycogen metabolism (e.g., *GSY1*, *GLC3*, *GPH1*). Surprisingly, instead of the mRNA sequence itself, the promoter sequence that sits in the nucleus directs the translation and cytoplasmic localization of the corresponding induced mRNAs. Specifically, Hsf1-target sequences were shown to direct mRNAs to be excluded from mRNP granules and well translated. However, the mechanism by which the promoter can couple steps of gene expression during glucose starvation is unclear. As the promoter exclusively resides in the nucleus, we hypothesize factors exist that interact with promoters and are co-transcriptionally loaded onto mRNA prior to nuclear export.

In this study, we developed a novel proteomics-based screening method that enabled us to identify Rvb1/Rvb2 as interacting proteins with the promoters of the Class II alternative glucose metabolism genes (e.g., *GLC3*) that are upregulated in transcription but downregulated in translation and have granular-localized mRNA transcripts. Rvb1/Rvb2 (known as RuvbL1/RuvbL2 in mammals) are two highly conserved AAA+ (ATPases Associated with various cellular Activities) proteins that are found in multiple nucleoprotein complexes. Structural studies have shown that they form a dodecamer comprised of a stacked Rvb1 hexametric ring and a Rvb2 hexametric ring. They were reported as the chaperones of multiprotein complexes involved in chromatin remodeling processes and other nuclear pathways including snoRNP assembly (Eickhoff & Costa, 2017; Huen et al., 2010; Jha & Dutta, 2009; Nano & Houry, 2013; Paci et al., 2012; Seraphim et al., 2021; Tian et al., 2017). These two proteins are generally thought to act on DNA but have been found to be core components of mammalian and yeast

cytoplasmic stress granules (Jain et al., 2016). Rvb1/Rvb2 have also been shown to regulate the dynamics and size of stress granules (Narayanan et al., 2019; Zaarur et al., 2015). The dual presence of Rvb1/Rvb2 at chromatin and stress granules hints to their potential in coupling activities in the nucleus and cytoplasm. Furthermore, a human homolog of Rvb2 was found to be an RNA-binding protein that promotes the degradation of translating HIV-1 *Gag* mRNA (Mu et al., 2015). Relatedly, in this study we found that Rvb1/Rvb2 have roles in coupling transcription, cytoplasmic mRNA localization, and translation of specific glucose starvation induced genes in yeast, providing insight into how gene expression can be coordinated during fluctuating environmental conditions.

2.3 Results

2.3.1 Rvb1/Rvb2 are identified as potential co-transcriptionally loaded protein factors on the alternative glucose metabolism genes

To identify proteins involved in the ability of promoter sequences directing the cytoplasmic fate of the mRNAs during stress, we developed Co-Transcriptional ImmunoPrecipitation (CoTrIP), a novel biochemical screening technique to identify co-transcriptionally loaded protein factors (Figure 2.1A). Here we modified a yeast plasmid containing LacO-binding sites that was previously used as an efficient purification system to isolate histones (Unnikrishnan, Akiyoshi, Biggins, & Tsukiyama, 2012; Unnikrishnan, Gafken, & Tsukiyama, 2010). To this plasmid we added a uniform open reading frame (ORF) and different promoters of interest. We then used FLAG-tagged LacI, which binds to the LacO sequences, and UV-crosslinking to purify the plasmid along with the nascent mRNAs, and co-transcriptionally loaded proteins. Thereafter, mass spectrometry was performed to identify proteins enriched in a promoter specific manner. Real-time quantitative PCR (RT-qPCR) validates that the CoTrIP method yields enrichment of the target nascent mRNAs, indicating that proteins enriched could be co-transcriptionally loaded (Figure supplement 2.1). Here, we performed CoTrIP of three plasmids (two heat shock genes' promoters, *HSP30* and *HSP26*, and an alternative glucose metabolism gene's promoter, *GLC3*) in cells subject to 10 minutes of glucose deprivation. Those promoters had previously been shown to be sufficient to determine the cytoplasmic fate of the uniform open reading frame (Zid & O'Shea, 2014).

After comparing the protein enrichment on *GLC3* promoter and on *HSP30/HSP26* promoters (Figure 2.1B, 2.1C), we were able to detect differences in protein factors across the specific classes of promoters. The ATP-dependent DNA RuvB-like helicase Rvb1 was enriched 10-fold more on *GLC3* promoter plasmids versus both *HSP30/HSP26* promoters (p-value = 0.02). To ensure that our data was sound, we compared our protein enrichment data against the CRAPome repository, a large database of contaminant proteins from various immunoprecipitation (IP) experiments, and we found that Rvb1 was significantly enriched on the *GLC3* promoter-containing plasmid (Figure 2.1C) (Mellacheruvu et al., 2013). Proteins that were both enriched in "promoter versus promoter comparison" as well as in comparison to the CRAPome are listed (Figure 2.1C).

Rvb1/Rvb2 are two highly conserved members of the AAA+ family that are involved in multiple nuclear pathways (Jha & Dutta, 2009). These two proteins are generally thought to act on DNA but have been found to be core components of mammalian and yeast cytoplasmic stress granules (Jain et al., 2016). Microscopy revealed that Rvb1/Rvb2 are predominately present in the nucleus when cells are not stressed but a portion of them becomes localized to cytoplasmic granules that are not P-bodies in both 15-minute and 30-minute glucose starvation conditions (Figure supplement 2.2). Rvb1/Rvb2's interactions with DNA in the nucleus and presence in the cytoplasm suggest the potential of Rvb1/Rvb2 to shuttle between the nucleus and cytoplasm.

2.3.2 Rvb1/Rvb2 are enriched at the promoters of endogenous alternative glucose metabolism genes

To validate the CoTrIP results as well as more globally explore the location on DNA of Rvb1/Rvb2 during stress, Chromatin ImmunoPrecipitation sequencing (ChIP-seq) was used to investigate Rvb1/Rvb2's enrichment across the genome. Because of the limitation in obtaining yeast Rvb1/Rvb2 antibodies and the convenience of the yeast cloning, Rvb1/Rvb2 were fused with a tandem affinity purification (TAP)-tag at the C-terminus and purified by rabbit IgG beads. The TAP-tagged strains grow at a normal rate (~90-minute doubling time), which suggests TAP-tagging does not disrupt the endogenous protein function or cellular health generally. Here, we performed ChIP-seq on Rvb1, Rvb2, and the negative control Pgk1 in 10 minutes of glucose starvation (Figure supplement 2.3, left). Rvb1/Rvb2 are enriched from the -500 bp to the transcription start site (TSS) along the genome in 10 minutes of glucose starvation, whereas ChIP-seq of the negative control Pgk1 is not enriched in the promoter region (Figure 2.2A). The overall enrichment on promoters is consistent with findings that Rvb's can function as chromatin remodelers (Zhou et al., 2017). We found Rvb1/Rvb2 are highly enriched on *GSY1*, *GLC3* and *HXK1* promoters but not *HSP30*, *HSP26* or *HSP104* promoters, which is consistent with our CoTrIP results (Figure 2.2C). Rvb1/Rvb2 are significantly more enriched on the proximal promoters of the transcriptionally upregulated, poorly translated genes versus the transcriptionally upregulated and well translated genes and the average genome (Figure 2.2D; Figure supplement 2.4). More generally we found that, for genes that show a greater than 3-fold increase in mRNA levels during glucose starvation, their promoters are significantly more enriched for Rvb2 binding. Previously we had found that Hsf1-

binding sequences were sufficient to exclude mRNAs from mRNP granules during glucose starvation (Zid & O'Shea, 2014). Interestingly we found that glucose starvation induced Hsf1-target promoters have no difference in Rvb1/Rvb2 binding than an average gene, and significantly lower Rvb1/Rvb2 enrichment than stress induced non-Hsf1 targets (Figure 2.2B).

Enrichment peaks of Rvb1/Rvb2 were called using the macs algorithm (Zhang et al., 2008). Consistently, enrichment peaks of Rvb1/Rvb2 were identified on the promoter regions of the Class II alternative glucose metabolism genes but not the Class I heat shock genes (Figure supplement 2.5). Rvb1 and Rvb2 also show a highly overlapped enrichment pattern across the genome, but neither of them shows overlapped enrichment with the negative control Pgk1 (Figure supplement 2.3). Structural studies have shown that Rvb1/Rvb2 can form a dodecamer complex. Their overlapped enrichment also indicates that Rvb1 and Rvb2 may function together.

2.3.3 Rvb1/Rvb2 are co-transcriptionally loaded on the alternative glucose metabolism mRNAs

Although Rvb1/Rvb2 are predominantly considered to act on DNA, they are also found to interact with various mRNAs and regulate mRNA translation and stability (Izumi, Yamashita, & Ohno, 2012; Mu et al., 2015). We next sought to test whether Rvb1/Rvb2 established similar enrichment patterns on mRNAs. To test the interaction, we performed RNA ImmunoPrecipitation (RIP) on Rvb1, Rvb2, and the negative control wild-type (WT) strain followed by RT-qPCR in both log phase and 15-minute glucose starved cells. Consistently, during 15 minutes of glucose starvation, Rvb1/Rvb2 are significantly more

enriched on the mRNAs of the Class II alternative glucose metabolism genes versus the Class I heat shock genes (Figure 2.3A). Rvb2 is specifically highly enriched on *GSY1* mRNA, where it is around twenty-fold more enriched than on *HSP30* mRNAs. However, in glucose-rich log phase conditions, Rvb1/Rvb2 are generally less enriched on the mRNAs compared to starvation conditions. Additionally, in log phase, Rvb1/Rvb2 do not show differential enrichment between the alternative glucose metabolism genes and the heat shock genes. (Figure supplement 2.6).

Since Rvb1/Rvb2 are enriched on both promoters and mRNAs of Class II alternative glucose metabolism genes, we hypothesized that Rvb1/Rvb2 are loaded from the interacting promoters to the nascent mRNAs via the transcription process. To test this, we eliminated the effects from the ORF sequences by designing a pair of reporter mRNAs with a uniform *CFP* ORF but driven by either the *GLC3* promoter or HSP26 promoter (Figure 2.3B). Interestingly, although the mRNA transcribed virtually identical mRNA sequences (Zid & O'Shea, 2014), Rvb1/Rvb2 are significantly more enriched on the mRNA driven by the *GLC3* promoter compared to the one driven by the *HSP26* promoter during 15-minute glucose starvation (Figure 2.3C). As a control, Rvb1/Rvb2 did not show an enrichment difference on the endogenous *GLC3* and *HSP26* mRNAs between the two reporter yeast strains (Figure supplement 2.7). This suggests that only the promoter itself can determine the transcribed mRNA's interaction with Rvb1/Rvb2, further indicating that Rvb1/Rvb2 are likely to be co-transcriptionally loaded from the promoters to mRNAs.

Class II alternative glucose metabolism mRNAs are localized to stress granules during stress and Rvb1/Rvb2 are found to be enriched in stress granules. Therefore, we tested whether these mRNAs and Rvb1/Rvb2 may be colocalized. We developed strains

with Rvb1 or Rvb2 labeled with the green fluorescent protein mNeongreen, and *GSY1* mRNA or the negative control *PGK1* mRNA labeled by MS2 sequences which bind to the MS2 coat protein fused with a red fluorescent protein mRuby2 (Tutucci et al., 2018). Microscopy revealed that Rvb1/Rvb2-containing granules are colocalized with *GSY1* mRNA-containing granules. 80% of the cells have colocalized Rvb1 and *GSY1* mRNA granules and 77% of cells have colocalized Rvb2 and *GSY1* mRNA granules. As a negative control, Rvb1/Rvb2 are not highly colocalized with *PGK1* mRNA-containing granules (Figure supplement 2.8). Taken together, Rvb1/Rvb2 are shown to be highly enriched on both the promoters and mRNAs of the Class II alternative glucose metabolism genes and Rvb1/Rvb2 are colocalized with *GSY1* mRNA containing granules during glucose starvation. This suggests that Rvb1/Rvb2 are recruited by promoters, co-transcriptionally loaded onto nascent mRNA, and then accompany mRNAs into the cytoplasm.

2.3.4 Engineered Rvb1/Rvb2 tethering to mRNAs directs the cytoplasmic localization and repressed translation

As Rvb1/Rvb2 were found to be located at both promoters in the nucleus and associated with mRNAs in the cytoplasm, we asked whether Rvb1/Rvb2 have an impact on the cytoplasmic fates of bound mRNAs. To test this, we engineered interactions between Rvb1 or Rvb2 and the mRNAs transcribed from various promoters of heat shock genes (e.g., *HSP30*, *HSP26*). We took advantage of the specific interaction between a phage-origin PP7 loop RNA sequence and the PP7 coat protein (Lim & Peabody, 2002). Here, in our engineered strains, a reporter construct consists of a promoter of interest, a

nanoluciferase reporter ORF to measure protein synthesis, a PP7 loop to drive the engineered interaction, and an MS2 loop for mRNA visualization. Along with the reporter, Rvb1 or Rvb2 are fused with PP7-coat protein to establish binding on the reporter mRNA (Figure 2.4A). As previously shown Rvb1/Rvb2 do not display strong binding on the promoters and mRNAs of heat shock genes (Figure 2.2C, 2.3A) (e.g., *HSP30*). Therefore, we specifically engineered the interaction between Rvb1 or Rvb2 and three mRNAs driven by the Class I heat shock promoters (*HSP30/HSP26/HSP12*). Strikingly, binding of both Rvb1 and Rvb2 alters the cytoplasmic fates of these Class I heat shock mRNAs to be similar to the Class II alternative glucose metabolism mRNAs (Figure 2.4; Figure supplement 2.9, 2.10, 2.11). Taking *HSP30* promoter-driven reporter mRNA as an example, during glucose starvation the binding of Rvb1 and Rvb2 reduces protein synthesis by ~35% and ~50% respectively (Figure 2.4B). It is important to consider that final protein abundance is determined by both mRNA levels and translation. Interestingly, we observed an increase in mRNA abundance when Rvb1 or Rvb2 are tethered to the reporter mRNA (Figure 2.4C). When the translational efficiency was normalized by the mRNA abundance, we were surprised to observe binding of either Rvb1 or Rvb2 reduces translational efficiency by greater than ~70% during glucose starvation (Figure 2.4D). Additionally, Rvb1/Rvb2 binding does not significantly repress the translational efficiency of mRNA in unstressed cells, indicating that Rvb1/Rvb2 has a more significant effect on mRNAs when mRNP granules have visibly formed (Figure supplement 2.9, 2.10, 2.11).

Since the translation of the mRNAs bound by Rvb1/Rvb2 was reduced, we further visualized the subcellular localization of those mRNAs. Consistent with reduced translation, Rvb1/Rvb2-tethering significantly increases the granular localization of the

heat shock mRNA reporters (Figure 2.4E; Figure supplement 2.9, 2.10, 2.11). Taking *HSP30* promoter-driven reporter mRNA as an example, only 9% of the cells form *HSP30* promoter-driven mRNA-containing granules when the mRNA is not bound by Rvb1 or Rvb2, yet Rvb2-tethering increases the mRNA's granular localization to 29% of the cells (Figure 2.4E). Furthermore, the binding of Rvb2 to mRNA increases the formation of granules that are non-colocalized with a P-body marker (Figure supplement 2.9, 2.10, 2.11). This indicates that Rvb2 guides the interacting mRNA to the presumed stress granule. To further eliminate any potential artifacts caused by the C-terminal modification on Rvb1/Rvb2, the negative controls were tested where Rvb1 or Rvb2 are fused with PP7 coat protein, but the mRNA does not have the PP7 loop. The negative control strains did not show a decrease in translation or increase in granular localization of the reporter mRNAs in glucose starvation. It indicates translation only decreases and the mRNA granular localization level only increases when the full Rvb-mRNA interaction was established (Figure supplement 2.9, 2.10, 2.11). These results support the ability of Rvb1/Rvb2 to significantly suppress the translation of the binding mRNAs, potentially through sequestering the mRNAs into cytoplasmic granules.

The coupling of induced transcription and repressed translation of the Class II alternative glucose metabolism genes may be an important adaptation for cells to survive from stress conditions. Results showed that after replenishing the glucose to the starved cells, the translation of those genes is quickly induced (Figure supplement 2.12), indicating the potential biological role of the stress granule as repository for these inactive translating Class II mRNAs during stress that does not preclude these mRNAs from potentially being quickly released and translated once the stress is removed.

2.3.5 Engineered Rvb1/Rvb2 binding to mRNAs increases the transcription of corresponding genes

Interestingly, Rvb1/Rvb2 not only suppress the translation of bound mRNAs, but also increases the abundance of the interacting mRNAs by more than 2-fold (Figure 2.4C). There are two possibilities for this increased mRNA abundance by Rvb1/Rvb2-tethering: increased transcription and/or slower mRNA decay. To address this, we performed time-course measurements on the *HSP30*-promoter-driven reporter mRNA abundance in 0, 5, 10, 15, 30, 45 minutes of glucose starvation. Here, we compared the mRNA abundance when mRNA is bound by Rvb2 and when mRNA is not bound by Rvb2 as a control. A mathematical modelling approach was performed to predict the mRNA induction abundance change caused by varied transcriptional efficiency or varied decay rate (Figure 2.5A) (Elkon, Zlotorynski, Zeller, & Agami, 2010). From the mathematical modelling, mRNA fold induction differs between varied transcriptional induction versus mRNA decay changes. For varied transcriptional rates differences in mRNA levels are the same (equal distance) at each time point on a log-log scale (Figure 2.5A upper panel). Although little difference is seen in mRNA abundance with varying mRNA fold induction and decay rates early in glucose starvation, our simulation predicts large differences in mRNA abundance after 10 and later minutes of glucose starvation (Figure 2.5A lower panel). By comparing experimental measurements of mRNA induction of the Rvb2-tethered condition to the unbound control condition, the mRNA induction differences are similar at each time point. When Rvb2 binds to the mRNA, the abundance of the mRNA is constantly greater than the unbound mRNA at all time points during glucose starvation, indicating that the greater mRNA abundance is mainly due to greater transcription

differences driven by the Rvb2 binding (Figure 2.5B). Also, the mRNA abundance does not differ in log phase, which indicates the effect is potentially stress-induced only.

To further experimentally validate that the greater mRNA abundance caused by Rvb2 binding is due to the increased transcription and not slower decay, we stopped cellular transcription after 15 minutes of glucose starvation by treatment with the transcription inhibitor drug 1,10-phenanthroline. Then we performed time-course measurements on mRNA abundance and compared the decay of mRNAs with and without Rvb2 binding. Consistently, mRNAs bound by Rvb2 decay at a slightly but not significantly faster rate, not a slower rate (Figure 2.5C). Whether or not bound by Rvb2, the reporter mRNA has around a 25-minute half-life (Figure 2.5D). These results further point to Rvb2 mRNA tethering driving transcriptional upregulation. Since Rvb2 is targeted to the mRNA, it is likely that local recruitment of Rvb2 to the nascently transcribed mRNA increases the local concentration of Rvb2 protein to the vicinity of the regulatory region of the corresponding gene, further showing the connections between the transcriptional and translational processes.

2.4 Discussion

In fluctuating environments, cells must quickly adjust the expression of different genes dependent upon cellular needs. Here, our results demonstrate a novel function of the AAA+ ATPases Rvb1/Rvb2 in the cytoplasm, and a novel mechanism of Rvb1/Rvb2 in coupling the transcription, mRNA cytoplasmic localization, and translation of specific genes (Figure 2.6). We identified Rvb1/Rvb2 as enriched protein factors on the promoters of the Class II alternative glucose metabolism genes that are upregulated in transcription but downregulated in translation during glucose starvation. Biochemical and microscopic results showed that Rvb1/Rvb2 have a strong preferred interaction with both promoters and mRNAs of these genes, suggesting Rvb1/Rvb2 are loaded from enriched promoters to the nascent mRNAs. More interestingly, when we tethered Rvb1/Rvb2 to the mRNAs, the binding of Rvb1/Rvb2 had a strong impact on reducing mRNA translation and increasing the mRNA granular localization, suggesting that co-transcriptional loading of Rvb1/Rvb2 directs post-transcriptional mRNA fate in the cytoplasm. Additionally, Rvb1/Rvb2's interaction with the mRNA can also induce transcription of the corresponding genes, further indicating that Rvb1/Rvb2 couple the transcription and translation of the interacting genes.

It is not clear how tethering Rvb1/Rvb2 to an mRNA reporter increases transcription of the corresponding DNA locus. Rvb1/Rvb2 were initially found to be associated with many chromatin-remodeling and transcription related complexes. This has further been expanded on and several studies have demonstrated a chaperone-like activity in the formation of various complexes including the assembly of chromatin

remodeling complexes and RNA polymerase II (Nano & Houry, 2013; Paci et al., 2012; Seraphim et al., 2021). It may be that recruiting Rvb1/Rvb2 to the nascent RNA increases the local concentration, driving further enhancement of transcription-related processes. It is also intriguing to think about Rvb1/Rvb2's reporter role in escorting client proteins to large macromolecular complexes. Like their escorting protein function, it is plausible to hypothesize that they might have additional functions in escorting mRNAs to the large macromolecule stress granule complex in stressful conditions.

The coupling of transcription and translation of specific genes may be an important adaptation for cells to survive during stress conditions. It has been postulated that to save energy during stress, mRNAs are temporarily stored in the cytoplasmic granules associated with inactive translation instead of mRNA decay (Guzikowski et al., 2019; Horvathova et al., 2017; Pitchiaya et al., 2019; Protter & Parker, 2016; Schutz, Noldeke, & Sprangers, 2017). Our results show that, after replenishing glucose to the starved cells, the translation of those genes is quickly induced (Figure 4-figure supplement 10). The stress-induced phase-separated granules may serve as temporary repositories for the inactive translating mRNAs of many genes that are regulated by Rvb1/Rvb2 in glucose starvation and involved in alternative glucose metabolism pathways. From the perspective of cell needs, many alternative glucose metabolism genes are involved in glycogen synthesis, which may be superfluous for survival during times of complete glucose starvation, but the cell may want to produce them as quickly as possible upon glucose replenishment to drive quick protein synthesis. The special coupling of increased transcription but repressed translation mediated by Rvb1/Rvb2 may serve as an emergency but prospective mechanism for cells to precisely repress the translation of

these alternative glucose metabolism mRNAs during stress but be able to quickly translate these pre-stored mRNAs once the cells are no longer starved (Jiang, AkhavanAghdam, Li, Zid, & Hao, 2020). Also, the genes regulated by Rvb1/Rvb2 are highly dependent on the type of stresses. We observed this interesting mechanism on the alternative glucose metabolism genes during glucose starvation stress. It will be interesting to test if there is similar regulation on different sets of genes that are related to other types of stresses, such as heat shock and osmotic stress responses. Rvb1/Rvb2 may regulate different sets of genes according to the different stresses or maybe different protein factors play a role in the mechanism. With our methodology, it is promising to generalize the mechanism toward to various stress conditions.

To further understand the function of Rvb1/Rvb2 mechanistically, it is crucial to understand how Rvb1/Rvb2 are recruited to these specific promoters initially. As we found that Rvb1/Rvb2 are enriched on the promoters of transcriptionally upregulated mRNAs except for those that are Hsf1-regulated (Figure 2.2B), we favor a model in which the default is for Rvb1/Rvb2 to be recruited to the active transcription sites but that Hsf1-regulated promoters circumvent this recruitment through an unknown mechanism, as the transcriptionally upregulated Hsf1 targets show reduced recruitment relative to non-Hsf1 targets. Intriguingly, Hsf1-regulated genomic regions have been found to coalesce during stressful conditions (Chowdhary, Kainth, & Gross, 2017; Pincus et al., 2018). Could Rvb1/Rvb2 be excluded from these coalesced regions? In the future, nuclear microscopy can be performed to identify the co-localization or exclusion of Rvb1/Rvb2 and the DNA loci of interest. Also, based on our current results, we prefer the hypothesis that the recruitment of Rvb1/Rvb2 is mediated by other DNA-binding proteins, as no specific

binding motif of Rvb1/Rvb2 were identified by ChIP-seq. Future tests will include identifying the potential DNA-binding proteins that mediate the interaction between Rvb1/Rvb2 and the specific DNA loci.

2.5 Conclusions

We discovered that Rvb1/Rvb2, predominantly implicated as protein assembly chaperons and chromatin remodelers, play an important role in coupling transcription, cytoplasmic localization, and translation of select mRNAs during glucose starvation. We identified Rvb1/Rvb2 as enriched protein factors on the promoters of the Class II alternative glucose metabolism genes that are upregulated in transcription but downregulated in translation during glucose starvation. Biochemical and microscopic results showed that Rvb1/Rvb2 have a strong preferred interaction with both promoters and mRNAs of these genes, suggesting Rvb1/Rvb2 are loaded from enriched promoters to the nascent mRNAs. More interestingly, when we tethered Rvb1/Rvb2 to the mRNAs, the binding of Rvb1/Rvb2 had a strong impact on reducing mRNA translation and increasing the mRNA granular localization, suggesting that co-transcriptional loading of Rvb1/Rvb2 directs post-transcriptional mRNA fate in the cytoplasm. Additionally, Rvb1/Rvb2's interaction with the mRNA can also induce transcription of the corresponding genes, further indicating that Rvb1/Rvb2 couple the transcription and translation of the interacting genes.

2.6 Availability of data and materials

ChIP-sequencing reads were deposited at GEO. The raw files and analyzed ChIP-seq enrichment data generated in this study is available at GEO: GSE184473.

Further information and requests for data, resources, scripts, and reagents should be directed to and will be fulfilled by the corresponding contact, B.M.Z. (zid@ucsd.edu).

2.7 Figures

Figure 2.1: Rvb1/Rvb2 are identified as potential co-transcriptional-loaded protein factors on the alternative glucose metabolism genes.

(A) A schematic view of CoTrIP. CoTrIP plasmid has an 8X lacO, a uniform ORF and various promoters of interest. The CoTrIP plasmid is independent in the yeast. CoTrIP plasmid was purified by immunoprecipitation on protein lacI-3XFlag. Co-transcriptional-loaded protein factors were identified by mass spectrometry. (B) Quantitative volcano plot of co-transcriptional-loaded protein candidates. X-axis: log2 scale of fold change of protein enrichment on 2 replicates of *GLC3* promoter-containing CoTrIP plasmid over on 2 replicates of *HSP30* promoter-containing and 1 replicate of *HSP26* promoter-containing plasmid. Y-axis: minus log10 scale of the p-values from 2-sample t-test. Null hypothesis: enrichment on *GLC3* promoter equals the enrichment on *HSP* promoters. Rvb1 and Rvb2 are highlighted in red dots and labeled. (C) Table of protein factors enriched on *GLC3* promoters. FC of *GLC3* vs *HSP*: fold change of protein enrichment on 2 replicates of *GLC3* promoter-containing CoTrIP plasmid over on 2 replicates of *HSP30* promoter-containing and 1 replicate of *HSP26* promoter-containing plasmid. FC of *GLC3* vs CRAPome: fold change of protein enrichment on 2 replicates of *GLC3* promoter containing CoTrIP plasmid over the CRAPome repository. CRAPome: a contaminant repository for affinity purification–mass spectrometry data. CRAPome was used as a negative control. P-values were from 2-sample t-test. Null hypothesis: enrichment on *GLC3* promoter equals the enrichment on *HSP* promoters. Protein factors were ranked from highest to lowest by “FC *GLC3* over *HSP*”.

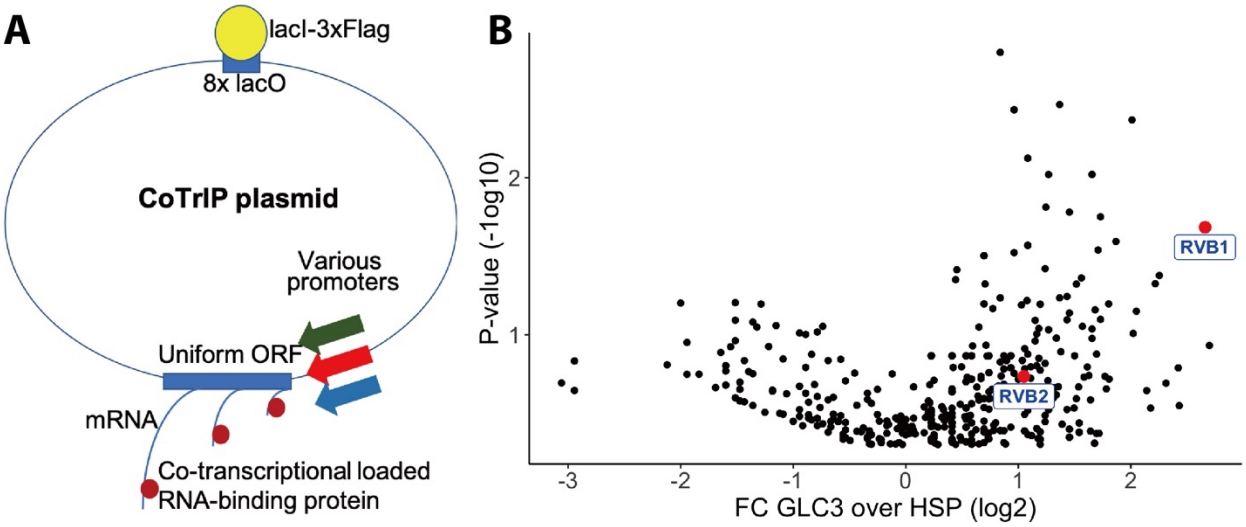

C

Protein factors	FC GLC3 over HSP	FC GLC3 over CRAPome	P-value
Rvb1	6.32	20.71	0.021
Rpp2a	4.77	1.46	0.042
Rps12	4.65	0.61	0.047
Ste20	4.03	12.75	0.004
Tef4	3.65	0.68	0.025
Rpn3	3.32	6.45	0.018
Hsp60	3.27	3.56	0.029
Rpl18a; Rpl18b	3.15	1.38	0.010

Figure 2.2: Rvb1/Rvb2 are enriched at the promoters of endogenous alternative glucose metabolism genes.

(A) Rvb1/Rvb2 are enriched on the promoters and nascent gene bodies. ChIP-seq of cells in 10-minute glucose starvation. X-axis: normalized scale of all genes containing -500 bp to TSS, TSS to TES and TES to +500 bp. TSS: transcription start site. TES: transcription end site. Y-axis: normalized density of target protein on the loci. Normalized density: RPKM of ChIP over RPKM of input. Input: 1% of the cell lysate. Rvb1/Rvb2/Pgk1 are C-terminally fused with TAP tag and immunoprecipitated by IgG-conjugating breads. TAP: tandem affinity purification tag. Pgk1: a negative control that considered as non-interactor on the genome. (B) Cumulative distribution of Rvb2's enrichment on genes. X-axis: log2 scale of Rvb2 ChIP read counts over Pgk1 ChIP read counts from -500 bp to TSS. Y-axis: cumulative distribution. >3 fold: genes that have more than 3-fold transcriptional induction during 10-minute glucose starvation. >3 fold Hsf1 targets: genes that have more than 3-fold transcriptional induction and are Hsf1-regulated. List of genes are in the supplementary. (C) Representative gene tracks showing Rvb1/Rvb2's enrichment. X-axis: gene track with annotation (in Mb). Arrow's orientation shows gene's orientation. Y-axis: normalized density of Rvb1/Rvb2 over Pgk1. Normalized density: RPKM of ChIP over RPKM of input. Class I genes are labeled in red and Class II genes are labeled in blue. Promoters are highlighted by red rectangles. (D) Enrichment profile of Rvb1/Rvb2 on Class I, II genes and genome. X-axis: normalized scale of genome containing -500 bp to TSS, TSS to TES. TES: transcription termination site. Y-axis: RPKM of ChIP over RPKM of input. P-values are from 2-sample t-test. Null hypothesis: normalized density from -500 bp to TSS on Class II promoters equals on Class I promoters.

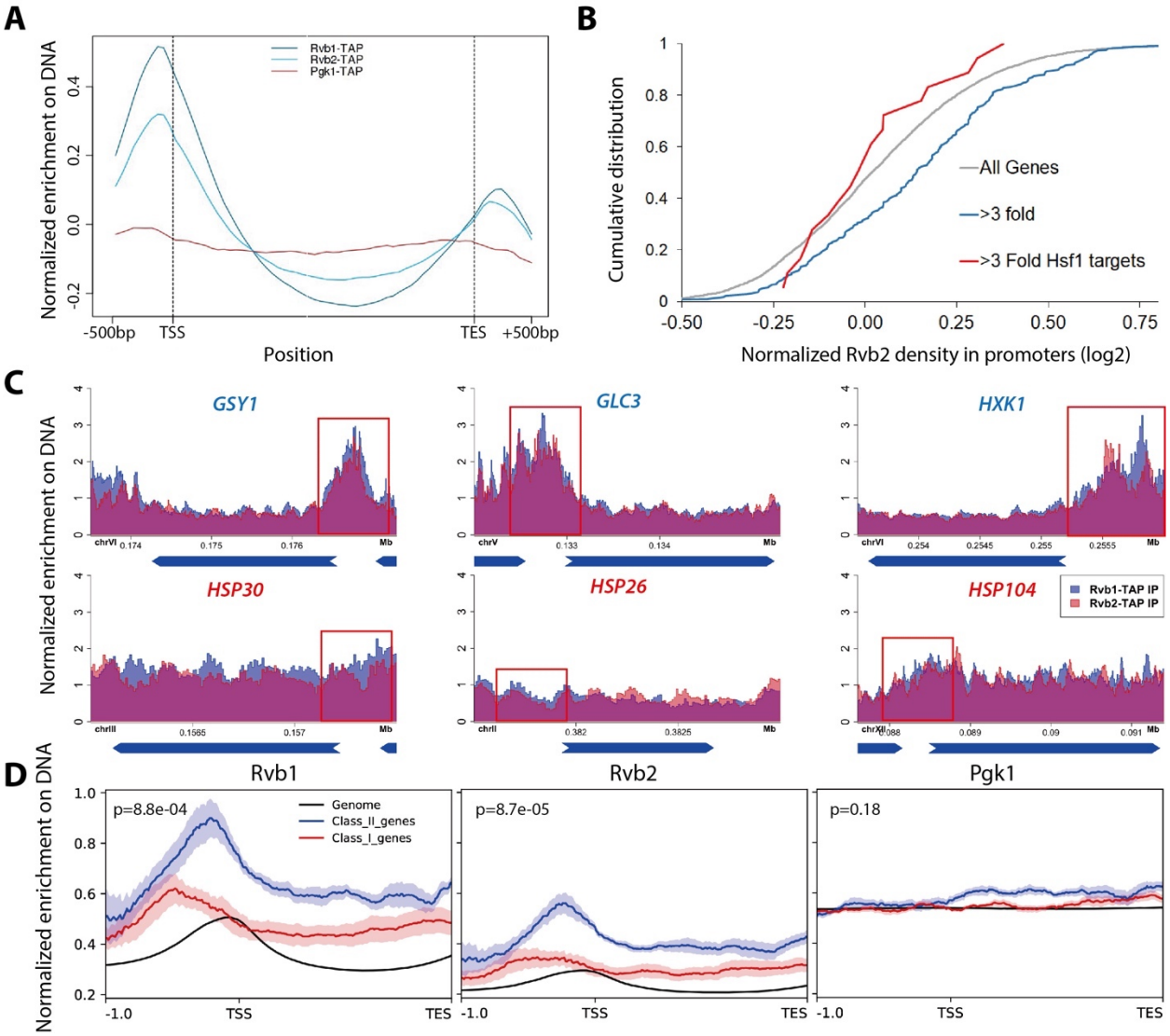
A
Rvb1-TAP
Rvb2-TAP
Pgk1-TAP
Normalized enrichment on DNA
-500bp
TSS
TES
+500bp
Position
B
Cumulative distribution
All Genes
>3 fold
>3 Fold Hsf1 targets
Normalized Rvb2 density in promoters (log2)
C
GSY1
GLC3
HXK1
HSP30
HSP26
HSP104
Rvb1-TAP IP
Rvb2-TAP IP
Normalized enrichment on DNA
D
Rvb1
Rvb2
Pgk1
p=8.8e-04
p=8.7e-05
p=0.18
Genome
Class_II_genes
Class_I_genes
Normalized enrichment on DNA
TSS
TES

Figure 2.3: Rvb1/Rvb2 are co-transcriptionally loaded on the alternative glucose metabolism mRNAs.

(A) Rvb1/Rvb2's enrichment on endogenous mRNAs in 15-minute glucose starvation. RNA immunoprecipitation qPCR of cells in 15-minute glucose starvation. Error bars are from 2 biological replicates. X-axis: 4 Class I mRNAs labeled in red and 4 Class II mRNAs in blue. Y-axis: Ct values were firstly normalized by internal control *ACT1*, then normalized by input control, finally normalized by the wild-type immunoprecipitation control group. Input: 1% of the cell lysate. (B) A schematic view of the reporter mRNA only swapping the promoter. 5UTR: 5' untranslated region. CDS: coding sequence. CFP: cyan fluorescent protein. (C) Rvb1/Rvb2's enrichment on the reporter CFP mRNAs in 15-minute glucose starvation. RNA immunoprecipitation qPCR of cells in 15-minute glucose starvation. X-axis: *HSP26* promoter-driven reporter mRNA labeled in red and *GLC3* promoter-driven mRNA in blue. Y-axis: Ct values were firstly normalized by internal control *ACT1*, then normalized by input control. Input: 1% of the cell lysate. Standard deviations are from 2 biological replicates. Statistical significance was assessed by 2-sample t-test (*$p<0.05$, **$p<0.01$). Null hypothesis: the enrichment on the 2 reporter mRNAs is equal.

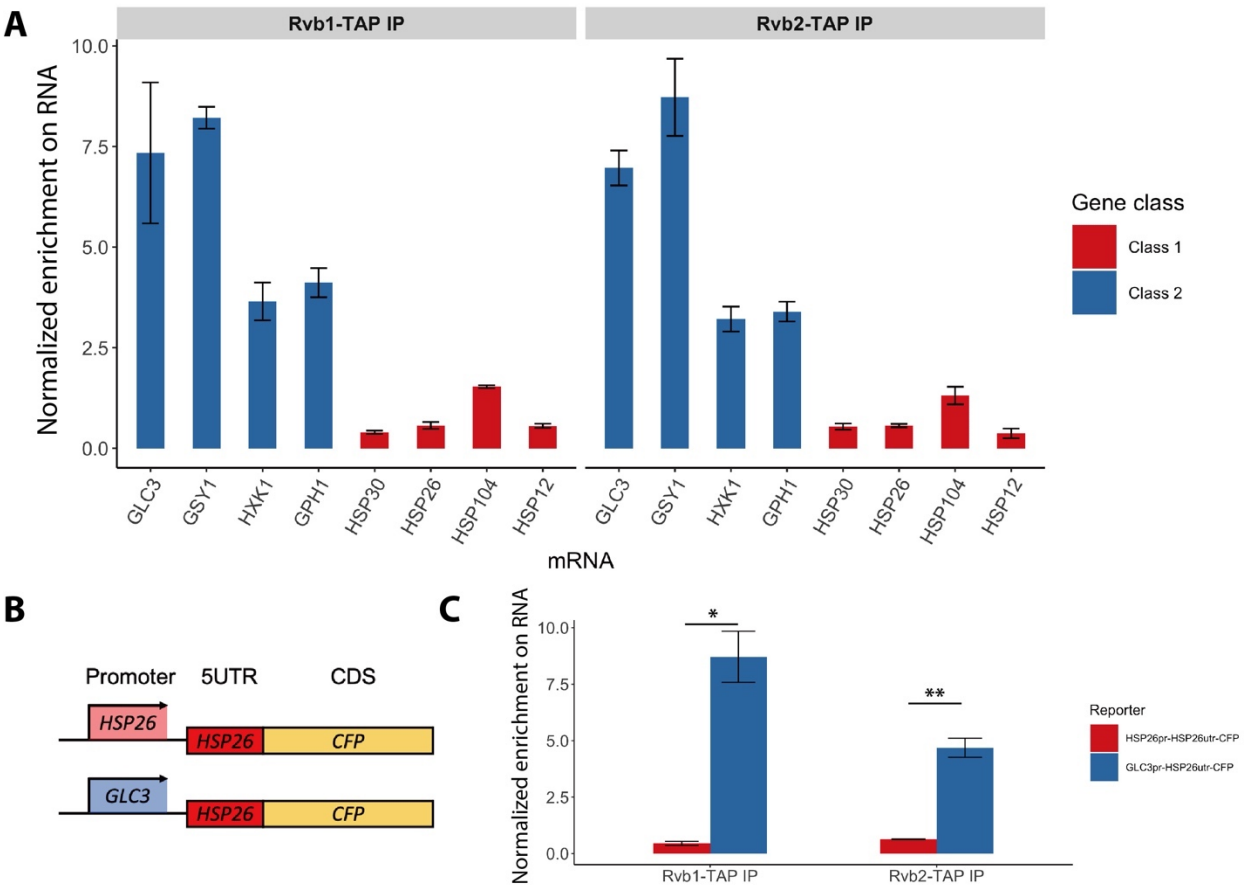
A
Rvb1-TAP IP
Rvb2-TAP IP
Normalized enrichment on RNA
10.0
7.5
5.0
2.5
0.0
GLC3
GSY1
HXK1
GPH1
HSP30
HSP26
HSP104
HSP12
mRNA
Gene class
Class 1
Class 2
B
Promoter
5UTR
CDS
HSP26
HSP26
CFP
GLC3
HSP26
CFP
C
Normalized enrichment on RNA
*
**
Rvb1-TAP IP
Rvb2-TAP IP
Reporter
HSP26pr-HSP26utr-CFP
GLC3pr-HSP26utr-CFP

Figure 2.4: Engineered Rvb1/Rvb2 tethering to mRNAs directs cytoplasmic granular localization and represses translation.

(A) A schematic view of Rvb-tethering methodology. The reporter mRNA contains promoter of interest (Class I promoters), nanoluciferase CDS, PP7 loop sequence, 12XMS2 sequence. Rvb1/Rvb2 are C-terminally fused with PP7-coat protein (CP). Upper panel shows cloning strategy and lower panel shows mRNA's situation upon engineering. (B) protein synthesis of *HSP30*-promoter driven reporter mRNA in log-phase and 25-minute glucose starvation. Y-axis: nanoluciferase synthesized within 5-minute time frame. Nanoluciferase reading was subtracted by the nanoluciferase reading of cycloheximide added 5 minutes earlier. (C) mRNA levels of *HSP30*-promoter driven reporter mRNA in log-phase and 15-minute glucose starvation. Y-axis: Ct values of reporter mRNAs were normalized by the internal control *ACT1*. (D) Translatability of *HSP30*-promoter driven reporter mRNA in log-phase and 15-minute glucose starvation. mRNA translatability: normalized protein level over normalized mRNA level. (B, C, D) Log-phase are labeled in blue and glucose starvation in red. Error bars are from 2 biological replicates. Statistical significance was assessed by 2-sample t-test. Null hypothesis: experimental groups and control groups have equivalent results (*$p<0.05$, **$p<0.01$, ***$p<0.001$). PP7 ctrl: negative control, cells only have the reporter mRNA with PP7 loop. PP7+Rvb1-PCP: Rvb1 is tethered to mRNA. PP7+Rvb2-PCP: Rvb2 is tethered to mRNA. (E) Live imaging showing the subcellular localization of the *HSP30* promoter-driven reporter mRNA in 30-minute glucose starvation. Reporter mRNA is labeled by the MS2 imaging system. P-body is labeled by marker protein Dcp2. PP7 ctrl: negative control, cells only have the reporter mRNA with PP7 loop. PP7+Rvb1-PCP: Rvb1 is tethered to mRNA. PP7+Rvb2-CP: Rvb2 is tethered to mRNA. Right: quantification of the subcellular localization of the reporter mRNA. Cells with foci: percentage of cells that have the reporter mRNA-containing granule foci. Co-localized: among cells that have a reporter mRNA-containing foci, the percentage of cells that have reporter mRNA granules co-localized with P-body. N=200.

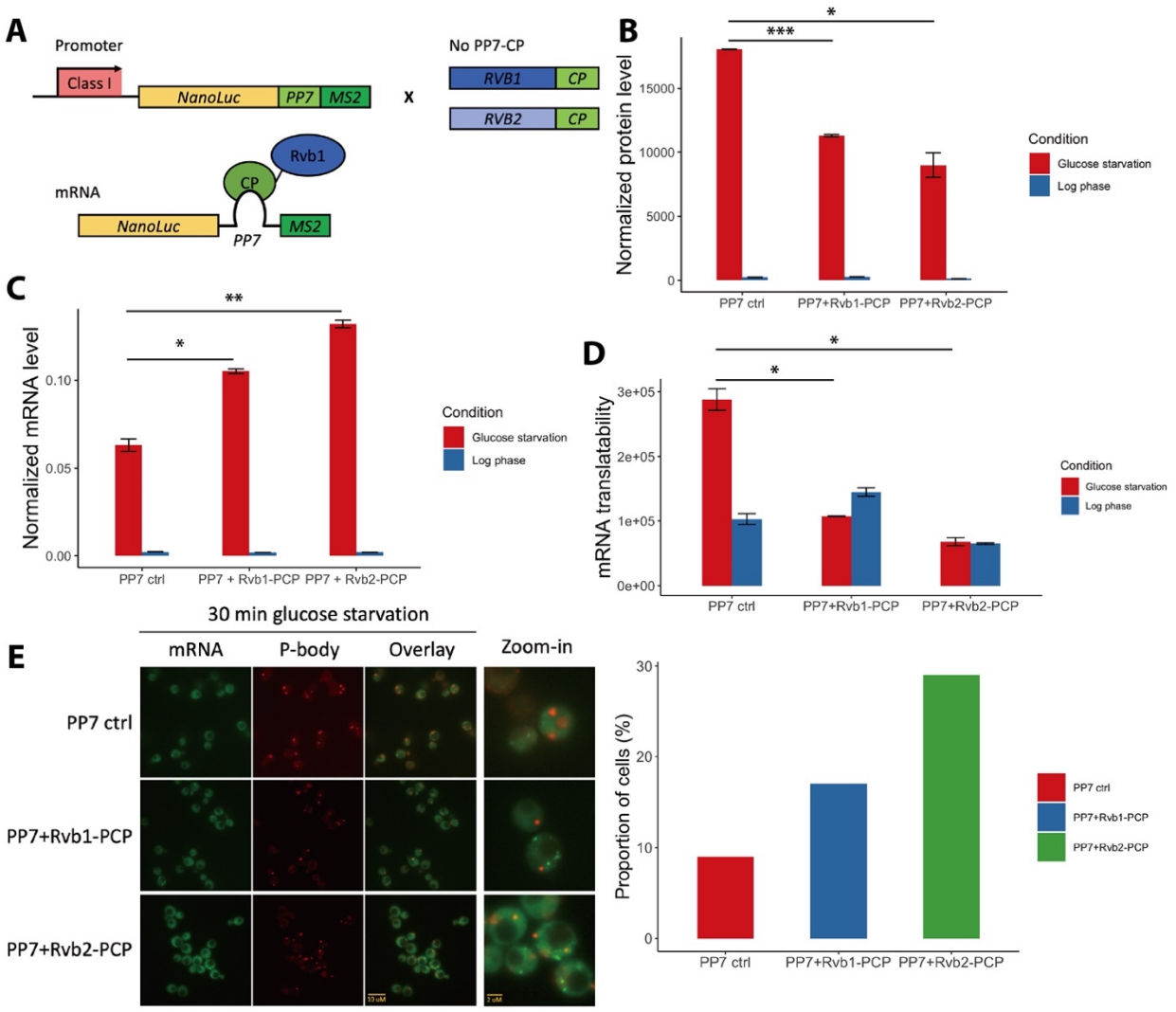
A
Promoter
Class I
NanoLuc
PP7
MS2
x
No PP7-CP
RVB1
CP
RVB2
CP
mRNA
Rvb1
CP
NanoLuc
PP7
MS2
B
Normalized protein level
15000
10000
5000
0
*
***
PP7 ctrl
PP7+Rvb1-PCP
PP7+Rvb2-PCP
Condition
Glucose starvation
Log phase
C
Normalized mRNA level
0.10
0.05
0.00
**
*
PP7 ctrl
PP7 + Rvb1-PCP
PP7 + Rvb2-PCP
Condition
Glucose starvation
Log phase
D
mRNA translatability
3e+05
2e+05
1e+05
0e+00
*
*
PP7 ctrl
PP7+Rvb1-PCP
PP7+Rvb2-PCP
Condition
Glucose starvation
Log phase
E
30 min glucose starvation
mRNA
P-body
Overlay
Zoom-in
PP7 ctrl
PP7+Rvb1-PCP
PP7+Rvb2-PCP
Proportion of cells (%)
30
20
10
0
PP7 ctrl
PP7+Rvb1-PCP
PP7+Rvb2-PCP
PP7 ctrl
PP7+Rvb1-PCP
PP7+Rvb2-PCP

Figure 2.5: Engineered Rvb1/Rvb2 binding to mRNAs increases the transcription of corresponding genes.

(A) Mathematical modeling on mRNA abundance upon varied transcription rates and varied mRNA degradation rates. X-axis: time (minute) after glucose is removed. Y-axis: mRNA fold induction compared to pre-stress condition. Modeling function: $\Delta X(t) = [\beta/\alpha - X0]*(1-e-\alpha t)$, $dX/dt = \beta - \alpha X$. α/a denotes the degradation rate constant. mRNA is produced at a constant rate (β/b). mRNA concentration is (X). (B) mRNA fold induction of Rvb2-tethered mRNAs and non-tethered mRNAs over time. Reporter mRNA is *HSP30* promoter driven. X-axis: time (minute) after glucose is removed. Y-axis: mRNA fold induction compared to pre-stress condition (log scale). PP7 ctrl: negative control, cells only have the reporter mRNA with PP7 loop, labeled in blue. PP7 + Rvb2-PCP: Rvb2 is tethered to mRNA, labeled in red. (C) mRNA decay curve of *HSP30* promoter-driven reporter mRNAs. X-axis: after cells were starved for 15 minutes, time (minute) after stopping the transcription using 1,10-phenanthroline. Y-axis: log2 scale of normalized mRNA levels. Ct values of reporter mRNAs were normalized by the internal control *ACT1.* Statistical significance was achieved by linear regression modeling. Null hypothesis: the mRNA levels of experimental and control groups are equivalent. PP7 ctrl: negative control, cells only have the reporter mRNA with PP7 loop, labeled in blue. PP7 + Rvb2-PCP: Rvb2 is tethered to mRNA, labeled in red.

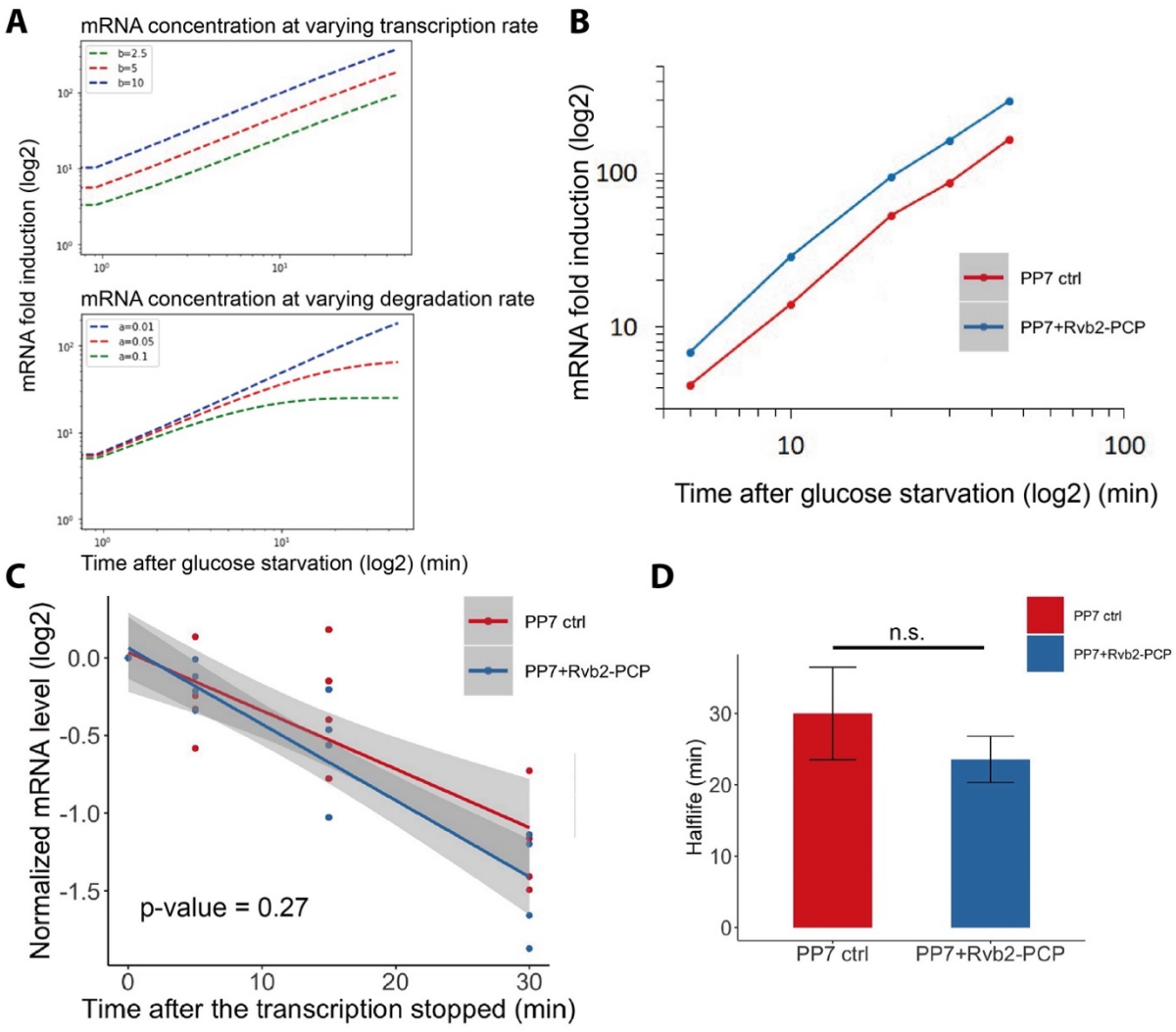
A
mRNA concentration at varying transcription rate
b=2.5
b=5
b=10
mRNA concentration at varying degradation rate
a=0.01
a=0.05
a=0.1
mRNA fold induction (log2)
Time after glucose starvation (log2) (min)
B
mRNA fold induction (log2)
100
10
PP7 ctrl
PP7+Rvb2-PCP
10
100
Time after glucose starvation (log2) (min)
C
Normalized mRNA level (log2)
0.0
-0.5
-1.0
-1.5
PP7 ctrl
PP7+Rvb2-PCP
p-value = 0.27
0
10
20
30
Time after the transcription stopped (min)
D
n.s.
PP7 ctrl
PP7+Rvb2-PCP
Halflife (min)
30
20
10
0
PP7 ctrl
PP7+Rvb2-PCP

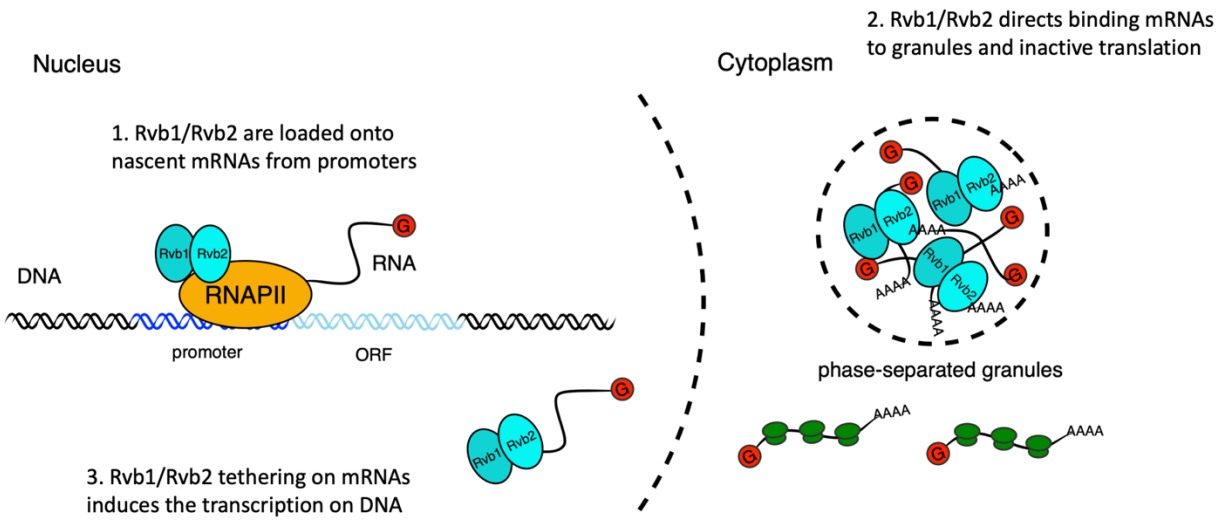

Figure 2.6: A working illustration of Rvb1/Rvb2's novel mechanism in coupling the transcription and translation of interacting genes.

First, Rvb1/Rvb2 are recruited by specific promoters and loaded onto the nascent mRNAs during glucose starvation. Then Rvb1/Rvb2 escort the interacting mRNAs to the cytoplasm and direct their localization in the cytoplasmic granules and associated repressed translation. Also, increased Rvb binding on the mRNA can backwards increase the transcription of the corresponding genes, further showing the coupling of transcription and translation.

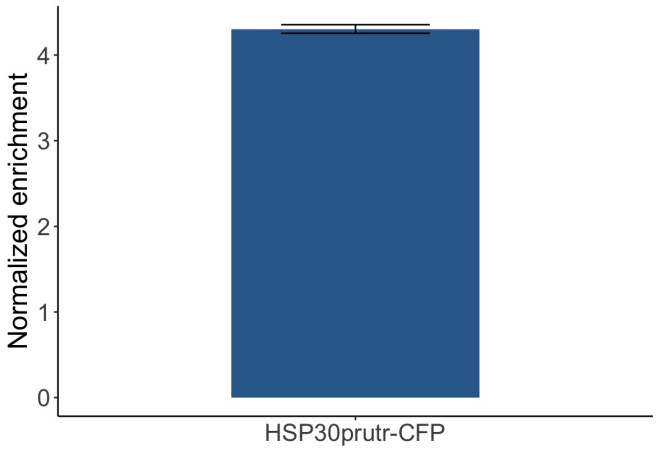

Figure supplement 2.1: Reporter RNA was enriched on the CoTrIP plasmid.

HSP30 promoter-driven reporter mRNA was tested via RT-qPCR. Y-axis: Ct value of the reporter mRNA was first normalized by housekeeping gene *PDC1* and further normalized by the promoter-less CoTrIP plasmid negative control.

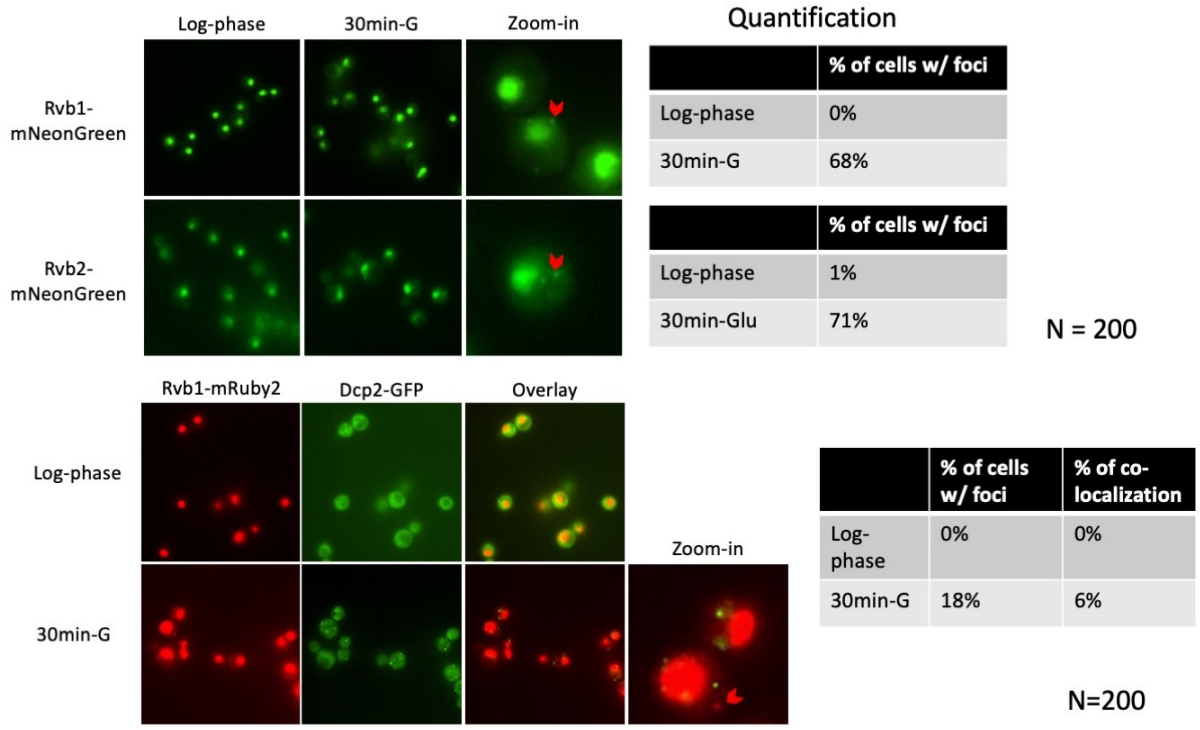

Figure supplement 2.2: Rvb1/Rvb2 form cytoplasmic granules that are not co-localized with P-body during glucose starvation.

In the upper panel, Rvb1/Rvb2 is C-terminally fused with green fluorescent protein mNeonGreen. In the lower panel, Rvb1/Rvb2 is C-terminally fused with red fluorescent protein mRuby2 and P-body marker Dcp2 is C-terminally fused with GFP. Cells are imaged lively in both log-phase and 30-minute glucose starvation condition. Quantification was performed on 200 cells in each imaging. % of cells w/ foci: among the cells analyzed, the percentage of cells that have a Rvb-containing foci. % of co-localization: among the cells with the Rvb-containing foci, the percentage of cells that have a co-localized foci with Dcp2-containing foci.

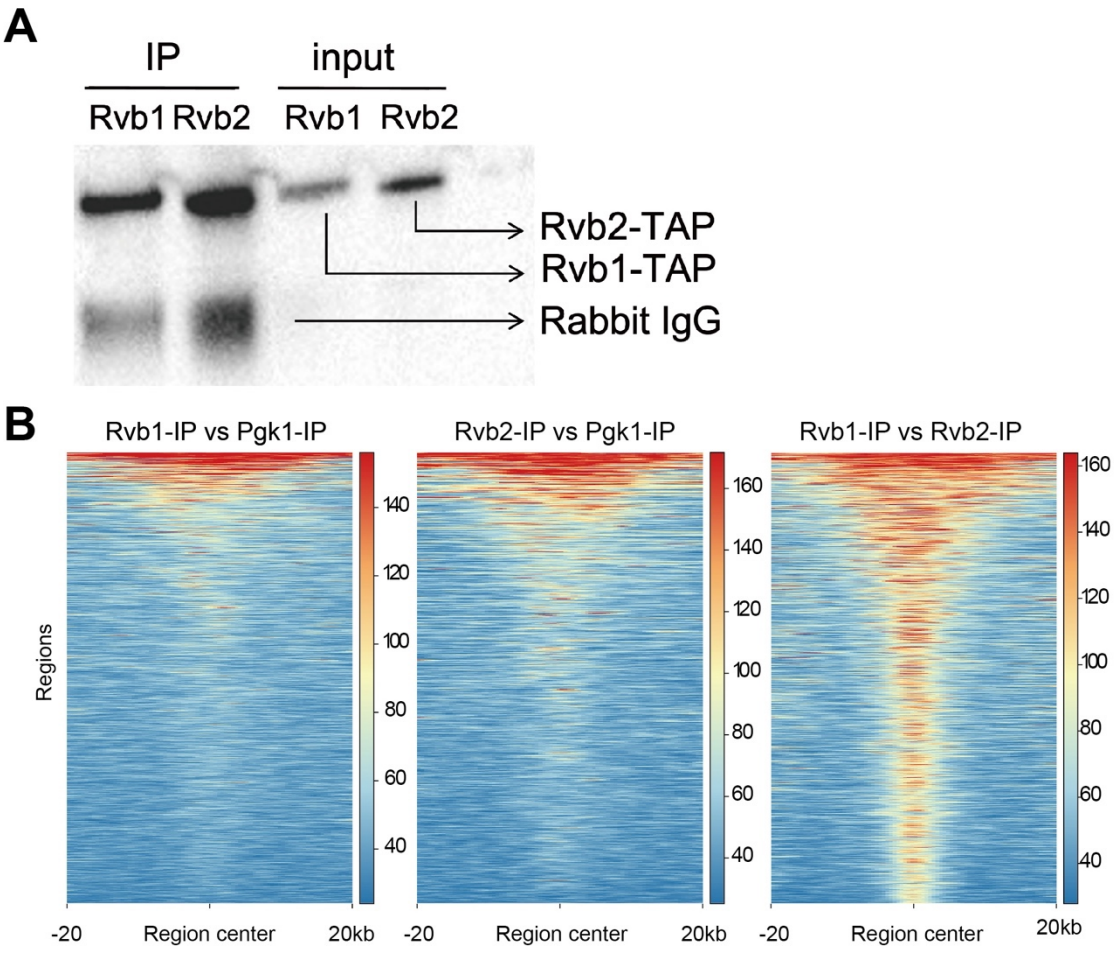

Figure supplement 2.3: Western validation of ChIP-seq and similarity analysis of Rvb1/Rvb2/Pgk1's enrichment.

(A) Western validating the efficiency of the immunoprecipitation (IP). Rvb1/Rvb2 are C-terminally fused with the tandem-affinity-purification tag (TAP), labeled as Rvb1-TAP and Rvb2-TAP. The proteins of interest were pulled down by rabbit IgG. Cells are harvested at 10-minute glucose starvation. Input is 1% of the total lysate. (B) comparison analysis of Rvb1/Rvb2/Pgk1's enrichment on the genome. X-axis: the enriched regions aligned by the center. Y-axis: regions arranged high to low by the level of overlapping. Color-code: red indicates that the two IPs are highly overlapped and blue means not overlapped. Left panel: use Pgk1's enriched regions as reference, score Rvb1's enrichment. Middle panel: use Pgk1's enriched regions as reference, score Rvb2's enrichment. Right panel: use Rvb2's enriched regions as reference, score Rvb1's enrichment.

Class I Upregulated High-Ribo genes

Systematic Name	Name	BY4741		EY0690	
		mRNA	Ribo	mRNA	Ribo
YCR021C	*HSP30*	5.9	2.5	6.9	0.8
YBR072W	*HSP26*	3.9	1.1	4.9	0.3
YLL026W	*HSP104*	3.8	0.7	3.1	0.3
YDR258C	*HSP78*	3.5	0.3	2.6	-0.2
YFL014W	*HSP12*	3.1	0.8	2.6	0.9
YPL240C	*HSP82*	2.8	0.1	2.2	0.1
YER067W	*RGI1*	6.7	0.6	4.6	-0.3
YLR327C	*TMA10*	5.9	2.9	6.0	0.9
YKR075C		4.6	1.3	4.4	-0.4
YGR142W	*BTN2*	5.0	2.0	5.2	0.6
YBL078C	*ATG8*	2.8	0.8	2.2	1.1

Class II Upregulated Low-Ribo genes

Systematic Name	Name	BY4741		EY0690	
		mRNA	Ribo	mRNA	Ribo
YEL011W	*GLC3*	5.5	-1.8	5.0	-2.7
YFR015C	*GSY1*	6.0	-1.7	3.7	-2.6
YFR053C	*HXK1*	5.5	-1.9	3.5	-1.3
YPR160W	*GPH1*	4.2	-1.8	3.6	-2.0
YGR088W	*CTT1*	3.9	-1.0	4.4	-1.2
YGL205W	*POX1*	4.1	-1.3	2.8	-1.8
YDR171W	*HSP42*	5.8	-2.0	4.7	-1.5
YGR249W	*MGA1*	5.1	-1.8	5.4	-2.2
YJL052W	*TDH1*	2.9	-1.5	2.7	-1.3
YBR147W	*RTC2*	2.5	-2.9	3.0	-2.6
YKL217W	*JEN1*	6.0	-1.6	5.0	-1.5
YLR258W	*GSY2*	3.3	-1.1	1.4	-1.1
YCR091W	*KIN82*	2.6	-2.1	2.9	-1.9

Figure supplement 2.4: List of Class I upregulated and high-ribo genes and Class II upregulated and low-ribo genes.

Data from Zid & O'Shea, 2014. Fold-change in mRNA levels and in ribosome occupancy after 15 minutes of glucose starvation from one measurement of BY4741 and one measurement of EY0690. mRNA: log2 mRNA fold change for glucose starvation vs. log-phase glucose-rich. Ribo: log2 ribosome occupancy fold change for glucose starvation vs. log-phase glucose-rich.

Gene	FC Rvb1 vs Pgk1	FDR%	FC Rvb2 vs Pgk1	FDR%
YDR171W	2.23	0.00	2.38	0.00
YELOIIW	3.43	0.00	3.58	0.00
YFR015C	3.57	0.00	3.07	0.00
YFR053C	4.13	0.00	3.45	0.00
YGR088W	3.34	0.00	2.85	0.00
YGR249W	2.81	0.00	2.75	0.00
YJL052W	3.5	0.00	4.26	0.00
YPR160W	3.97	0.00	3.52	0.00

Figure supplement 2.5: List of peaks called of Rvb1/Rvb2 on the genome.

From the ChIP-seq results of Rvb1/Rvb2 in 10-minute glucose starvation. MACS algorithm was applied. Genes are showed under systematic names. FC: fold change of Rvb's peak versus Pgk1's peak. FDR: false discovery rate.

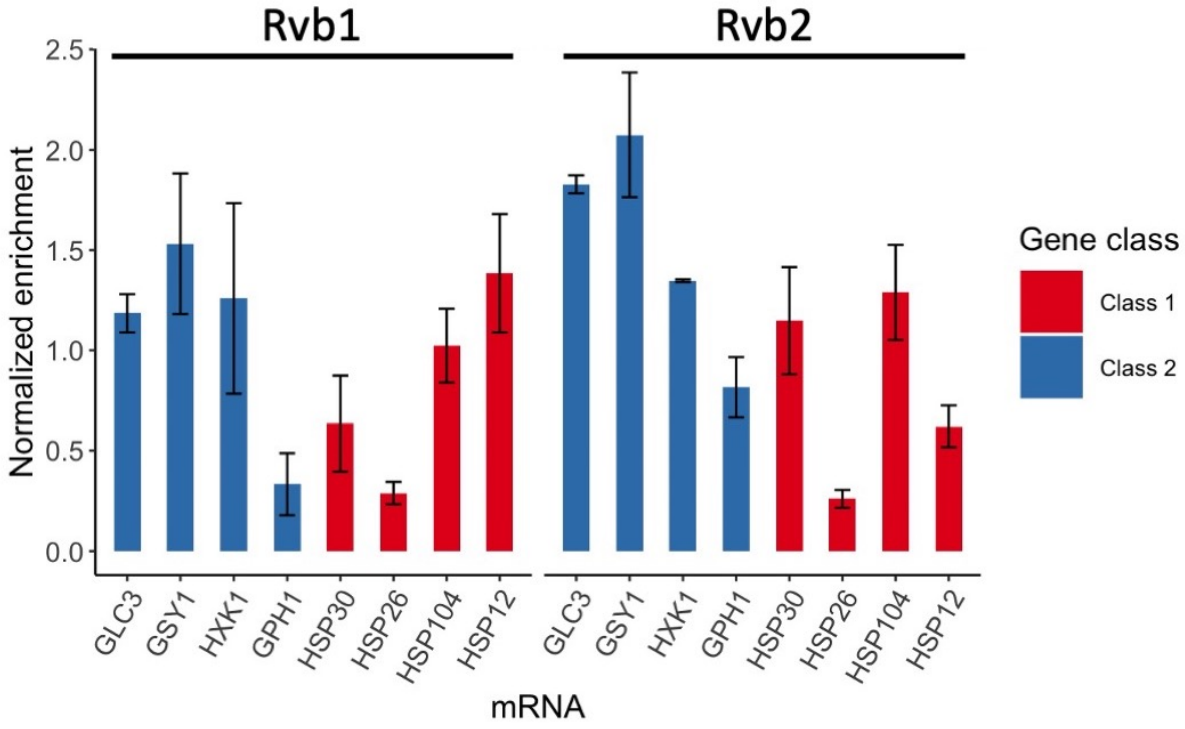

Figure supplement 2.6: Rvb1/Rvb2 did not show differential enrichment between Class I and Class II mRNAs in glucose-rich log-phase cells.

RNA immunoprecipitation qPCR of cells in log phase. Error bars are from 2 technical replicates. X-axis: 4 Class I mRNAs labeled in red and 4 Class II mRNAs in blue. Y-axis: Ct values were firstly normalized by internal control *ACT1*, then normalized by input control, finally normalized by the wild-type immunoprecipitation control group. Input: 1% of the cell lysate.

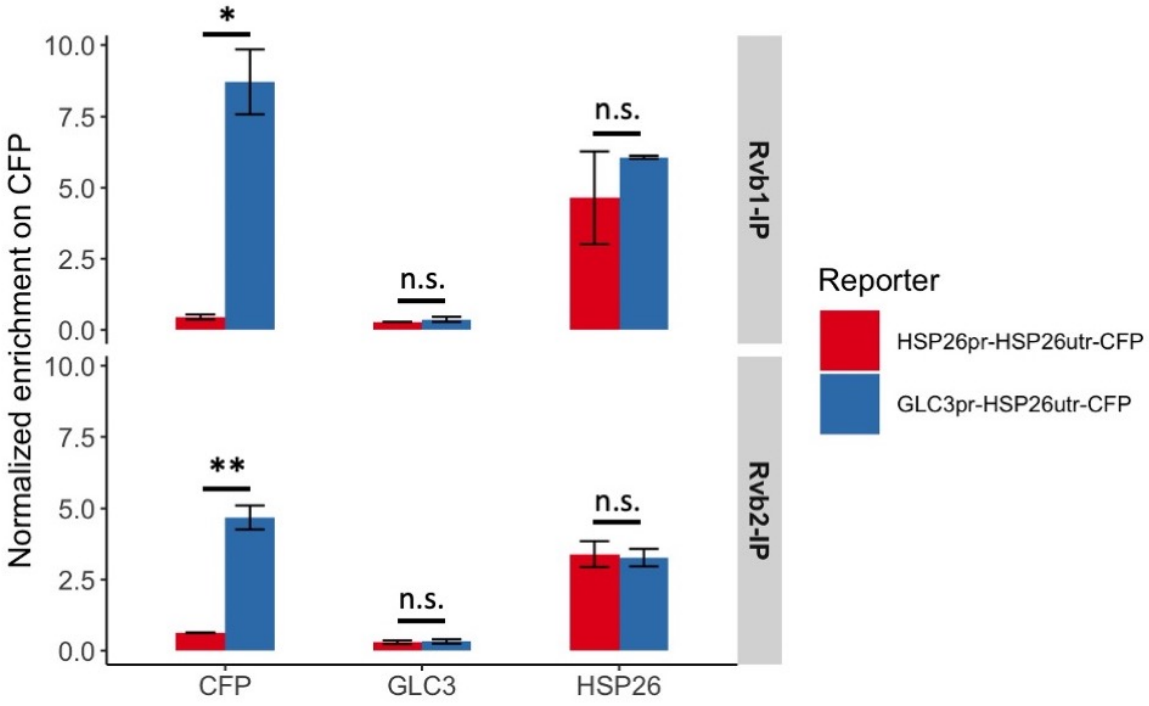

Figure supplement 2.7: Rvb1/Rvb2's enrichment on the reporter CFP mRNAs and endogenous *GLC3/HSP26* mRNAs as control in 15-minute glucose starvation.

RNA immunoprecipitation qPCR of cells in 15-minute glucose starvation. X-axis: *HSP26* promoter-driven reporter mRNA labeled in red and *GLC3* promoter-driven mRNA in blue. Y-axis: Ct values were firstly normalized by internal control *ACT1*, then normalized by input control. Input: 1% of the cell lysate. Error bars are from 2 biological replicates. Statistical significance was assessed by 2-sample t-test (*p<0.05, **p<0.01). Null hypothesis: the enrichment on the 2 reporter mRNAs is equal.

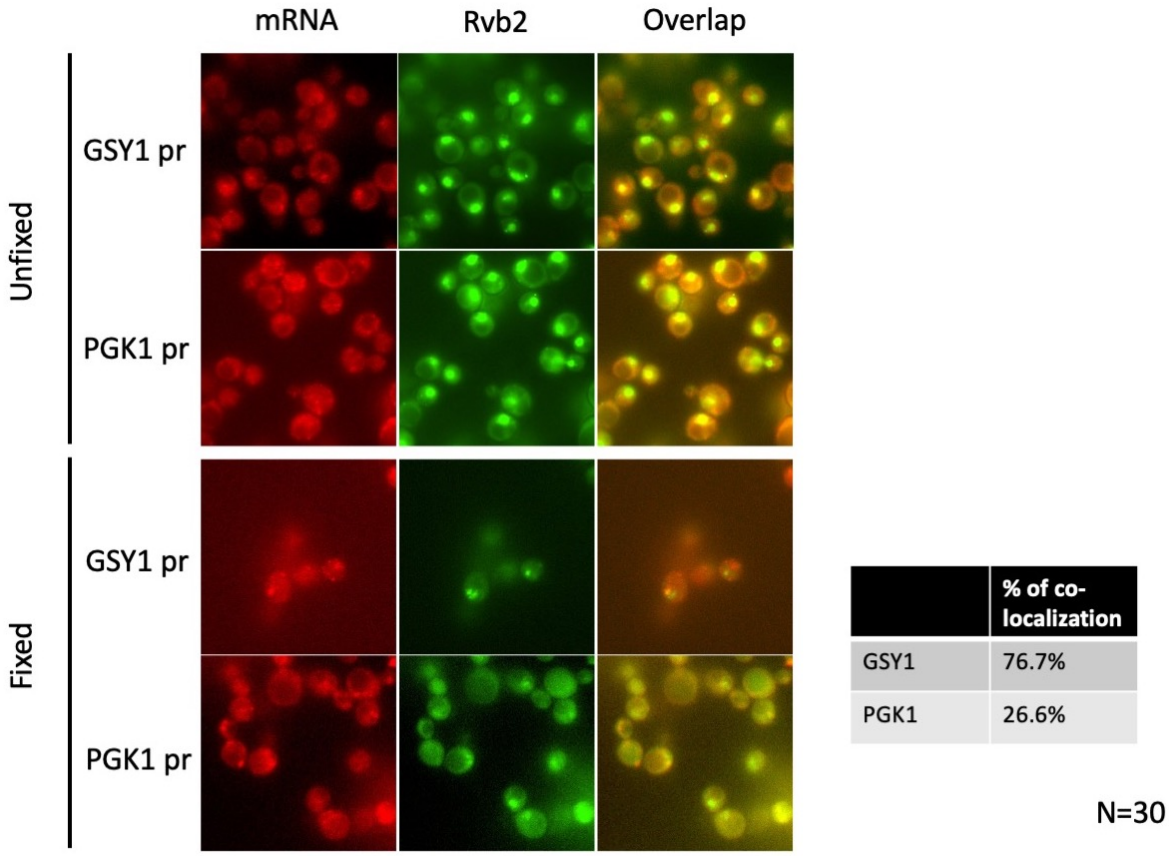

Figure supplement 2.8: Imaging of colocalization of Rvb2 and *GSY1* promoter-driven reporter mRNA.

Cells were harvested after 15-minute glucose starvation. Fixed: cells were fixed by 3% glyoxal. Unfixed: cells are imaged right after glucose starvation. Reporter mRNA was fused by 12XMS2 sequences, which is labelled by MS2CP-mRuby2. Reporter mRNAs contains promoter of interest, uniform nanoluciferase ORF, PET ORF and 12XMS2 sequence. Rvb2 is C-terminally fused with GFP. *PGK1* promoter-driven reporter mRNA was a negative control because it is considered not co-localized with Rvb2. Table: quantification of percentage of cells that have colocalized mRNA-containing granules and Rvb2-containing granules. N=30.

Figure supplement 2.9: Engineered Rvb1/Rvb2 tethering to *HSP30* promoter-driven reporter mRNA directs cytoplasmic granular localization and repressed translation.

(A) protein synthesis of *HSP30*-promoter driven reporter mRNA in log-phase and 25-minute glucose starvation. Y-axis: nanoluciferase synthesized within 5-minute time frame. Nanoluciferase reading was subtracted by the nanoluciferase reading of cycloheximide added 5 minutes earlier. X-axis: different Rvb-tethering conditions. Ctrl: negative control, no PP7 and PP7-coat protein. Rvb1-PCP ctrl: negative control, Rvb1 is fused with PP7-coat protein but no reporter mRNA with PP7 loop. Rvb2-PCP ctrl: negative control, Rvb2 is fused with PP7-coat protein but no reporter mRNA with PP7 loop. PP7 ctrl: negative control, cells only have the reporter mRNA with PP7 loop. PP7+Rvb1-PCP: Rvb1 is tethered to mRNA. PP7+Rvb2-PCP: Rvb2 is tethered to mRNA. Log-phase are labeled in blue and glucose starvation in red. Error bars are from 2 biological replicates. Statistical significance was assessed by 2-sample t-test. Null hypothesis: experimental groups and control groups have equivalent results (*$p<0.05$, **$p<0.01$, ***$p<0.001$). (B) Live imaging showing the subcellular localization of the *HSP30* promoter-driven reporter mRNA in 15-minute and 30-minute glucose starvation. Reporter mRNA is labeled by the MS2 imaging system. P-body is labeled by marker protein Dcp2. PP7 ctrl: negative control, cells only have the reporter mRNA with PP7 loop. PP7+Rvb1-PCP: Rvb1 is tethered to mRNA. PP7+Rvb2-CP: Rvb2 is tethered to mRNA.

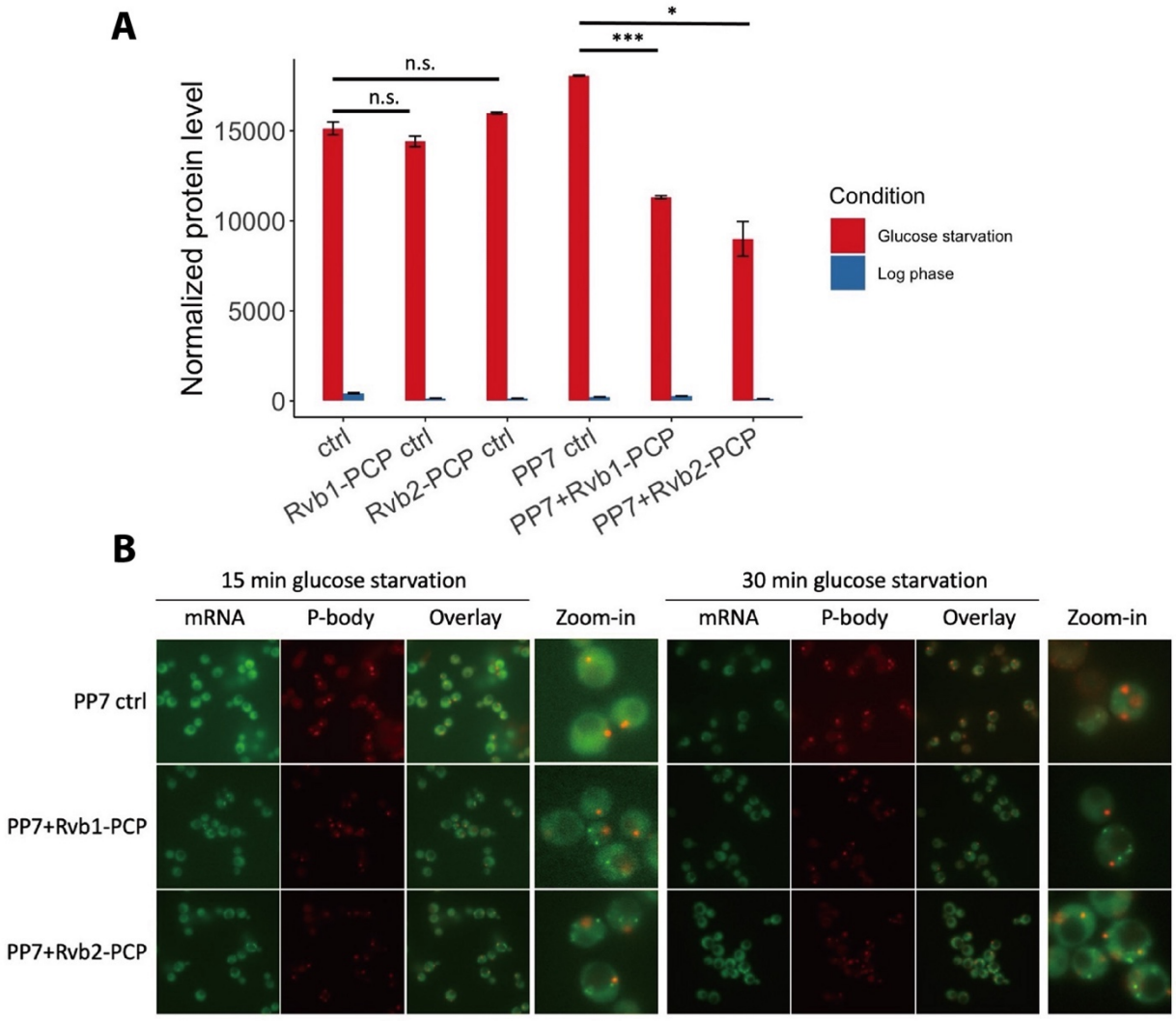
A
Normalized protein level
15000
10000
5000
0
n.s.
n.s.
*
***
ctrl
Rvb1-PCP ctrl
Rvb2-PCP ctrl
PP7 ctrl
PP7+Rvb1-PCP
PP7+Rvb2-PCP
Condition
Glucose starvation
Log phase
B
15 min glucose starvation
30 min glucose starvation
mRNA
P-body
Overlay
Zoom-in
PP7 ctrl
PP7+Rvb1-PCP
PP7+Rvb2-PCP

Figure supplement 2.10: Engineered Rvb1/Rvb2 tethering to *HSP26* promoter-driven reporter mRNA directs cytoplasmic granular localization and repressed translation.

(A) protein synthesis of *HSP26*-promoter driven reporter mRNA in log-phase and 25-minute glucose starvation. Y-axis: nanoluciferase synthesized within 5-minute time frame. Nanoluciferase reading was subtracted by the nanoluciferase reading of cycloheximide added 5 minutes earlier. (B) mRNA levels of *HSP26*-promoter driven reporter mRNA in log-phase and 15-minute glucose starvation. Y-axis: Ct values of reporter mRNAs were normalized by the internal control *ACT1*. (C) Translatability of *HSP26*-promoter driven reporter mRNA in log-phase and 15-minute glucose starvation. mRNA translatability: normalized protein level over normalized mRNA level. (A, B, C) Log-phase are labeled in blue and glucose starvation in red. Error bars are from 2 biological replicates. Ctrl: negative control, no PP7 and PP7-coat protein. Rvb1-PCP ctrl: negative control, Rvb1 is fused with PP7-coat protein but no reporter mRNA with PP7 loop. Rvb2-PCP ctrl: negative control, Rvb2 is fused with PP7-coat protein but no reporter mRNA with PP7 loop. PP7 ctrl: negative control, cells only have the reporter mRNA with PP7 loop. PP7+Rvb1-PCP: Rvb1 is tethered to mRNA. PP7+Rvb2-PCP: Rvb2 is tethered to mRNA. (D) Live imaging showing the subcellular localization of the *HSP26* promoter-driven reporter mRNA in 30-minute glucose starvation. Reporter mRNA is labeled by the MS2 imaging system. P-body is labeled by marker protein Dcp2. PP7 ctrl: negative control, cells only have the reporter mRNA with PP7 loop. Rvb1-PCP: Rvb1 is fused with PP7-coat protein. Rvb2-CP: Rvb2 is fused with PP7-coat protein. Non-PP7 control: cells don't have reporter mRNA with PP7. PP7 sets: cells have reporter mRNA with PP7. (E) Quantification of subcellular localization of the reporter mRNA. Y-axis: percentage of cells that have the reporter mRNA-containing granule foci. N=100. Ctrl: negative control, no PP7 and PP7-coat protein. Rvb1-PCP ctrl: negative control, Rvb1 is fused with PP7-coat protein but no reporter mRNA with PP7 loop. Rvb2-PCP ctrl: negative control, Rvb2 is fused with PP7-coat protein but no reporter mRNA with PP7 loop. PP7 ctrl: negative control, cells only have the reporter mRNA with PP7 loop. PP7+Rvb1-PCP: Rvb1 is tethered to mRNA. PP7+Rvb2-PCP: Rvb2 is tethered to mRNA.

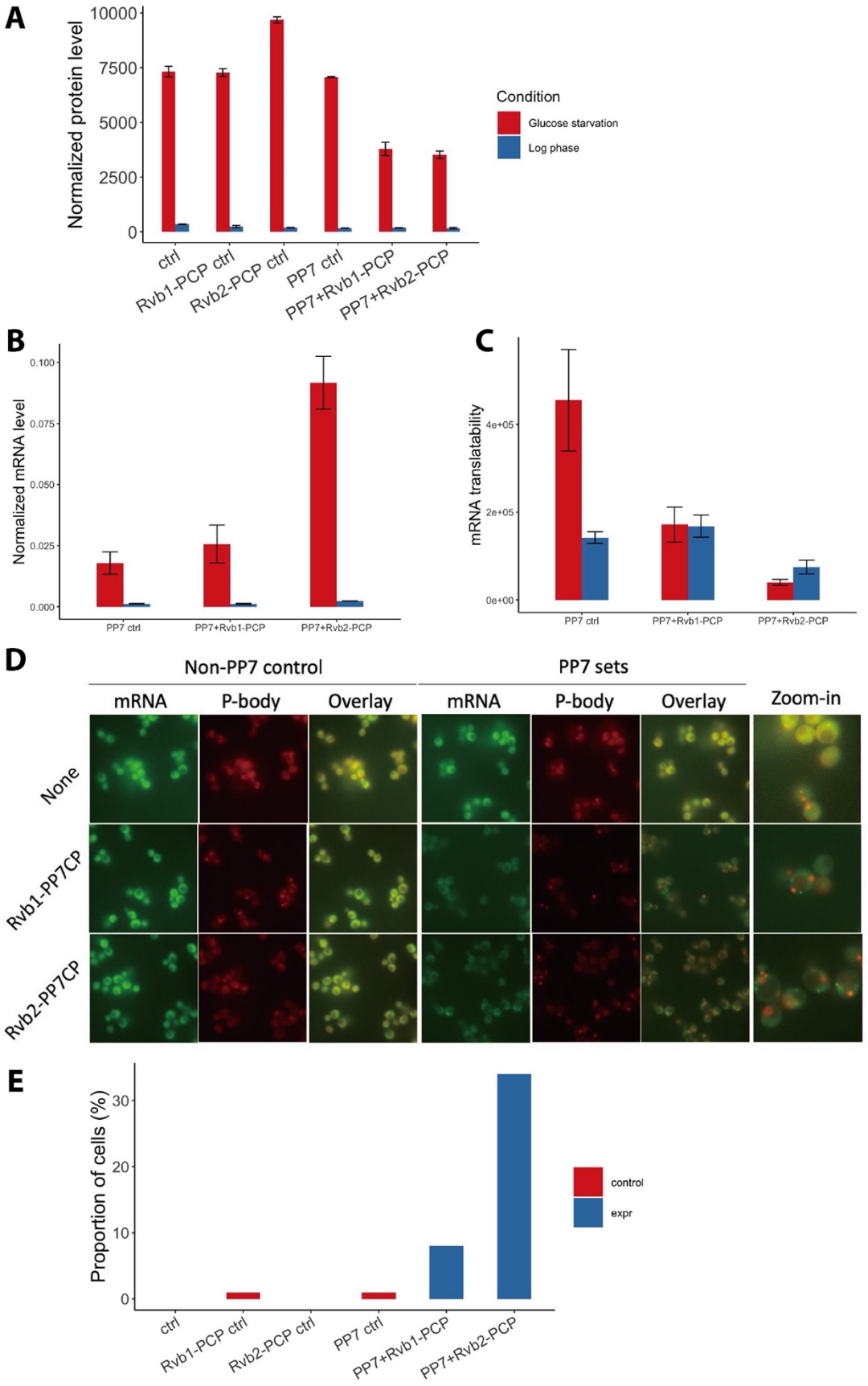
A
Normalized protein level
10000
7500
5000
2500
0
Condition
Glucose starvation
Log phase
ctrl
Rvb1-PCP ctrl
Rvb2-PCP ctrl
PP7 ctrl
PP7+Rvb1-PCP
PP7+Rvb2-PCP
B
Normalized mRNA level
0.100
0.075
0.050
0.025
0.000
PP7 ctrl
PP7+Rvb1-PCP
PP7+Rvb2-PCP
C
mRNA translatability
4e+05
2e+05
0e+00
PP7 ctrl
PP7+Rvb1-PCP
PP7+Rvb2-PCP
D
Non-PP7 control
PP7 sets
mRNA
P-body
Overlay
mRNA
P-body
Overlay
Zoom-in
None
Rvb1-PP7CP
Rvb2-PP7CP
E
Proportion of cells (%)
30
20
10
0
control
expr
ctrl
Rvb1-PCP ctrl
Rvb2-PCP ctrl
PP7 ctrl
PP7+Rvb1-PCP
PP7+Rvb2-PCP

Figure supplement 2.11: Engineered Rvb1/Rvb2 tethering to *HSP12* promoter-driven reporter mRNA directs cytoplasmic granular localization and repressed translation.

(A) protein synthesis of *HSP12*-promoter driven reporter mRNA in log-phase and 25-minute glucose starvation. Y-axis: nanoluciferase synthesized within 5-minute time frame. Nanoluciferase reading was subtracted by the nanoluciferase reading of cycloheximide added 5 minutes earlier. Error bars are from 2 technical replicates. (B) mRNA levels of *HSP12*-promoter driven reporter mRNA in log-phase and 15-minute glucose starvation. Y-axis: Ct values of reporter mRNAs were normalized by the internal control *ACT1*. (C) Translatability of *HSP12*-promoter driven reporter mRNA in log-phase and 15-minute glucose starvation. mRNA translatability: normalized protein level over normalized mRNA level. (A, B, C) Log-phase are labeled in blue and glucose starvation in red. Ctrl: negative control, no PP7 and PP7-coat protein. Rvb1-PCP ctrl: negative control, Rvb1 is fused with PP7-coat protein but no reporter mRNA with PP7 loop. Rvb2-PCP ctrl: negative control, Rvb2 is fused with PP7-coat protein but no reporter mRNA with PP7 loop. PP7 ctrl: negative control, cells only have the reporter mRNA with PP7 loop. PP7+Rvb1-PCP: Rvb1 is tethered to mRNA. PP7+Rvb2-PCP: Rvb2 is tethered to mRNA. (D) Live imaging showing the subcellular localization of the *HSP12* promoter-driven reporter mRNA in 30-minute glucose starvation. Reporter mRNA is labeled by the MS2 imaging system. P-body is labeled by marker protein Dcp2. PP7 ctrl: negative control, cells only have the reporter mRNA with PP7 loop. Rvb1-PCP: Rvb1 is fused with PP7-coat protein. Rvb2-CP: Rvb2 is fused with PP7-coat protein. Non-PP7 control: cells don't have reporter mRNA with PP7. PP7 sets: cells have reporter mRNA with PP7. (E) Quantification of subcellular localization of the reporter mRNA. Y-axis: percentage of cells that have the reporter mRNA-containing non-P-body granule foci. N=100. Ctrl: negative control, no PP7 and PP7-coat protein. Rvb1-PCP ctrl: negative control, Rvb1 is fused with PP7-coat protein but no reporter mRNA with PP7 loop. Rvb2-PCP ctrl: negative control, Rvb2 is fused with PP7-coat protein but no reporter mRNA with PP7 loop. PP7 ctrl: negative control, cells only have the reporter mRNA with PP7 loop. PP7+Rvb1-PCP: Rvb1 is tethered to mRNA. PP7+Rvb2-PCP: Rvb2 is tethered to mRNA.

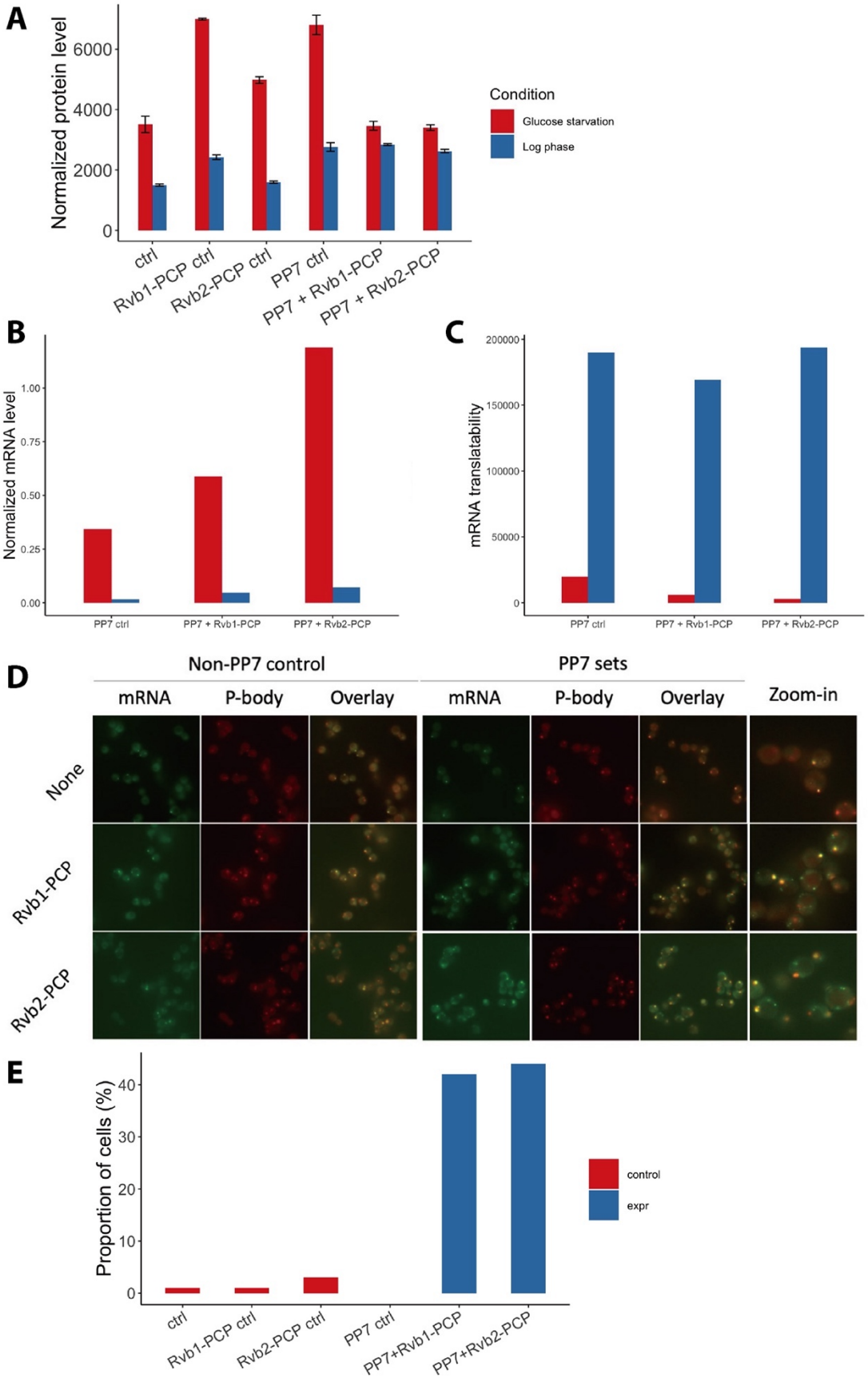
A
Normalized protein level
6000
4000
2000
0
Condition
Glucose starvation
Log phase
ctrl
Rvb1-PCP ctrl
Rvb2-PCP ctrl
PP7 ctrl
PP7 + Rvb1-PCP
PP7 + Rvb2-PCP
B
Normalized mRNA level
1.00
0.75
0.50
0.25
0.00
PP7 ctrl
PP7 + Rvb1-PCP
PP7 + Rvb2-PCP
C
mRNA translatability
200000
150000
100000
50000
0
PP7 ctrl
PP7 + Rvb1-PCP
PP7 + Rvb2-PCP
D
Non-PP7 control
PP7 sets
mRNA
P-body
Overlay
mRNA
P-body
Overlay
Zoom-in
None
Rvb1-PCP
Rvb2-PCP
E
Proportion of cells (%)
40
30
20
10
0
control
expr
ctrl
Rvb1-PCP ctrl
Rvb2-PCP ctrl
PP7 ctrl
PP7+Rvb1-PCP
PP7+Rvb2-PCP

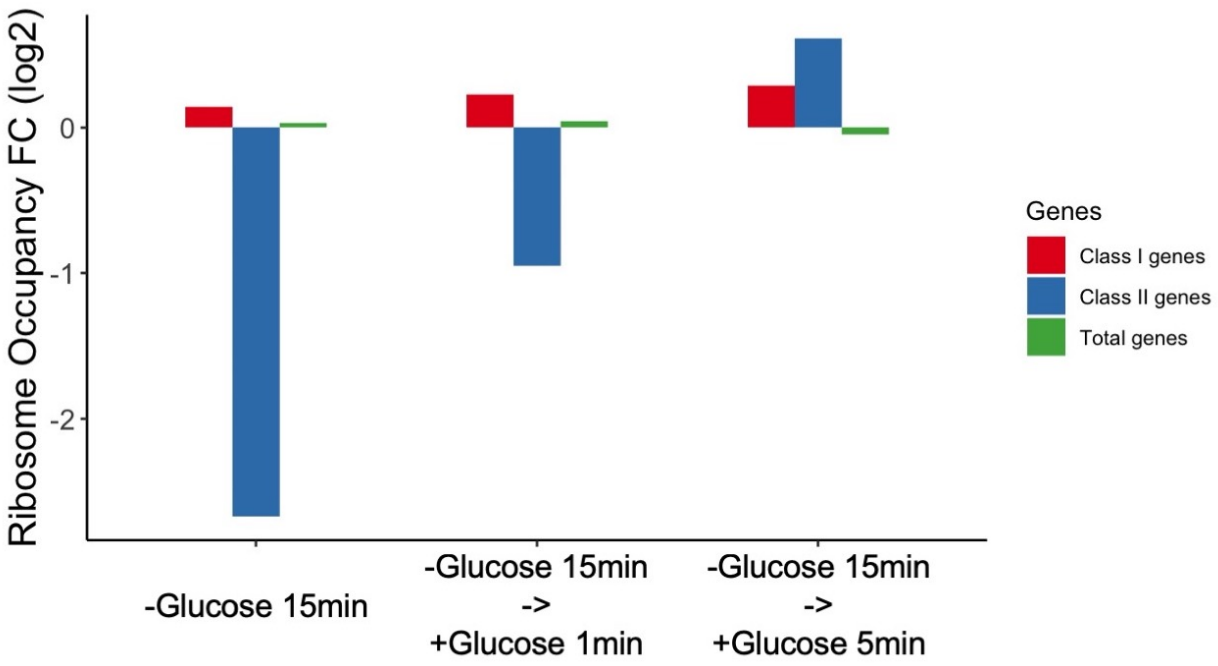

Figure supplement 2.12: Ribosome occupancy of endogenous glucose metabolism mRNAs was quickly induced after glucose replenishment.

Ribosome profiling was performed on cells in 15-minute glucose starvation and followed by 1-minute and 5-minute glucose addback. Y-axis: log 2 scale of ribosome occupancy fold changes on mRNAs compared to log-phase condition. X-axis: each bar represents a gene group. Bars are grouped by conditions. Class I genes and Class II genes refer to figure supplement 4.

2.8 Methods

2.8.1 Yeast strains and plasmids:

The yeast strains and plasmids used in this study are listed in Supplementary file 1 and the oligonucleotides used for the plasmid construction, yeast cloning and RT-qPCR are described in Supplementary file 2. The strains were created through genomic integration of a linear PCR product, or a plasmid linearized through restriction digest or the transformation of an episomal vector. The background strain used was W303 (EY0690), one laboratory strain that is closely related to S288C. In yeast cloning for the C-terminal fusion on the endogenous proteins (e.g. Rvb1-mNeongreen, Rvb1-PP7CP, Rvb1-TAP etc.), we used plasmids of Pringle pFA6a and pKT system (Lee, Lim, & Thorn, 2013; Longtine et al., 1998; Zid & O'Shea, 2014), gifts from the E. K. O'Shea laboratory and the K. Thorn laboratory. We modified the pFA6a and pKT plasmids by inserting in the peptides of interest into the plasmids. The primers used to amplify the fragments from these plasmids contain 2 parts from 3' to 5': a uniform homolog sequence to amplify the plasmid and a homolog sequence to direct inserting the fragments to the genomic loci of interest. The fragments were transformed into the yeasts and integrated to the genome by homologous recombination. The integrations were confirmed by genomic DNA PCR (Yeast DNA Extraction Kit from Thermo Fisher). In the cloning of the reporter strains, we used a strain that was derived from W303 and has one-copied genomic insertion of MYOpr-MS2CP-2XGFP and an endogenous fusion Dcp2-mRFP (Zid & O'Shea, 2014), as the background strain. Further we transformed the linearized MS2-loop-containing reporter plasmids into the strain by restriction digest and genomic integration. RT-qPCR

was performed to verify the one-copied genomic integration. To generate the MS2-loop-containing reporter plasmids (e.g., ZP207 pRS305-HSP30prUTR-nLuc-PEST-12XMS2-tADH1), we started from the plasmid ZP15 pRS305-12XMS2-tAdh1 (Zid & O'Shea, 2014). ZP15 was linearized by the restriction enzymes SacII and NotI (NEB). Promoter fragments, nanoluciferase-pest CDS fragments were inserted into linearized ZP15 using Gibson Assembly. Promoter sequences were amplified by PCR from the W303 genomic DNA. Nanoluciferase-pest CDS was amplified by PCR from the geneblock (Masser, Kandasamy, Kaimal, & Andreasson, 2016). To generate the PP7-MS2-containing reporter plasmids (e.g., ZP296 pRS305-HSP30prUTR-nLuc-PEST-1XPP7-12XMS2-tADH1), ZO680 and ZO679 were firstly annealed using the primer annealing protocol described by Thermo Fisher (https://www.thermofisher.com/us/en/home/brands/invitrogen/molecular-biology-technologies/spotlight-articles/pcr-annealing-optimization-universal-annealing.html). ZP15 was linearized by restriction enzymes BamHI and NotI. Then annealed oligos were inserted into linearized ZP15 by T4 ligation to generate ZP440. ZP440 was further linearized by restriction enzymes SacII and NotI. Promoter fragments, nanoluciferase-pest CDS fragments were inserted into linearized ZP440 using Gibson Assembly. In the cloning of the CoTrIP experiments, detailed procedures were described in the "CoTrIP and CoTrIP analysis".

2.8.2 Yeast growth and media:

The background yeast strain w303 (EY0690) was used for all experiments. For cells cultured in the functional experiments, cells were streaked out on the yeast extract

peptone dextrose (YPD) agarose plate (BD) from the frozen stocks and grew at 30 °C for 2 days. Single colony was selected to start the over-night culture for each biological replicate. Cells were grown at 30°C in batch culture with shaking at 200 r.p.m. in synthetic complete glucose medium (SCD medium: yeast nitrogen base from RPI, glucose from Sigma-Aldrich, SC from Sunrise Science). When the OD_{660} of cells reached 0.4, half of the culture was harvested as the pre-starved sample. The other half of the culture was transferred to the prewarmed synthetic complete medium lacking glucose (SC -G medium) by centrifugation method. Cells are centrifuged at 3000 xg, washed once by SC medium and resuspended in the same volume as the pre-starvation medium of SC medium. Glucose starvation was performed in the same 200 r.p.m shaking speed and 30°C. The length of the glucose starvation time varies from 10 minutes to 30 minutes depending on the experiments.

2.8.3 CoTrIP and CoTrIP analysis:

The protocol was developed based on (Unnikrishnan et al., 2012). ZP64 PRS406-CMV-lacI-FLAG was integrated into the W303 yeast background by linearization withing the *URA3* gene with BstBI digestion and transformation into yeast. The CoTrIP plasmid was constructed by modifying the ZP66 pUC-TALO8 plasmid which contains 8 copies of the Lac operator. The EcoRI sites in ZP66 were mutated to NotI using QuikChange II Site-directed mutagenesis kit (Stratagene). Promoter specific reporters driving CFP were inserted into pUC-TALO8-NotI by digesting with NheI followed by Gibson assembly. The plasmid backbone was then digested with NotI, gel purified, ligated, and transformed into yeast using standard Lithium Acetate transformation. 1L of yeast were grown overnight

in SCD medium -Trp to maintain selection on the CoTrIP plasmid, until an OD_{660} 0.3-0.4. Cells were filtered, washed with SC -G -Trp media, and resuspended in 1L of prewarmed media and grown at 30°C for 5 mins. Cells were then refiltered, resuspended in 4mLs of PBS in a glass petri dish and crosslinked using UV from a Stratalinker 1800 (254 nm, 9999 microjoules × 100, 5 cm from the UV bulb). Crosslinked cells were pelleted and resuspended in 2 mLs of Buffer H 150 (25mM HEPES KOH pH 7.6, 2mM MgCl2, 0.5mM EGTA, 0.1mM EDTA, 10% Glycerol, 150mM KCl, 0.02% NP40) plus protease inhibitor (P8215 Millipore Sigma) and then dripped into liquid N2 to be cryogenically ball milled using a Retsch PM100. Ground lysate was clarified by spinning at 3500 xg for 5 mins at 4°C, isolating the supernatant and spinning at 12K for 5 min at 4°C. Supernatant was aliquoted and frozen at –80°C. 10 µL of unpacked Anti-FLAG® M2 Magnetic Beads (M8823 Millipore Sigma) per sample were pre-washed with Buffer H 150. 300 µL of extract was added to magnetic beads and incubated at 4°C for 3 hrs with rotation. Beads were then washed 3 times with Buffer H 150, 3 times with Buffer H 300 (300mM KCl), and once with Buffer H 150. 500 µg/mL 3xFLAG peptide (F4799 Millipore Sigma) was diluted in Buffer H 150 and CoTrIP plasmids were eluted with 100 µL elution buffer with FLAG peptide. Elutions were taken forward for DNA, RNA, and mass spectrometry. Mass spectrometry was performed through the Yeast Resource Center by James Moresco of the Yates lab and was funded through a P41GM103533 Biomedical Technology Resource Center grant. Data-dependent acquisition of MS/MS spectra was performed with an LTQ-Orbitrap. Tandem mass spectra were extracted from raw files using RawExtract 2.9.9 (McDonald et al., 2004) and were searched against a yeast protein database (http://www.yeastgenome.org) using ProLuCID (Peng et al., 2003; Xu et al.,

2015). Enrichment analysis was performed using the CRAPome online data analysis software (https://reprint-apms.org/) (Mellacheruvu et al., 2013)

2.8.4 ChIP-sequencing:

The protocol was developed based on (Grably & Engelberg, 2010). 100 mL of yeast were grown overnight in SCD medium, until an OD_{660} around 0.4. 50 mL of cells were filtered, washed with SC -G media, and resuspended in 50 mL of prewarmed media and grown at 30°C for 10 mins. 50 mL of pre-starved and 50 mL of 10-minute glucose-starved cell culture was fixed by incubating in the freshly made crosslink buffer (1% formaldehyde, 10 mM NaCl, 0.1 mM EDTA, 5 mM HEPES pH 7.5), respectively, with gentle shaking at room temperature for 15 minutes. Crosslink was quenched by introducing 0.5 M of glycine for 5 minutes at room temperature. Cells were harvested by centrifugation at 3000 xg at 4°C, washed twice in the ice-cold TBS buffer (20 mM Tris pH 7.5, 150 mM NaCl). Cells were resuspended in 400 µL of ChIP lysis buffer (50 mM Hepes-KOH pH 7.5, 150 mM NaCl, 1 mM EDTA, 1% Triton X-100, 0.1% sodium deoxycholate, 1 mM PMSF, 0.5% SDS), and lysed by bead-beating (Biospec Products) for 1 minute for 5 times. Lysis was verified under microscope. Lysates were sonicated by Covaris Sonicator to ~500 bp fragments (130 µL/tube, 105 PIP, 5% Duty F, 200 cycles/burst, 80 seconds). Lysates were centrifuged at 15,000 xg at 4°C to remove the cell debris and diluted to 1 mL. Save 10% of the clear lysate to verify the sonication by protein digestion using Pronase, reverse crosslinking, RNA digestion using RNase A and running the samples on 1% agarose gel. 50 µL of IgG-Dynabeads per sample was used. The protocol of making the IgG-Dynabeads from Dynabeads M-270 Epoxy (Thermo Fisher) was taken

from (X. Li, 2011). IgG-Dynabeads were pre-washed 3 times with ChIP lysis buffer. 1% of the lysate was saved as the input and for Western blotting, respectively. The immunoprecipitation (IP) sample was incubated with IgG-Dynabeads, rotating at 4°C for 4 hours. The IP samples were further washed twice by ChIP lysis buffer with 0.1% SDS, twice by ChIP lysis buffer with 0.1% SDS and 0.5 M NaCl, once by ChIP wash buffer (50 mM Tris pH 7.5, 0.25 mM LiCl, 1 mM EDTA, 0.5% NP-40, 0.5% sodium deoxycholate), and once by TE buffer pH 7.5. Before the last wash, save 10% of the sample for Western blotting. Western blotting was performed to verify the successful enrichment and purification of the protein of interest. Samples were later eluted from beads in 250 µL 2X Pronase buffer (50 mM Tris pH 7.5, 10 mM EDTA, 1% SDS) at 65°C for 10 minutes and beads were removed. Samples were then digested by 2.6 mg/mL Pronase (20 µL of 20 mg/mL Pronase, Sigma-Aldrich) at 42°C for 2 hours and reverse-crosslinked at 65°C for 6 hours. DNA was extracted from the sample using phenol-chloroform, washed once with chloroform, and pelleted using ethanol, washed twice with 75% ethanol (Sigma-Aldrich), and resuspended in 200 µL TE buffer. DNA sequencing libraries were prepared and sequenced following the NextSeq 500 SR 75 protocol at The UCSD IGM Genomics Center (Illumina).

2.8.5 ChIP-sequencing analysis:

Sequencing reads were demultiplexed and the quality was verified by FastQC (Anders, 2010). The reads were mapped to S288C *S. cerevisiae* genome using Bowtie2 (Langmead & Salzberg, 2012). The mapped reads were then sorted, indexed and converted into BAM files using SAMtools (H. Li et al., 2009). Duplicated reads were

removed using Picard Tools (Broad Institute, 2009). The genome browser files for visualizing the reads were generated by igvtools and were visualized on Integrative Genomics Viewer by Broad Institute and Sushi.R (Phanstiel, Boyle, Araya, & Snyder, 2014; Robinson et al., 2011; Thorvaldsdóttir, Robinson, & Mesirov, 2013). Enriched peaks for Rvb1/Rvb2 were called using MACS (Zhang et al., 2008). deepTools was used to calculate and plot the enrichment of Rvb1/Rvb2 on genome and selected genes (Ramírez et al., 2016). The coverage of reads (BigWig files) was calculated from indexed BAM files using bamCoverage. To compare the enrichment of 2 targets, the matrix was computed from BigWig files of 2 targets using computeMatrix and further presented as a heatmap by plotHeatmap. To visualize Rvb1/Rvb2's enrichment, the matrix was computed from BigWig files of the target and S288C genome annotation as the reference using computeMatrix and further presented by plotProfile. Additionally, BEDtools was used to calculate the coverage of regions of interest and a home-made R script was generated to analyze and plot the enrichment of Rvb1/Rvb2 on genome and specific gene groups (Quinlan & Hall, 2010).

2.8.6 RNA immunoprecipitation (RIP):

The RIP protocol was developed based on the protocol from (Van Nostrand et al., 2016; Zander et al., 2016). 100 mL of yeast were grown overnight in SCD medium, until an OD_{660} around 0.4. 50 mL of cells were filtered, washed with SC -G media, and resuspended in 50 mL of prewarmed media and grown at 30°C for 15 mins. 50 mL of pre-starved and 15-minute glucose-starved cell culture was washed and resuspended in 10 mL of ice-cold PBS buffer, fixed by UV irradiation on a 10-cm petri dish using a

Stratalinker 1800 (254 nm, 9999 microjoules × 100, 5 cm from the UV bulb), and harvested. Cells were resuspended in 400 µL of ice-cold RIP lysis buffer (50 mM Tris pH 7.5, 100 mM NaCl, 1% NP-40, 0.5% SDS, 0.2 mM PMSF, 1 mM DTT, 10U RNase inhibitor from Promega, cOmplete Protease Inhibitor Cocktail from Roche), and lysed by bead-beating (Biospec Products) for 1 minute for 5 times. Bright-field microscopy was used to verify that more than 90% of cells were lysed. The lysates were centrifuged softly at 1000 xg at 4°C for 10 minutes to remove cell debris and diluted to 500 µL. Clear lysates were treated with 5U RQ1 DNase and 5U RNase inhibitor (Promega) at 37°C for 15 minutes. Then 1% of the lysate was saved as the input and for Western blotting, respectively. 50 µL of IgG-Dynabeads per sample was used. The protocol of preparing the IgG-Dynabeads from Dynabeads M-270 Epoxy (Thermo Fisher) was taken from (X. Li, 2011). IgG-Dynabeads were pre-washed 3 times with RIP lysis buffer. The immunoprecipitation (IP) samples were incubated with IgG Dynabeads, rotating at 4°C for 4 hours. The IP samples were further washed 6 times by RIP wash buffer (50 mM Tris pH 7.5, 100 mM NaCl, 0.1% NP-40) at 4°C. Samples were later eluted from the beads in 100 µL of PK buffer (100 mM Tris pH 7.5, 50 mM NaCl, 10 mM EDTA) at 65°C for 15 minutes and later the proteins were digested by 10U Proteinase K (NEB) at 37°C for 30 minutes. Digestion was later activated by incubation with Urea (210 mg/mL) at 37°C for 20 minutes. RNA was extracted using TRIzol reagent (Thermo Fisher) according to the vendor's protocol. RNA was washed twice by 70% EtOH and eluted in 10 µL of RNase-free water. RNA samples were further digested fully by RQ1 DNase (Promega) in 10 µL system and were reverse transcribed by ProtoScript II reverse transcriptase (NEB) (a 1:1 combination of

oligo dT18 and random hexamers was used to initiate reverse transcription). The cDNA was investigated by real-time quantitative PCR (RT-qPCR).

2.8.7 Live-cell microscopy and analysis:

Cells were grown to an OD_{660} to ~0.4 in SCD medium at 30°C and glucose-starved in SC -G medium for 15 and 30 minutes. 100 µL of cell culture was loaded onto a 96-well glass-bottom microplate (Cellvis). Cells were imaged using an Eclipse Ti-E microscope (Nikon) with an oil-immersion 63X objective. Imaging was controlled using NIS-Elements software (Nikon). Imaging analysis was performed on Fiji software.

2.8.8 Nanoluciferase assay and analysis:

The nanoluciferase assay was adapted from methods previously described by (Masser et al., 2016). Cells were grown to an OD_{660} to ~0.4 in SCD medium at 30°C and glucose-starved in SC -G medium for 20 minutes. 90 µL of cell culture was loaded onto a Cellstar non-transparent white 96-well flat-bottom plate (Sigma-Aldrich). OD_{660} of cells was taken for each sample. For cells treated with cycloheximide (CHX), CHX was added to a final concentration of 100 µg/mL to stop the translation for 5 minutes. To measure the nanoluciferase signal, 11 µL of substrate mix (10 µL of Promega Nano-Glo® Luciferase Assay Buffer, 0.1 µL of Promega NanoLuc® luciferase substrate and 1 µL of 10 mg/mL CHX) was added and mixed with the samples by pipetting. Measurements were taken immediately after addition of substrate mix by Tecan Infinite Lumi plate reader. To analyze the data, the luciferase level of samples was firstly divided by the OD_{660} level

of the samples. Then the normalized luciferase level of non-CHX-treated sample was further normalized by subtracting the luciferase level of CHX-treated sample.

2.8.9 Western blotting:

The Western blotting protocol was adapted from (Tsuboi et al., 2020). IP and input samples were mixed with the same volume of 2X Laemmli buffer (Bio-Rad) and were boiled at 95 °C for 10 minutes. The samples were then resolved by SDS-PAGE (Bio-Rad), and a rabbit polyclonal antibody specific for calmodulin-binding peptide (A00635-40, GenScript), a Goat anti-Rabbit IgG (H+L) Secondary Antibody, HRP (Thermo Fisher) and SuperSignal™ West Femto Maximum Sensitivity Substrate (Thermo Fisher) were used to detect TAP-tagged proteins. The blotting was imaged using a Gel Doc XR+ Gel Documentation System (Bio-Rad).

2.8.10 Real-time quantitative PCR (RT-qPCR):

The RT-qPCR protocol was adapted from (Tsuboi et al., 2020). RNA was extracted using the MasterPure Yeast RNA Purification Kit (Epicentre). cDNA was prepared using ProtoScript II Reverse Transcriptase (NEB #M0368X) with a 1:1 combination of oligodT 18 primers and random hexamers (NEB) according to the manufacturer's instructions. mRNA abundance was determined by qPCR using a home-brew recipe with SYBR Green at a final concentration of 0.5X (Thermo Fisher #S7564). Primers specific for each transcript were described in Supplementary file 2. The mRNA levels were normalized to *ACT1* abundance, and the fold change between samples was calculated by a standard $\Delta\Delta$Ct analysis.

2.8.11 Mathematical modeling on the mRNA induction:

The mathematical modeling method was adapted from (Elkon et al., 2010) and performed in Python Jupyter Notebook (https://jupyter.org/). To accurately describe the dynamics of induced mRNA transcription, we used an ordinary differential equation as follows,

$$\frac{dX}{dt} = \beta - \alpha X$$

where X is the mRNA concentration, α is the degradation constant, and β is the transcription rate.

We assumed that transcription and degradation rates play essential roles in shaping the overall curve of mRNA increase, and these parameters stay constant over the course of induced expression. We then hypothesized that Rvb1/Rvb2 binding to mRNAs could either increase β or decrease α, leading to greater mRNA abundance than the PP7 control. To observe the effects of varied transcription or degradation rates on the mRNA abundance, we solved the differential equations with different parameters using ODEINT algorithm, and generated time profiles of the mRNA fold in log2 scale. Solution to the differential equation was expressed as the following function of change in X with respect to time:

$$\Delta X(t) = (\frac{\beta}{\alpha} - X_0)(1 - e^{-\alpha t})$$

where X_0 is the mRNA level at t=0, the initial time of mRNA induction. Since the degradation rate was proportional to the mRNA concentration, we expected the curves to have a steady increase, followed by a gradual leveling off where the mRNA concentrations stay constant over time. Closer look at the differential equation showed

that at steady state (dX/dt = 0), the mRNA concentration is determined by the ratio of β to α:

$$X_{ss} = \frac{\beta}{\alpha}$$

whereas for the time it takes for the curve to transition into steady state, inversely proportional to the degradation constant, is given by:

$$T_{1/2} = \ln\left(\frac{2}{\alpha}\right)$$

Thus, we showed that for log2 plots, the expected shape of the curves can be altered by varying α and β. At constant α, increasing β would only shift the curve up, while at constant β, increasing α would cause the mRNA abundance to enter steady state more rapidly. Through the comparison between mathematical modeling and experimental data, we could infer the actual effects of Rvb1/Rvb2 binding to mRNA on the transcription and decay rates.

2.8.12 Ribosome profiling:

The ribosome profiling protocol was adpated from (Zid & O'Shea, 2014). Yeast was grown in SCD to an OD_{660} between 0.3 and 0.4. Then, cells were collected by filtration, resuspended in SC -G medium. After 15 minutes glucose was adding back. CHX was added to a final concentration of 0.1 mg/mL for 1 min, and cells were then harvested. Cells were pulverized in a PM 100 ball mill (Retsch), and extracts were digested with RNase I followed by the isolation of ribosome-protected fragments by purifying RNA from the monosome fraction of a sucrose gradient. Isolated 28-base sequences were polyadenylated, and reverse transcription was performed using OTi9pA. OTi9pA allowed

samples to be multiplexed at subsequent steps. RNA-seq was performed on RNA depleted of rRNA using a yeast Ribo-Zero kit (Epicentre). Samples were multiplexed and sequenced on a HiSeq analyzer (Illumina).

To analyze the ribosomal profiling and RNA-seq sequences, reads were trimmed of the 39 run of poly(A)s and then aligned against *S. cerevisiae* rRNA sequences using Bowtie sequence aligner (Langmead & Salzberg, 2012). Reads that did not align to rRNA sequences were aligned against the full *S. cerevisiae* genome. Reads that had an unambiguous alignment with less than 3 mismatches were used in the measurements of ribosome occupancy and mRNA levels. Since there were many reads mapping to the initiation region (216 bp to120 bp in relation to the AUG), the ribosome occupancy for each mRNA was calculated by taking the total number of ribosome reads (normalized to the total number of aligned reads in reads per million reads (RPM)) in the downstream region (120 bp from the AUG to the end of the ORF) and dividing this by the number of mRNA reads (RPM) in the same region. The ribosome occupancy along the mRNA was calculated by dividing the ribosome read counts at each base pair along the gene by the average number of mRNA reads per base pair for each gene.

2.9 Acknowledgements

We acknowledge support by the Zid lab startup funds from UCSD and MIRA grant from the National Institutes of Health R35GM128798 (to B.M.Z).

Chatper 2, in full, is prepared for publication: Chen, Yang S.; Tracy, Sharon; Harjono, Vince; Xu, Fan; Moresco, James J.; Yates III, John R.; Zid, Brian M. 2021. “Rvb1/Rvb2 proteins couple transcription and translation during glucose starvation”. The dissertation author was the first author of this paper.

2.10 References

Anders, S., 2010. Babraham Bioinformatics - FastQC A Quality Control tool for High Throughput Sequence Data [WWW Document]. Soil. URL https://www.bioinformatics.babraham.ac.uk/projects/fastqc/ (accessed 9.9.21).

Attwood, K.M., Robichaud, A., Westhaver, L.P., Castle, E.L., Brandman, D.M., Balgi, A.D., Roberge, M., Colp, P., Croul, S., Kim, I., McCormick, C., Corcoran, J.A., Weeks, A., 2020. Raloxifene prevents stress granule dissolution, impairs translational control and promotes cell death during hypoxia in glioblastoma cells. Cell Death Dis. 11, 1–18.

Bregman, A., Avraham-Kelbert, M., Barkai, O., Duek, L., Guterman, A., Choder, M., 2011. Promoter Elements Regulate Cytoplasmic mRNA Decay. Cell 147, 1473–1483.

Broad Institute, 2009. Picard Tools - By Broad Institute [WWW Document]. Github. URL https://broadinstitute.github.io/picard/ (accessed 9.9.21).

Chowdhary, S., Kainth, A.S., Gross, D.S., 2017. Heat Shock Protein Genes Undergo dynamic alteration in their Three-Dimensional Structure and Genome organization in response to thermal Stress. Mol. Cell. Biol. 37, 1–22.

De Nadal, E., Ammerer, G., Posas, F., 2011. Controlling gene expression in response to stress. Nat. Rev. Genet.

Eickhoff, P., Costa, A., 2017. Escorting Client Proteins to the Hsp90 Molecular Chaperone. Structure.

Elkon, R., Zlotorynski, E., Zeller, K.I., Agami, R., 2010. Major role for mRNA stability in shaping the kinetics of gene induction. BMC Genomics 11, 1–8.

Grably, M., Engelberg, D., 2010. A detailed protocol for chromatin immunoprecipitation in the yeast Saccharomyces cerevisiae. Methods Mol. Biol. 638, 211–224.

Guzikowski, A.R., Chen, Y.S., Zid, B.M., 2019. Stress-induced mRNP granules: Form and function of processing bodies and stress granules. Wiley Interdiscip. Rev. RNA 10, e1524.

Horvathova, I., Voigt, F., Kotrys, A. V., Zhan, Y., Artus-Revel, C.G., Eglinger, J., Stadler, M.B., Giorgetti, L., Chao, J.A., 2017. The Dynamics of mRNA Turnover Revealed by Single-Molecule Imaging in Single Cells. Mol. Cell 68, 615-625.e9.

Huen, J., Kakihara, Y., Ugwu, F., Cheung, K.L.Y., Ortega, J., Houry, W.A., 2010. Rvb1-Rvb2: Essential ATP-dependent helicases for critical complexes. In: Biochemistry and Cell Biology. pp. 29–40.

Ivanov, P., Kedersha, N., Anderson, P., 2019. Stress granules and processing bodies in translational control. Cold Spring Harb. Perspect. Biol. 11, a032813.

Izumi, N., Yamashita, A., Ohno, S., 2012. Integrated regulation of PIKK-mediated stress responses by AAA+ proteins RUVBL1 and RUVBL2. Nucleus.

Jain, S., Wheeler, J.R., Walters, R.W., Agrawal, A., Barsic, A., Parker, R., 2016. ATPase-Modulated Stress Granules Contain a Diverse Proteome and Substructure. Cell 164, 487–498.

Jha, S., Dutta, A., 2009. RVB1/RVB2: running rings around molecular biology. Mol Cell 34, 521–533.

Jiang, Y., AkhavanAghdam, Z., Li, Y., Zid, B.M., Hao, N., 2020. A protein kinase A–regulated network encodes short- And long-lived cellular memories. Sci. Signal. 13.

Kedersha, N., Anderson, P., 2002. Stress granules: sites of mRNA triage that regulate mRNA stability and translatability. Biochem. Soc. Trans.

Langmead, B., Salzberg, S.L., 2012. Fast gapped-read alignment with Bowtie 2. Nat. Methods 9, 357–359.

Lee, S., Lim, W.A., Thorn, K.S., 2013. Improved Blue, Green, and Red Fluorescent Protein Tagging Vectors for S. cerevisiae. PLoS One 8, e67902.

Li, H., Handsaker, B., Wysoker, A., Fennell, T., Ruan, J., Homer, N., Marth, G., Abecasis, G., Durbin, R., 2009. The Sequence Alignment/Map format and SAMtools. Bioinformatics 25, 2078–2079.

Li, X., 2011. Rabbit IgG Conjugation to Dynabeads. BIO-PROTOCOL 1.

Lim, F., Peabody, D.S., 2002. RNA recognition site of PP7 coat protein. Nucleic Acids Res.

Longtine, M.S., McKenzie III, A., Demarini, D.J., Shah, N.G., Wach, A., Brachat, A., Philippsen, P., Pringle, J.R., 1998. Additional modules for versatile and economical PCR-based gene deletion and modification in Saccharomyces cerevisiae. Yeast 14, 953–961.

Majmundar, A.J., Wong, W.J., Simon, M.C., 2010. Hypoxia-Inducible Factors and the Response to Hypoxic Stress. Mol. Cell.

Masser, A.E., Kandasamy, G., Kaimal, J.M., Andreasson, C., 2016. Luciferase NanoLuc as a reporter for gene expression and protein levels in Saccharomyces cerevisiae. Yeast 33, 191–200.

McDonald, W.H., Tabb, D.L., Sadygov, R.G., MacCoss, M.J., Venable, J., Graumann, J., Johnson, J.R., Cociorva, D., Yates, J.R., 2004. MS1, MS2, and SQT - Three unified,

compact, and easily parsed file formats for the storage of shotgun proteomic spectra and identifications. Rapid Commun. Mass Spectrom. 18, 2162–2168.

Mellacheruvu, D., Wright, Z., Couzens, A.L., Lambert, J.P., St-Denis, N.A., Li, T., Miteva, Y. V, Hauri, S., Sardiu, M.E., Low, T.Y., Halim, V.A., Bagshaw, R.D., Hubner, N.C., Al-Hakim, A., Bouchard, A., Faubert, D., Fermin, D., Dunham, W.H., Goudreault, M., Lin, Z.Y., Badillo, B.G., Pawson, T., Durocher, D., Coulombe, B., Aebersold, R., Superti-Furga, G., Colinge, J., Heck, A.J., Choi, H., Gstaiger, M., Mohammed, S., Cristea, I.M., Bennett, K.L., Washburn, M.P., Raught, B., Ewing, R.M., Gingras, A.C., Nesvizhskii, A.I., 2013. The CRAPome: a contaminant repository for affinity purification-mass spectrometry data. Nat Methods 10, 730–736.

Mu, X., Fu, Y., Zhu, Y., Wang, X., Xuan, Y., Shang, H., Goff, S.P., Gao, G., 2015. HIV-1 Exploits the Host Factor RuvB-like 2 to Balance Viral Protein Expression. Cell Host Microbe 18, 233–242.

Nano, N., Houry, W.A., 2013. Chaperone-like activity of the AAAþproteins RVb1 and RVb2 in the assembly of various complexes. Philos. Trans. R. Soc. B Biol. Sci.

Narayanan, A., Meriin, A., Andrews, J.O., Spille, J.-H., Sherman, M.Y., Cisse, I.I., 2019. A first order phase transition mechanism underlies protein aggregation in mammalian cells. Elife 8.

Paci, A., Liu, X.H., Huang, H., Lim, A., Houry, W.A., Zhao, R., 2012. The stability of the small nucleolar ribonucleoprotein (snoRNP) assembly protein Pih1 in Saccharomyces cerevisiae is modulated by its C terminus. J. Biol. Chem. 287, 43205–43214.

Peng, J., Schwartz, D., Elias, J.E., Thoreen, C.C., Cheng, D., Marsischky, G., Roelofs, J., Finley, D., Gygi, S.P., 2003. A proteomics approach to understanding protein ubiquitination. Nat. Biotechnol. 21, 921–926.

Phanstiel, D.H., Boyle, A.P., Araya, C.L., Snyder, M.P., 2014. Sushi.R: Flexible, quantitative and integrative genomic visualizations for publication-quality multi-panel figures. Bioinformatics 30, 2808–2810.

Pincus, D., Anandhakumar, J., Thiru, P., Guertin, M.J., Erkine, A.M., Gross, D.S., 2018. Genetic and epigenetic determinants establish a continuum of Hsf1 occupancy and activity across the yeast genome. Mol. Biol. Cell mbc.E18-06-0353.

Pitchiaya, S., Mourao, M.D.A., Jalihal, A.P., Xiao, L., Jiang, X., Chinnaiyan, A.M., Schnell, S., Walter, N.G., 2019. Dynamic Recruitment of Single RNAs to Processing Bodies Depends on RNA Functionality. Mol. Cell 74, 521-533.e6.

Protter, D.S.W., Parker, R., 2016. Principles and Properties of Stress Granules. Trends Cell Biol.

Quinlan, A.R., Hall, I.M., 2010. BEDTools: A flexible suite of utilities for comparing

genomic features. Bioinformatics 26, 841–842.

Ramírez, F., Ryan, D.P., Grüning, B., Bhardwaj, V., Kilpert, F., Richter, A.S., Heyne, S., Dündar, F., Manke, T., 2016. deepTools2: a next generation web server for deep-sequencing data analysis. Nucleic Acids Res. 44, W160–W165.

Richter, K., Haslbeck, M., Buchner, J., 2010. The Heat Shock Response: Life on the Verge of Death. Mol. Cell.

Robinson, J.T., Thorvaldsdóttir, H., Winckler, W., Guttman, M., Lander, E.S., Getz, G., Mesirov, J.P., 2011. Integrative genomics viewer. Nat. Biotechnol.

Sahoo, P.K., Lee, S.J., Jaiswal, P.B., Alber, S., Kar, A.N., Miller-Randolph, S., Taylor, E.E., Smith, T., Singh, B., Ho, T.S.Y., Urisman, A., Chand, S., Pena, E.A., Burlingame, A.L., Woolf, C.J., Fainzilber, M., English, A.W., Twiss, J.L., 2018. Axonal G3BP1 stress granule protein limits axonal mRNA translation and nerve regeneration. Nat. Commun. 9, 1–14.

Schutz, S., Noldeke, E.R., Sprangers, R., 2017. A synergistic network of interactions promotes the formation of in vitro processing bodies and protects mRNA against decapping. Nucleic Acids Res. 45, 6911–6922.

Seraphim, T. V., Nano, N., Cheung, Y.W.S., Aluksanasuwan, S., Colleti, C., Mao, Y.-Q., Bhandari, V., Young, G., Höll, L., Phanse, S., Gordiyenko, Y., Southworth, D.R., Robinson, C. V., Thongboonkerd, V., Gava, L.M., Borges, J.C., Babu, M., Barbosa, L.R.S., Ramos, C.H.I., Kukura, P., Houry, W.A., 2021. Assembly principles of the human R2TP chaperone complex reveal the presence of R2T and R2P complexes. Structure 0.

Thorvaldsdóttir, H., Robinson, J.T., Mesirov, J.P., 2013. Integrative Genomics Viewer (IGV): High-performance genomics data visualization and exploration. Brief. Bioinform. 14, 178–192.

Tian, S., Yu, G., He, H., Zhao, Y., Liu, P., Marshall, A.G., Demeler, B., Stagg, S.M., Li, H., 2017. Pih1p-Tah1p Puts a Lid on Hexameric AAA+ ATPases Rvb1/2p. Structure 25, 1519-1529.e4.

Trcek, T., Larson, D.R., Moldón, A., Query, C.C., Singer, R.H., 2011. Single-Molecule mRNA Decay Measurements Reveal Promoter- Regulated mRNA Stability in Yeast. Cell 147, 1484–1497.

Tsuboi, T., Viana, M.P., Xu, F., Yu, J., Chanchani, R., Arceo, X.G., Tutucci, E., Choi, J., Chen, Y.S., Singer, R.H., Rafelski, S.M., Zid, B.M., 2020. Mitochondrial volume fraction and translation duration impact mitochondrial mRNA localization and protein synthesis. Elife 9, 1–24.

Unnikrishnan, A., Akiyoshi, B., Biggins, S., Tsukiyama, T., 2012. An efficient purification system for native minichromosome from saccharomyces cerevisiae. Methods Mol.

Biol. 833, 115–123.

Unnikrishnan, A., Gafken, P.R., Tsukiyama, T., 2010. Dynamic changes in histone acetylation regulate origins of DNA replication. Nat. Struct. Mol. Biol. 17, 430–437.

Van Nostrand, E.L., Pratt, G.A., Shishkin, A.A., Gelboin-Burkhart, C., Fang, M.Y., Sundararaman, B., Blue, S.M., Nguyen, T.B., Surka, C., Elkins, K., Stanton, R., Rigo, F., Guttman, M., Yeo, G.W., 2016. Robust transcriptome-wide discovery of RNA-binding protein binding sites with enhanced CLIP (eCLIP). Nat Methods 13, 508–514.

Vera, M., Pani, B., Griffiths, L.A., Muchardt, C., Abbott, C.M., Singer, R.H., Nudler, E., 2014. The translation elongation factor eEF1A1 couples transcription to translation during heat shock response. Elife 3.

Xu, T., Park, S.K., Venable, J.D., Wohlschlegel, J.A., Diedrich, J.K., Cociorva, D., Lu, B., Liao, L., Hewel, J., Han, X., Wong, C.C.L., Fonslow, B., Delahunty, C., Gao, Y., Shah, H., Yates, J.R., 2015. ProLuCID: An improved SEQUEST-like algorithm with enhanced sensitivity and specificity. J. Proteomics 129, 16–24.

Youn, J.Y., Dyakov, B.J.A., Zhang, J., Knight, J.D.R., Vernon, R.M., Forman-Kay, J.D., Gingras, A.C., 2019. Properties of Stress Granule and P-Body Proteomes. Mol. Cell.

Zaarur, N., Xu, X., Lestienne, P., Meriin, A.B., McComb, M., Costello, C.E., Newnam, G.P., Ganti, R., Romanova, N. V, Shanmugasundaram, M., Silva, S.T., Bandeiras, T.M., Matias, P.M., Lobachev, K.S., Lednev, I.K., Chernoff, Y.O., Sherman, M.Y., 2015. RuvbL1 and RuvbL2 enhance aggresome formation and disaggregate amyloid fibrils. EMBO J. 34, 2363–2382.

Zander, G., Hackmann, A., Bender, L., Becker, D., Lingner, T., Salinas, G., Krebber, H., 2016. mRNA quality control is bypassed for immediate export of stress-responsive transcripts. Nature 540, 593–596.

Zhang, Y., Liu, T., Meyer, C.A., Eeckhoute, J., Johnson, D.S., Bernstein, B.E., Nussbaum, C., Myers, R.M., Brown, M., Li, W., Shirley, X.S., 2008. Model-based analysis of ChIP-Seq (MACS). Genome Biol. 9, 1–9.

Zhou, C.Y., Stoddard, C.I., Johnston, J.B., Trnka, M.J., Echeverria, I., Palovcak, E., Sali, A., Burlingame, A.L., Cheng, Y., Narlikar, G.J., 2017. Regulation of Rvb1/Rvb2 by a Domain within the INO80 Chromatin Remodeling Complex Implicates the Yeast Rvbs as Protein Assembly Chaperones. Cell Rep. 19, 2033–2044.

Zid, B.M., O'Shea, E.K., 2014. Promoter sequences direct cytoplasmic localization and translation of mRNAs during starvation in yeast. Nature 514, 117–121.

Chapter 3: Stress-induced mRNP granules: form and function of P-bodies and stress granules

3.1 Abstract

In response to stress, cells must quickly reprogram gene expression to adapt and survive. This is achieved in part by altering levels of mRNAs and their translation into proteins. Recently, the formation of two stress-induced messenger ribonucleoprotein (mRNP) assemblies named stress granules and processing bodies has been postulated to directly impact gene expression during stress. These assemblies sequester and concentrate specific proteins and RNAs away from the larger cytoplasm during stress, thereby providing a layer of posttranscriptional gene regulation with the potential to directly impact mRNA levels, protein translation, and cell survival. The function of these granules has generally been ascribed either by the protein components concentrated into them or, more broadly, by global changes that occur during stress. Recent proteome- and transcriptome-wide studies have provided a more complete view of stress-induced mRNP granule composition in varied cell types and stress conditions. However, direct measurements of the phenotypic and functional consequences of stress granule and processing body formation are lacking. This leaves our understanding of their roles during stress incomplete. Continued study into the function of these granules will be an important part in elucidating how cells respond to and survive stressful environmental changes.

3.2 Introduction

Cells are frequently exposed to fluctuating, potentially adverse environmental conditions. To survive adverse changes, they must rapidly alter gene expression in order to maintain internal homeostasis. The cellular reprogramming that occurs in response to a disruptive or inimical external fluctuation is broadly termed as stress response. Cellular stress response typically includes slowing or ceasing growth that is concomitant with repression of overall translation, although certain genes important for survival and repair are highly induced. Concurrently, while overall translation is repressed, many posttranscriptional regulatory proteins and mRNAs undergo a process called phase separation that results in the formation of concentrated, nonmembranous cytoplasmic structures generally described as granules or foci. During stress, this phase separation process might segregate proteins and mRNAs in a way that is functionally important for the cell and that promotes survival. Therefore, these structures are a subject of emergent interest. Although much progress has been made recently to identify the proteins and mRNAs that reside in these granules and the physical characteristics that underlie their formation, there is little known about the phenotypic or functional consequences of their formation during stress and therefore how significantly they contribute to stress response.

There are many different types of cellular granules involved in a wide variety of biological processes such as nucleoli, paraspeckles, PML bodies, and Cajal bodies in the nucleus as well as the stress-induced processing bodies (PBs) and stress granules (SGs) in the cytoplasm. Here, we highlight the cytoplasmic PBs and SGs, two well-studied messenger ribonucleoprotein (mRNP) granules that are present across eukaryotes

during a variety of stressful conditions such as exposure to heat shock, oxidative stress, UV irradiation, osmotic stress, and nutrient starvation. The formation of these mRNP granules, which occurs on the scale of minutes after exposure to stress stimuli, is mediated by a physical process called liquid–liquid phase separation (LLPS). There are common biophysical characteristics and some shared components between SGs and PBs as well as granule-specific features. It should be noted that, while the aptly named SGs are broadly induced during stress, PBs are a bit more organismal-specific. *Saccharomyces cerevisiae* induces visible PBs primarily during stress response while, in mammalian cells, small, microscopically visible PBs are constitutive but they become much larger and more abundant during stress. It should also be noted that the majority of research into these stress-induced granules is performed with yeast and mammalian cell culture systems. Ultimately, we posit SGs and PBs should be considered as distinct yet closely related mRNP granules; their properties and role in posttranscriptional gene expression during stress response is the focus of this review and we will address them individually, as SGs or PBs, and together more generally, as stress-induced mRNP granules, when appropriate.

Initial characterization of conditions that bring about stress-induced mRNP granules began in the late 1990s when researchers observed that impairment of translation initiation causes SG formation (Bashkirov, Scherthan, Solinger, Buer- stedde, & Heyer, 1997; Kedersha, Gupta, Li, Miller, & Anderson, 1999). A decrease in initiation is one hallmark of stress response; the canonical mechanism of eIF2α-phosphorylation can drive robust granule formation in some stress conditions (Kedersha et al., 1999). Importantly, however, the formation of SGs is not dependent on eIF2α-phosphorylation

as the addition of small molecules that block translation initiation through different mechanisms are sufficient to drive granule assembly (Dang et al., 2006; Mazroui et al., 2006; Mokas et al., 2009). Moreover, the genetic knockdown of specific translation initiation factor proteins (Mokas et al., 2009) or the overexpression of RNA-binding proteins (RBPs) that function to repress translation (De Leeuw et al., 2007; Gilks, 2004; Kedersha et al., 2005; Mazroui et al., 2006; Wilczynska, 2005) also lead to mRNP granule formation.

The observation that impaired translation drives SG and PB formation spurred further inquiry into their induction and the degree of interrelation between the two granules during stress response. Evidence emerged that SGs and PBs, each lacking membranes, are able to interact, potentially docking and swapping components (Buchan, Muhlrad, & Parker, 2008; Kedersha et al., 2005; Wilbertz et al., 2019). Nonetheless, it is known that these granules retain unique protein content and presumably RNA content, though the dynamics and degree of retention of RNAs with an individual granule is more poorly understood than it is for proteins. Interestingly, one study found SG assembly was dependent on and promoted by the presence of preexisting PBs in yeast cells, demonstrating the akin yet distinct nature of SGs and PBs (Buchan et al., 2008). On the other hand, a different study found that induction of PBs and SGs occurs via independent signaling pathways in yeast and reported no such dependency (Shah, Zhang, Ramachandran, & Herman, 2013). These results highlight the complexity that underlies stress-induced mRNP granule formation. Ultimately, it is not only a loss of translation initiation but also complex networks of signaling pathways, granule–granule interactions,

protein–RNA interactions, protein–protein interactions, and RNA–RNA interactions that shape and define both types of distinct but closely related stress-induced mRNP granules.

Understanding when SGs and PBs form is an important first step in recognizing what purpose they have in the broader changes elicited during stress. During the stress response a cell must confront a potential dearth of resources, including of resources necessary to synthesize new proteins, as it responds to the challenge of environmental stress. The direct connection between SG and PB induction coincident with the overall reduction of translation during stress suggests mRNP granule formation may directly control the rapidly changing proteome, yet the extent of this is not clear. The function and molecular relevance of SGs and PBs have been attributed largely based on the protein components concentrated within them. Specifically, the majority of mRNP granule proteins function in translation initiation, translational repression, or mRNA degradation. Consequently, it is generally thought that SGs and PBs function to segregate mRNAs from the larger cytoplasm to regulate their fate, either by storage, decay, or eventual reintroduction to the translating pool. In the section below, we discuss the protein and RNA content of SGs and PBs. We then switch to a discussion of what information is both known and lacking about their function during stress.

3.3 Stress-Induced mRNP Granules: Characteristics and Composition

The function of a stress-induced mRNP granule is presumably related to its molecular composition and so it is important to understand the identity of resident proteins and RNAs in both SGs and PBs. Insight into the ever-expanding catalog of SG and PB

residents, discussed below, has enabled informed speculation about granule function; however, it is important to note that simply knowing what is inside these structures has, thus far, been insufficient to clearly elucidate their roles during stress response.

3.3.1 Protein composition of stress-induced mRNP granules

Over the past decade, more and more protein factors residing in PBs and SGs were detected and characterized biochemically and genetically (Buchan & Parker, 2009; Parker & Sheth, 2007). For example, dozens of PB protein components were identified originally in yeast, including Lsm1-7, Xrn1, and Pop2 (Decker, Teixeira, & Parker, 2007). However, due to the challenge of capturing and isolating an intact, membraneless granule structure in the cytoplasm, a comprehensive profile of the hundreds of resident proteins in mRNP granules under various conditions remained experimentally challenging and therefore elusive. More recently, by taking advantage of mass spectrometry-based high-throughput proteomics and proximity labeling techniques, several studies profiled the larger proteome of PBs and SGs in yeast and different mammalian cell types under various stresses and, for mammalian PBs, native conditions. More than 100 protein factors were newly identified and extensive interactomes within mRNP granules were characterized (Alberti, 2018; Hubstenberger et al., 2017; S. Jain et al., 2016; Markmiller et al., 2018; Youn et al., 2018). Overall, mammalian mRNP granule proteomes are larger than yeast proteomes but they have substantial overlap with each other. Therefore, mammalian granules are more complex but stress-induced phase separation is an evolutionarily conserved event. In both mammals and yeast, PBs and SGs only share 10–25% of their protein components (5 are shared in yeast and 28 in mammalian cells),

leaving the majority of the proteome granule-specific (Figure 3.1A). Intriguingly, even though the majority of the proteome is granule-specific, several protein families and classifications are highly enriched in both types of mRNP granules across species. Most notably, there is very high enrichment in RBPs, with over 50% of proteins present in human SGs and yeast or human PBs having annotated RNA-binding functionality. There are also many proteins that contain of IDRs, which will be discussed in more detail later.

Amid a general ability to bind RNA, many other sub-categorizations of stress-induced mRNP granule proteins arise from a thorough analysis of their proteomes (Figure 3.1B). For example, in PBs, the majority of protein components are involved in RNA decay and translational repression in yeast and mammals. They include RNA decay factors (EIF4E-T, LSM14A [Scd6 in yeast], LSM14B, and IGF2BP2), decapping complex components (DCP1A/1B, DCP2, EDC4, DDX6 [Dhh1 in yeast], Edc3, and Pat1), factors in the microRNA (miRNA) pathway (Ge-1, GW182, AGO1/2/3, TRNC6A, and ZCCHC3), deadenylation complex components (CCR4-NOT, LSM1-7), ribonucleases (XRN1), nonsense-mediated decay (NMD) factors (UPF1, SMG5/7), and finally, translation repressors (EIF4E-T, CPEB1) (Andrei et al., 2005; Luo, Na, & Slavoff, 2018; Serman et al., 2007; Sheth & Parker, 2003). Like PBs, SGs harbor proteins that are related to RNA decay, such as ribonucleases (XRN1, G3BP, SND1) and components in the miRNA pathway (ZFP36, TNRC6B, AGO2), although mRNAs in SGs are not typically considered targets for decay (Lavut & Raveh, 2012). SGs also house translation repressors (CIRP, DDX3 [Ded1 in yeast], FXR1/2, Staufen1). Unlike PBs, SGs contain many components involved in translation including initiation factors (EIF2A/3/4A/4B/4G) and, notably, 40S ribosomal subunits. Transcripts stalled at the initiation step of translation are thought to

be enriched in SGs though, to our knowledge, this has not been directly validated. Furthermore, whether these translation factors are directly associated with mRNAs as complete pre-initiation complexes remains to be tested.

The classifications of proteins discussed above are notable in how broad they are. After all, factors involved in general cellular processes like decay and translation have to be able to recognize and regulate the diverse set of mRNAs that comprise a cell's transcriptome. This raises the question of how specificity arises in targeting the mRNAs that proteins interact with to cytoplasmic granules during stress. To find clues into potential mechanisms one can look to more specific functions in the categories of proteins that arise from classification of PB and SG proteomes. Interestingly, proteins that recognize both RNA secondary structures like G-quadruplexes (FXR1, FMR1) and the epitranscriptional RNA modification N6-methyladenosine (m6A) (YTHDF1/2/3) are enriched in SGs. Relatedly, YTHDF2, a m6A reader, is a recently identified PB component (Luo et al., 2018; X. Wang et al., 2013). Therefore, RNA structures and modifications recognized by these proteins may provide means to determine specificity in targeting certain mRNAs to mRNP granules, though experimental validation of this potential mechanism is not yet realized.

In addition to enabling classification of the functions of proteins found in SGs and PBs, approaches that combine proximity labeling with mass spectrometry have provided insight into the degree of heterogeneity in the proteomes of stress-induced mRNP granules formed in different cell types and in response to different stresses. Certain proteins are thought to be present in all SGs, particularly those that have been shown to nucleate SG formation, but the protein composition of SGs does vary across different

conditions. For example, comparison of SGs formed during arsenite stress with those formed during heat shock showed that 23% of protein components are stress-type-specific (S. Jain et al., 2016; Markmiller et al., 2018). Markmiller et al. also reported differences in SG composition in different cell types as well as different stress and disease conditions; SGs in amyotrophic lateral sclerosis (ALS) motor neurons contained particularly distinct proteins. They estimated that up to 20% of the SG proteome is stress and cell-type-specific. This context-dependence and diversity of SG composition suggests SGs arise and potentially function according to the specific cellular needs and demands brought about by a given stress condition. Similarly, studies of PB composition showed that PB protein content changes during stress compared to native conditions in mammalian systems (Ohn, Kedersha, Hickman, Tisdale, & Anderson, 2008). PBs were found uniquely enriched with ubiquitination-related proteins under arsenite stress (Youn et al., 2018). Understanding how the protein composition of mRNP granules changes in specific conditions may reveal mechanisms of how these granules are fine-tuned to allow the cell to best survive specific stressors and regulate gene expression to meet stress-dependent challenges. This may ultimately help ascertain the function of stress-induced mRNP granules.

3.3.2 Protein-dependent dynamics, assembly, and interactions in stress-induced mRNP granules

3.3.2.1 Dynamics: liquid and solid states of stress-induced granules

One of the initial observations made about stress-induced mRNP granules was their dynamic nature, reflected in both their rapid formation during stress and dissolution upon recovery. Recently, the biophysical basis of this has been ascribed to LLPS. The biophysical properties inherent to LLPS also lead to dynamic granule states during the duration of stress response as both proteins and mRNAs can rapidly exchange with the non-phase separated cytoplasm while stress-induced granules are present. Much of the insight into stress-induced granule dynamics has come from fluorescence recovery after photobleaching (FRAP) studies. FRAP of mRNP granule proteins showed that these granules can hold liquid-like and therefore dynamic structures, with components moving in and out after photobleaching (Brangwynne et al., 2009; Kroschwald et al., 2015). However, it is important to note that not all stress-induced mRNP granules have been found to be liquid-like.

The type and duration of stress stimuli seems to influence the material state of the granules it induces and can shift them to a more solid-like state in certain contexts. For instance, yeast SGs induced by heat shock were found to be less dynamic and more solid-like generally (Kroschwald et al., 2015). This contrasts with mammalian SGs induced by sodium arsenite, which were very dynamic and liquid-like (Kroschwald et al., 2015). The extent of species-specific or stress-specific influences in determining the material state of SGs is indeed a complicated matter. One cannot simply assume that, in general, yeast SGs are more solid-like and mammalian SGs are more liquid-like. More recently, the same research group has shown that yeast SGs induced by lowered pH are dynamic and behave in a more liquid-like manner akin to mammalian arsenite-induced

SGs (Kroschwald et al., 2018). At the same time, ALS-linked mutations that increase protein misfolding drove the material state of heat shock-induced mammalian SGs from fluid to more solid-like state (Mateju et al., 2017). This indicates that differences in material state are more strongly influenced by the specific stress stimuli used to induce them rather than species-specific differences (Kroschwald et al., 2018). Moreover, other studies have found that SGs can have differing material states within an individual granule. Specifically, mammalian SGs in lysate were found to be smaller than those in cells, suggesting that individual granules have a distinct, less liquid-like core inside a more soluble, outer shell structure (S. Jain et al., 2016). Protein components in the shell are more dynamic and fast moving, while components in the core dwell within the structure longer. Taken together, these results indicate that the material states of stress-induced mRNP granules cannot be assumed without direct study and that continued, careful parsing of their dynamics in different contexts will be important to fully understand the nuances of phase separation in biological systems.

3.3.2.2 Assembly: the necessity of certain proteins in stress-induced mRNP granule formation

As previously discussed, proteomic studies revealed hundreds of proteins that reside in PBs and SGs. Though hundreds of proteins reside in these granules, only a fraction of them are considered important for granule assembly or maintenance during stress. Some proteins have been reported to be critical for granule assembly and maintenance as their disruption abolished or decreased the size and number of granules while overexpression had the opposite effect. For instance, in PBs, some translation

repressors (CPEB, EIF4E-T), RBPs related to RNA decay and stabilization (LSM14A [Scd6 in yeast], DDX6 [Dhh1 in yeast]), and components in decapping and deadenylation complexes (DCP1/2, EDC3/4, PATL1, LSM1-7, CCR-NOT) were shown to be essential (Ayache et al., 2015; Eulalio et al., 2007; Franks & Lykke-Andersen, 2008; Luo et al., 2018; Sheth & Parker, 2003). In SGs, translation repressors (Caprin-1, TIA-1/TIAR [Pub1/Ngr1 in yeast]), RBPs related to RNA decay and stabilization (G3BP, DDX6 [Ded1 in yeast], TDP-43, PAB1), and enzymes with ATPase activity (RUVBL1/2 [Rvb1/2], MCM, CCT) were all shown to be essential (Buchan & Parker, 2009; Gilks, 2004; S. Jain et al., 2016; Kedersha et al., 2016; Tourriere et al., 2003). The latter class stands out in particular as it indicates that granule assembly likely depends on ATP. In fact, the ATPase complexes CCT, RVB, and MCM were shown to regulate distinct steps of SG assembly and disassembly, indicating that the properties and functions of SGs are modulated and maintained by active ATPases in an energy-consuming manner (S. Jain et al., 2016). Similarly, DEAD-box proteins with ATPase activity were also found to be important for main- taining and regulating PB dynamics and turn-over of mRNAs and protein components (Kim & Myong, 2016; Mugler et al., 2016).

Laboratory techniques like genetic screens and knockdown approaches are particularly useful for identifying which proteins mediate granule assembly but are not without caveats. For instance, a screen of yeast SG-defective mutants identified many factors related to translation such as eIF4G2 (Tif4632) and Arc1 (Yang et al., 2014). However, the results of this screen are complicated because the necessity of a given factor for SG nucleation can change in different stress conditions and cell types. For example, G3BP is not required for SG assembly in some osmotic or heat shock stresses

but is thought essential for assembly under arsenite-induced oxidative stress (Kedersha et al., 2016). To further add to this complexity, the necessity of these components can be redundant. For example, double-deletion of Edc3 and Lsm4 abolished PB formation in yeast but this was rescued by overexpressing Dhh1 (Rao & Parker, 2017). This complexity calls to mind the complexity that underlies stress-dependent differences in mRNP material state discussed above. Understanding what proteins are necessary for stress-induced mRNP granule formation must be done with proper care; consideration of cell-type and stressor used must be accounted for when one determines what proteins are essential for both SG and PB assembly. Tracking differences in the necessity and redundancy of proteins that mediate stress-induced mRNP granule assembly across stress conditions will likely offer clues into the different functions that these granules have in responding to distinct environmental cues.

3.3.2.3 Interaction networks between proteins influence stress-induced mRNP granules

Complex networks of interactions mediate mRNP granule assembly, maintenance, and disassembly. Understanding the interactions between macromolecular components may give insight into why some proteins are more important than others in granule assembly and maintenance. Resident protein components can be classified as scaffolds or clients (Ditlev, Case, & Rosen, 2018). Scaffolds are proteins required for mRNP granule assembly as described above, while clients are concentrated in the granule via interactions with scaffold components. The distinction between scaffolds and clients can be blurred and condition-dependent in varied biological contexts. Scaffolds are

considered to be more concentrated than clients in the granule and are supposed to have higher degrees of interactions. We analyzed the interactions of SG and PB protein components (Figure 3.2); the hubs in these interaction networks have higher likelihoods to function as scaffolds that are essential for granule assembly (Hubstenberger et al., 2017; S. Jain et al., 2016; Youn et al., 2018). It is important to note that many interactions identified during stress were preexistent in nonstressed conditions, although no SGs and only small numbers of PBs were formed. One possible explanation for this observation is that interactions during normal growth states are sub-stoichiometric, while interactors become more concentrated in granules during stress. Additionally, these preexisting interactions may drive the preassembly of sub-microscopic granules in normal conditions that simply cannot be observed with conventional microscopy techniques. These possibilities remain to be tested (Youn et al., 2018). Regardless, there is little doubt that understanding protein–protein interaction networks will shed light on the formation of stress-induced mRNP granules and offer potential insight into their function during stress.

The interactions in mRNP granules can be classified as specific interactions when proteins or mRNAs have limited binding partners or as promiscuous, nonspecific interactions when they do not. Specific interactions in granules are usually mediated by well-folded domains or short linear motifs of IDRs that specifically interact with well-folded domains of other RBPs (Fromm et al., 2014). For example, Edc3 dimerization via a YjeF-N domain is important for PB formation in yeast (Decker et al., 2007). G3BP dimerization and interactions with Caprin-1 are important for mammalian SG formation (Kedersha et al., 2016). Also, posttranslational modifications (PTMs) can regulate granule formation by altering specific interactions. For example, methylation of the RGG domains of FUS or

EWS recruits Tudor domain-containing proteins (Goulet, Boisvenue, Mokas, Mazroui, & Cote, 2008). NEDDylation of SRSF3 in SGs is required for interaction with TIA-1 (Jayabalan et al., 2016). Banani et al. showed one possibility of how specific interactions drive scaffolds to recruit specific clients and promote LLPS through the use of a SUMO/SIM system. Despite these specific interactions, formation of complex, in vivo granules also requires promiscuous interactions mediated by longer IDRs (Figure 3.3). Since IDRs do not hold well-folded structure they can interact with other proteins nonspecifically. It has been shown that in vitro LLPS driven by specific protein–RNA interactions is enhanced by addition of promiscuously interacting IDRs. In yeast, PB formation is promoted by IDRs in cooperation with specific interactions (Protter et al., 2018). It is generally thought that neither specific nor nonspecific interactions are individually sufficient to drive stress-induced granule formation, as promiscuous IDRs are not sufficient to form granules in vivo if specific interactions are not also present in certain contexts. For example, high expression levels of fusion proteins hnRNPA1-Cry2 or DDX4-Cry2 cannot phase separate in cells, unless the Cry2 protein is triggered to assemble via light-activated, specific interactions (Shin et al., 2017). Notably, as previously described, RBPs are vastly enriched in both SGs and PBs, suggesting that interactions between RBPs and mRNA transcripts might also play an important role granule assembly that goes beyond protein–protein interactions (S. Jain et al., 2016). In fact, in addition to multivalent proteins, some longer RNAs can actually serve as scaffolds and thus promote LLPS (Schütz, Nöldeke, & Sprangers, 2017). Overall, synergistic and tuned networks of interactions mediate the formation and maintenance of stress-induced mRNP granules. The identity of these protein components and their interactions potentially drive the

specificity of what mRNA transcripts are enriched and excluded from these granules and parsing them might further inform our understanding of how SGs and PBs influence gene expression during cellular stress response.

3.3.3 RNA properties and composition in stress-induced mRNP granules

Although a thorough and accurate understanding of the proteins found in SGs and PBs across organisms, cell types, and stressors is necessary to gain deep insight into granule function, one must take an equally deep look at RNA content, particularly at mRNA, to fully realize granule influence on gene expression during stress. The identity and fate of mRNAs in SGs and PBs have remained more elusive than those of proteins for many reasons. First, RNA is more transient and unstable in the cell relative to protein. This makes isolation and subsequent characterization of RNA from a liquid-like, membraneless granule contained within the larger cytoplasm a challenge. There are also larger varieties of RNAs relative to proteins in SGs and PBs; recent studies identify hundreds of proteins but thousands of RNA species, indicating the necessity of genome-wide approaches for systematic identification (Hubstenberger et al., 2017; Khong et al., 2017). Furthermore, initial studies that provided insight into granule formation and utility during stress paid limited attention to the contribution of individual RNA components in stress-induced granules relative to protein components. Researchers proposed roles based on the functions and identities of proteins, rather than RNAs, identified within them and it was not until recently that studies began to provide genome-wide analyses of enriched RNAs. The protein components of granules enable one to make informed speculations about how these structures influence the fate of mRNAs. However, it is

important to directly study the fate of mRNAs that are recruited to RNP granules in order to fully appreciate their function. Fortunately, advances in mRNP granule purification, RNA sequencing, and single-molecule resolution mRNA imaging have provided valuable insight into the RNAs of SGs and PBs and have advanced and refined our understanding of their regulation. We discuss below a current view of RNA properties relevant to phase separation, RNA components in both SGs and PBs, and how this understanding further informs our perception of the role that RNP granules might have in gene expression during stress.

3.3.3.1 General, biophysical properties of RNAs can influence mRNP granule dynamics

When considering mRNP granule-mediated translation regulation from an RNA-centric perspective, it is prudent to consider how general biophysical properties of RNAs influence phase separation. Unsurprisingly, mRNP granule stability is dependent on RNA concentration and identity, in addition to the presence of previously discussed mRNP-nucleating proteins. For instance, PBs can be dissolved by RNase treatment (Teixeira, Sheth, Valencia-Sanchez, Brengues, & Parker, 2005). Positively charged IDRs on proteins interact with negatively charged mRNAs via electrostatic interactions that influence LLPS propensity (Aumiller & Keating, 2015; Schütz et al., 2017). In addition to charge, RNA secondary structure can influence the properties of phase-separated granules and in fact can control whether LLPS occurs at all. For example, an in vitro reconstitution system shows that recruitment of CLC3 RNA as well as other RNAs into droplets of Whi3, a disordered RBP found in PBs and SGs, is dependent upon CLC3 RNA

secondary structure (Langdon et al., 2018). A similar system demonstrated that some RNAs prevent Whi3 droplets from aggregating and help to maintain their liquid-like state (Zhang et al., 2015). Conversely, disease-associated RNAs with repeat expansions can serve as templates for multivalent base pairing that drives granule self-assembly and shifts the equilibrium towards phase separation in vitro and in human cells (A. Jain & Vale, 2017). Ultimately, an appreciation of how RNA's physical properties affect its capacity to act as a protein scaffold and influence granule formation will be important considerations during analysis of sequence and structural elements both shared and lacking in the mRNAs present in SGs and PBs. One must understand and appreciate both RNA–RNA and RNA–protein interactions to determine to what extent a given RNA species may be found in a granule.

3.3.3.2 RNA-polysome interactions influence mRNP dynamics

The degree of interaction between ribosomes and mRNAs is of particular importance when considering the relationship between stress-induced mRNP granule formation, protein translation, and changing gene expression during stress. The repression of translation during stress response yields an abundance of nontranslating mRNAs disengaged from polysomes in the cytoplasm within minutes (Kershaw & Ashe, 2017). As previously stated, stress also induces SG and PB formation on the same time scale. Both types of stress-induced mRNP granules accumulate nontranslating mRNAs (Buchan et al., 2008). These observations suggest that there is a direct balance or stoichiometry between levels of polysome engagement, free mRNAs, and stress-induced mRNP granule abundance (Figure 3.4). This balance, in turn, might help to control or limit

protein production during a period when overall translation is greatly reduced. Levels of polysome engagement and RNA abundance have been shown to directly influence granule assembly in an RNA-dependent manner. For example, cycloheximide, an inhibitor of ribosomal translocation that traps mRNAs in polysomes, can repress formation of both PBs and SGs and even dissolve preformed granules (Teixeira et al., 2005). Conversely, addition of puromycin, a drug that dissociates ribosomes from mRNAs actually triggers SG formation (Buchan et al., 2008; Kedersha et al., 2000). This implies that one must consider the translational status of mRNAs as well as the more general biophysical properties of RNAs discussed above to understand RNA's roles in granule assembly, maintenance, and disassembly as well as broader mRNP function during stress.

Finally, to fully parse the biological function of SGs and PBs in the context of stress response, one needs to understand not only general changes in polysome engagement but also what transcripts are localized where in the cytoplasm, how transient this localization is, and what distinguishes mRNAs selected for translation into protein during and after stress. It has been suggested that mRNAs can move in and out of mRNP granules due to their liquid-like state. In fact, some mRNAs have been proposed not only to move in and out of a PB or SG but to actually shuttle between granules and polysomes on the timescale of minutes, linking mRNPs to highly controlled regulation of translation during stress even more directly (Brengues, Teixeira, & Parker, 2005; Mollet et al., 2008). These observations, in turn, lead to many questions: what are the proportions and identities of cytoplasmic mRNAs and their bound proteins recruited into granules when translation is downregulated, how dynamically does the mRNA pool actually move into

and out of these granules during and after stress in living cells, what proteins accompany such movements, how specific or promiscuous is mRNA recruitment to granules, and how are stressinduced, pro-survival genes excluded from these granules during times of stress to ensure their robust translation? It was not until very recently that we had a genome-wide snapshot of the mRNAs included and excluded from SGs and PBs (Hubstenberger et al., 2017; Namkoong, Ho, Woo, Kwak, & Lee, 2018; C. Wang et al., 2018). The datasets generated by these studies, discussed in more detail below, provide a newfound opportunity to begin to answer to some of the questions outlined above and provide clues or directions for research that can begin to address the others.

3.3.3.3 Characteristics of mRNAs Targeted to mRNPs During Stress

A surge of recent studies has provided the broadest look into the RNP granule transcriptome to date for both yeast and mammalian models (Hubstenberger et al., 2017; Namkoong et al., 2018; C. Wang et al., 2018). These studies used varied methods to purify intact RNP granules and report that approximately 10–20% of bulk RNAs in the cytoplasm localize to them; the vast majority (~80%) are mRNAs though non-coding RNAs are also recruited. A portion of these studies discovered a relationship between certain 3’ untranslated region (UTR) features and favorable granule recruitment. For instance, swapping the endogenous 3’ UTRs of specific PB-localized transcripts with noneukaryotic 3’ UTRs was sufficient to halt PB localization of those mRNAs in stressed yeast (C. Wang et al., 2018). Additionally, a motif search revealed 3’ AU-rich elements (AREs) are most strongly correlated with SG-targeting of mRNAs upon analysis of motifs in the SG-enriched transcriptome isolated during mammalian endoplasmic reticulum

stress (Namkoong et al., 2018). This suggests the possibility that interactions between certain 3' UTRs and ARE-binding, SG-localized proteins such as TIAR and TIA-1 might contribute to directing and sequestering mRNAs to mRNP granules. More generally, it is likely that 3' UTR sequences and other untranslated features influence localization of some mRNAs into SGs and PBs.

Although the presence of ARE motifs and the 3' UTR dependence of some granule-localized RNAs is intriguing, it is not sufficient to explain the complex regulatory interactions that target the huge range of mRNAs that localize to granules during stress. Nonetheless, deeper dives into other motifs or sequence features common to stress-induced mRNP granule-localized RNAs have provided very limited insight into what other characteristics intrinsic to mRNAs might drive them to PBs and SGs. Systematic analysis of binding motifs is complicated by the huge variety of RBPs found in these granules, which in turn, have an even larger range of client mRNAs. Furthermore, not all RBPs that localize to PBs or SGs have strong binding motifs. In fact, for many prominent mRNP granule-localized RBPs researchers have failed to identify consensus binding motifs (Ishigaki et al., 2012; Mitchell, Jain, She, & Parker, 2013; Rogelj et al., 2012). For instance, for the P-body proteins Pat1, Dhh1, and Lsm1, cross-linking immunoprecipitation-Seq data failed to identify any strong consensus sequence (Mitchell et al., 2013). More generally, the degree of promiscuity and randomness versus tightly regulated specificity of mRNA recruitment into mRNP granules during stress remains unclear. Therefore, there might not be all that many RNA sequence features that cause recruitment to SGs and PBs through recognition by specific RBPs. It is possible that the concentrated environment of a phase-separated granule promotes more nonspecific protein–RNA

interactions and so identifying consensus sequences in RNA targets will continue to be elusive. Furthermore, it has been shown that RNA–RNA interactions also contribute to granule formation (Van Treeck & Parker, 2018). Therefore, taken together, not only do some specific RNA–protein interactions contribute to the identity and proportion of mRNAs that are recruited into a PB or SG during a specific stress, but so do RNA–RNA and nonspecific RNA–protein interactions. Importantly, the relative extent of each contribution is an open question.

Although the search for sequence commonalities has returned limited results, there is another characteristic of mRNAs more strongly correlated with SG and PB enrichment: length. Khong et al. performed RNA sequencing of purified SG cores from U2OS cells and found that SG-enriched mRNAs are, on average, thousands of base pairs longer than those depleted from SGs. Similarly, bulk purification of all cytoplasmic mRNP granules (PBs and SGs) from stressed NIH3T3 cells revealed that granule-enriched mRNAs are thousands of base pairs longer than mRNAs not targeted to granules (Namkoong et al., 2018). If the length of a transcript is indeed the most correlative indicator of RNP granule localization during stress this also sheds relatively little light on how sequences within mRNAs target them to granules, thus leaving the specificity in targeting an open question. It might even indicate that longer mRNAs are recruited into SGs and PBs more often simply because a longer mRNA necessarily has a longer primary sequence and this provides more chances for potential nonspecific, promiscuous interactions with RBPs or other RNAs.

The lion's share of analysis on transcriptome-wide sequencing data from stress-induced mRNP-isolated RNAs has focused on parsing characteristics and identities of

genes that reside within SGs and PBs. However, to fully understand how stress impacts translation, one must consider the other side of the data: what mRNAs are not found in SGs and PBs and what mechanisms prevent certain RNAs from recruitment into them? It is known that some transcripts such as those encoding certain heat-shock proteins (HSPs) remain diffusely localized and well-translated in the cytoplasm during stress. These are predominantly stress associated mRNAs such as HSP30, HSP26, HSP12, HSP70, and HSP90 (Kedersha & Anderson, 2002; Lavut & Raveh, 2012; Stöhr et al., 2006; Zid & O'Shea, 2014). Our previous data implied that during glucose starvation in yeast, it is not the mRNA sequence that determines exclusion of HSP mRNAs from mRNP granules. Instead, information in the promoter sequence drives cytoplasmic mRNA localization (Zid & O'Shea, 2014). The details of mechanisms that enable this exclusion remain elusive and could likely be informed by a thorough parsing of the SG- and PB-excluded transcriptome. In general, we expect that researchers will need to think outside the box and look beyond primary sequences of mRNAs that are recruited to SGs and PBs to solve the puzzle of what directs their recruitment to mRNP granules during stress. Fortunately, some preliminary clues to this puzzle might have already been discovered. For example, it is known that ribosomal proteins, which interact with mRNAs during nonstress conditions, are depleted from PBs while protein-coding mRNAs are enriched. At the same time, noncoding RNAs are depleted from PBs (Hubstenberger et al., 2017). This hints that previous translation and engagement with ribosomes might be factors that drive mRNA localization to PBs through an unknown mechanism. When it comes to SGs, very recent work has highlighted how the compaction status of a transcript influences its propensity for recruitment. Two separate groups used single-molecule fluorescence in

situ hybridization (FISH) to observe the distance between the 5' and 3' ends of mRNAs; both found that compaction increased for mRNAs recruited into granules, indicating that the spatial organization of a transcript influences its localization (Adivarahan et al., 2018; Khong & Parker, 2018). Lastly, a correlation exists between a transcript's mRNP enrichment and its translational efficiency (TE), as determined by ribosome profiling. Ribosome profiling is an RNA sequencing-based technique that provides a nucleotide-resolution "snapshot" of translation by generating a library of RNA fragments engaged with ribosomes. Traditionally, the occupancy of ribosomes across a gene is quantified and compared to whole transcriptome measurements to generate a measurement of TE (Ingolia et al., 2009). It was found that TE measurements are lower for mRNAs enriched in SGs and PBs relative to depleted mRNAs (Hubstenberger et al., 2017; Khong et al., 2017). This information begets speculation that characteristics that determine the translatability of an mRNA might impact its propensity for ribosome engagement and mRNP localization in an interrelated way, hinting that well-translated mRNAs have characteristics that confer granule exclusion. What exactly these characteristics are remains to be seen.

3.4 Stress-Induced mRNP Granules: Function

The stress-inducible formation of SGs and PBs is conserved from yeast to mammals in response to a broad array of stresses. It has also been found that mutants that cannot appropriately form these mRNP granules are more sensitive to stress (Eisinger- Mathason et al., 2008; Kwon, Zhang, & Matthias, 2007; Lavut & Raveh, 2012;

Riback et al., 2017; Yang et al., 2014). These data imply that mRNP granules play an important role during stress, yet identifying the actual molecular function of the membraneless compartments in the cell has proven challenging. One reason for this is that stress in itself has such dramatic effects on gene expression. It can be hard to decouple the formation of mRNP granules from the broad changes induced by stress. While stress-induced mRNP granules were originally posited to have functions related to the function of the proteins concentrated within them, it is unclear if the physical properties of the cytoplasm that govern protein–RNA interactions under normal growth conditions can be directly compared to those inside phase separated mRNP granules (Helder, Blythe, Bond, & Mackay, 2016). Therefore, many established hypotheses on mRNP granule function are currently being reassessed through in vitro models of phase separation that can be tested outside of the context of stress response as well as through modern technological advances that allow higher resolution in imaging and sequencing. Below we discuss current attitudes about SG and PB function, unresolved questions related to their functions, and potential experimental approaches that might help to elucidate them.

3.4.1 Stress Granule Function:

As described above, many translation initiation components and translational repressors are concentrated in SGs. While certain mRNAs are enriched in SGs, the impact this sequestration has on gene expression is unclear. Only ~10–20% of bulk mRNA species reside in SGs yet there is a global shutdown of translation during stress. Some speculate that SGs assist with this aspect of stress response but it is unclear how

SGs can act as broad and global translational repressors during stress if up to ~80–90% of mRNAs remain excluded and distributed through the cytoplasm. Secondly, inhibiting visible SG formation was shown to have no effect on global translation during stress (Buchan et al., 2008; Kedersha et al., 2016) or on mRNA half-life (Bley et al., 2015; Buchan et al., 2008). While some specific mRNAs have been found to be altered translationally when specific SG proteins are mutated and SG formation is perturbed (Damgaard & Lykke-Andersen, 2011; Gilks, 2004; Mazroui, Marco, Kaufman, & Gallouzi, 2007; Moeller, Cao, Li, & Dewhirst, 2004; Tsai, Ho, & Wei, 2008), it is unclear whether these effects are mediated by aberrant SG localization itself or if they simply reflect changes made by the absence of the wild-type protein.

An alternative function for SGs may be in helping cells recover upon cessation of the stress response. As much of the translation initiation machinery is present in SGs, it may be that mRNAs enriched in SGs are translationally repressed during stress but some portion of this population is translationally primed for protein synthesis upon stress relief. The knowledge of which mRNAs are enriched in SGs combined with the advent of ribosome profiling provides opportunity for an exciting direction: measurement of the effects that SG dissolution has on mRNA-specific ribosome loading as well as comparison of the timing of ribosome loading onto SG-enriched versus SG-depleted mRNAs after stress ends. Such an experiment would provide insight into the possibility that SGs form to enable rapid engagement of translation machinery with sequestered mRNAs and provide insight into the purpose of SG formation more generally. A very exciting application of this approach would be to isolate SGs and perform profiling specifically on the 40S subunit, as described in Archer, Shirokikh, Beilharz, and Preiss (2016). The

abundance and identities of transcripts found by this approach would shed light on the presumed but unverified notion that SGs house mRNAs that are engaged with pre-initiation complexes and are primed for reintroduction into the translating pool upon cessation of stress and resumption of growth.

3.4.2 P-Body Function:

PBs were historically proposed to be sites of mRNA degradation due to the abundance of decapping factors and exonucleases found within them. Furthermore, yeast strains that had mutations in mRNA degradation machinery showed a large increase in the number and size of visible PBs (Sheth & Parker, 2003). Finally, an unstable mRNA that had a polyG sequence inserted to block the exonuclease Xrn1 from fully degrading it accumulated in PBs (Sheth & Parker, 2003). From these results it was concluded that PBs are likely concentrated hubs of mRNA degradation. While these results did point to mRNA decay intermediates, which presumably have very low translatability, accumulating in PBs they did not show whether the actual processing of these mRNAs was taking place inside or outside of the membraneless compartments. A number of papers have presented contradictory evidence to the notion that PBs serve as hubs of decay and the field is now considering the possibility of a more storage-based role for PBs during stress, leaving active mRNA decay as a process that takes place in the larger cytoplasm. Researchers have found that visible PB formation is not directly necessary for RNA decay; these granules can be disrupted without inhibiting global RNA decay pathways (Ayache et al., 2015; Eulalio et al., 2007). There has also been a lack of degradation intermediates present in recently sequenced, PB-enriched mRNAs

(Hubstenberger et al., 2017). This same study reports that depletion of the PB protein DDX6 causes PB dissolution but does not increase levels of PB-enriched mRNAs. Further studies have used fluorescent microscopy to follow the decay of single mRNAs that are labeled at their 5' and 3' ends with different fluorescently tagged coat proteins. Over time there was no accumulation of degradation products in PBs (Horvathova et al., 2017). It was also found that there is a general decline in mRNA degradation during stress that is independent of where the reporter mRNA was localized, either in PBs or outside of PBs. This general stabilization of mRNAs during stress has also been previously seen in both yeast and mammalian cells (Gowrishankar et al., 2006; Hilgers, Teixeira, & Parker, 2006). Further microscopy-based studies found that inhibition of reporter mRNA degradation continues for about 2 hr after stress removal and that the kinetics of degradation appear to be independent of whether an mRNA was localized to a PB or not (Wilbertz et al., 2019). Finally, using purified decapping proteins along with accessory proteins and RNA, studies were able to drive in vitro LLPS, potentially reconstituting PBs (Schütz et al., 2017). It was found that RNA contained within these in vitro reconstituted PBs was protected from endonucleolytic cleavage and that enzymatic activity of the decapping enzyme was greatly decreased (Schütz et al., 2017). Combined, this evidence strongly points towards a storage role for PBs that house a subset of translationally repressed mRNAs during stress and, more generally, demonstrates that caution should be applied when speculating about the function of stress-induced granules.

3.4.3 mRNP Granules: Alternative Functions

While much of the research on mRNP granules has rightly focused on the function of the proteins and mRNAs within the granules, an alternative possibility is that the phase separation of translation initiation factors and mRNA degradation machinery into SGs and PBs, respectively, is to reduce the working concentration of these proteins in the aqueous regions of the larger cytoplasm. This possibility would help to remedy the contradiction that, though only a small portion of mRNAs in the cell are present in SGs or PBs, the majority of mRNAs present during early stages of stress are from nonstress-induced mRNAs. We have observed that after 15 min of glucose starvation in yeast, about 90% of the mRNAs present within the cell are from nonstress-induced mRNAs (B.M. Zid, unpublished data). One factor that must be taken into account when considering this alternative possibility is the intracellular volume that SGs and PBs occupy. Generally, mRNP granules constitute only a minor portion of cellular volume, approximately 1% or less. And while proteins are very highly concentrated within granules (e.g., in mammalian SGs, G3BP1 protein is 13-fold more concentrated in the SG shell than the cytoplasm and about 30-fold more concentrated in the core than it is in the shell; S. Jain et al., 2016), it is unclear if this would cause significant enough depletion from the cytoplasm to have a functional impact. Very recently, quantitative measurements have been performed on yeast PB proteins to compare their concentration inside and outside of PBs (Xing et al., 2018). For Dcp2 protein, the catalytic subunit of the decapping enzyme complex, more than 30% becomes sequestered in PBs. Other accessory decapping proteins such as Edc3 and Pat1 have greater than 20% of their protein content sequestered into P-bodies. The supports the notion that the function of PBs would be to reduce mRNA decapping

activity in the bulk cytoplasm, rather than to concentrate it in a granule. This is consistent with the previously mentioned observation that there is a general decline in mRNA degradation during stress regardless of whether a transcript is sequestered into PBs or not.

A different possibility is that visible phase separation during stress is just an indicator or consequence of broader remodeling happening globally to smaller mRNP complexes that exist throughout the cell. Proteins interact with a transcript throughout its life, creating sub-microscopic mRNP complexes that can be translationally active or inactive. At any given point in time, a relatively small number of total cellular protein and RNA is contained in a granule. However, we know that both proteins and mRNAs are dynamically exchanging between mRNP granules and the cytoplasm. Could mRNP complexes that are competent to enter or have previously exited an mRNP granule be in a “modified” state, even outside of the granule? To date, we do not know if there are changes to the molecular composition of interacting RNAs and proteins as they leave membrane-less compartments; current techniques only capture granules at a given point in time and do not reveal how many molecules in the general cytoplasm were prior mRNP residents. This alternative proposal is not without some grounding in previous research. For example, during nonstress conditions, the SG component protein Pab1 is predominantly in a soluble and nonpelletable, state when cell extracts are treated with RNase I (Riback et al., 2017). Yet, during a mild heat stress, about half of the Pab1 molecules transition to insoluble, pelletable quinary assemblies, though no visible SGs form. At higher temperatures when visible SGs do form, over 90% of Pab1 transitions to a pelletable state even though a much smaller portion of total Pab1 resides within phase

separated mRNP granules. Therefore, it could be that some mRNAs not directly contained within mRNP granules still interact with their protein partners in “altered,” mRNP-dependent states. These would be distinct from interactions that take place before stress and might be relevant for survival during stress. For instance, posttranslational modifications of proteins have been implicated in granule formation. If these proteins are rapidly exchanging with the environment, presumably many proteins not found in the granule at any specific time will still be modified upon leaving the granule. What percent of proteins are modified? How would these modifications affect protein function when they exist as part of mRNP complexes that are sub-microscopic and are no longer contained within the granule? Further investigations into the changes that mRNP complexes undergo both within and outside of granules during stress will need to be undertaken to address these possibilities. One exciting, relevant direction would be to perform a time-course experiment that employs a proximity labeling and proteomics approach to see if certain PTMs are upregulated on PB- or SG-enriched proteins in both granule and cytoplasmic fractions. If a certain protein is modified in the granule and then released back into the cytoplasm, thereby changing its function, you would expect this to be reflected over the time-course.

Finally, the role of stress-induced mRNP granules could be entirely passive. As previously described, one proposed function of mRNP granules is to store RNAs throughout the duration of stress to allow optimal growth upon recovery as this provides avoidance of extraneous transcription and nuclear export. A recently considered possible, complementary function of mRNP granules is that instead of only serving as RNA storage depots they may also serve as protein storage depots for growth proteins that are not

needed during stressful conditions but that the cell may not want to immediately degrade. After all, stress is transitory and dynamic in nature. As evidence consider the yeast pyruvate kinase protein Cdc19, a key regulator of glycolytic metabolism and cell growth. This protein has been found to form reversible aggregates that co-localize with SGs during stress. This aggregation was found to be a protective mechanism from stress-induced degradation as, upon stress relief, it proves to be reversible and allows quick reentry into the cell cycle because these proteins do not have to be reexpressed (Saad et al., 2017). It is possible, therefore, that stress-induced granule formation evolved as a means to coordinate cellular machinery in a way that enables its rapid and efficient deployment in the cell once conditions are more favorable for growth and energy consumption.

3.5 Conclusion

There has been a recent surge in research focusing on phase separation in biological processes. The formation of stress-induced mRNP granules is a broadly conserved example of this phase separation, but for all of this intense study the importance of this phase separation remains unclear. Overall, there has been much progress in understanding the formation and composition of stress-induced mRNP granules. Yet, somewhat surprisingly, this knowledge has only led to marginal increases in our understanding of the function of these membraneless compartments within the cell. Moving forward, there are a number of distinct directions that may prove fruitful in elucidating the function of stress-induced mRNP granules. in vitro reconstitution has been

an important tool for understanding many biochemical and biophysical processes. Several recent advances that helped to elucidate mechanisms of biological LLPS have come from reconstitution of these systems in vitro (Banani et al., 2016; Han et al., 2012; A. Jain & Vale, 2017; P. Li et al., 2012; Molliex et al., 2015). While progress has been made in making reductionist systems in vitro, some of the properties of mRNP granules may arise because of their complexity. Thus, reduction of granules to limited protein or mRNA components may mask some emergent properties and it would be worth studying if and how an increase in protein and RNA types alters in vitro phase separation to more closely mimic granules in cells. in vitro studies of stress-induced mRNP granules will also need to be cognizant of role that ATP plays in the dynamics of mRNP granules (S. Jain et al., 2016) and ATP's ability to directly solubilize molecules in aqueous solutions as a biological hydrotrope (Patel et al., 2017). Lastly, a worthwhile avenue would be combined use of techniques like single molecule FISH and SHAPE (selective 20 hydroxyl acylation analyzed by primer extension) probing of RNA secondary structure before and after in vitro phase separation to address the relationship between RNA compaction and granule entry to determine the extent to which RNAs undergo compaction before, during, or after entry into granules.

Another exciting direction important to understand how the assembly of these granules directly affects function is the ability to perturb phase separation in a more controlled, stress-independent manner in vivo. While overexpression of certain proteins is sufficient to drive phase separation without stress, an exciting new direction is using the Arabidopsis thaliana cryptochrome 2 photolyase homology region to drive light-inducible phase separation (Shin et al., 2017; Taylor et al., 2018). This technique

potentially allows experiments to dynamically drive phase separation in cells and might provide an understanding of what effect LLPS has on the physiology of the cell in a way that is decoupled from stress and unobscured by consequences of overexpression. Intriguingly, recent experiments have shown that light-induced phase separation of the SG protein G3BP1 is sufficient to recruit many other core SG components and polyadenylated RNA (Taylor et al., 2018). Lastly, more work must be done that employs methods to directly measure the impact of mRNP granules on gene expression. Recent work using microscopy based in vivo reporters of translation and mRNA decay have given interesting insights into what these mRNP granules may and may not be doing (Horvathova et al., 2017; Moon et al., 2019; Pitchiaya et al., 2018; Wilbertz et al., 2019). Further single molecule measurements are needed, particularly in live cells, to increase the diversity of mRNA species analyzed and to directly follow mRNAs that were previously localized to mRNP granules after stress is abated to resolve their fate. Such single molecule approaches could be complemented by a genome-wide approach described in two exciting, recently posted preprints that utilize a novel technique that applies APEX-based proximity labeling to RNA called APEX-seq (Fazal et al., 2018; Padròn, Iwasaki, & Ingolia, 2018). The latter preprint analyzed stress-specific impacts on mRNA localization and offers powerful insight into the relationship between protein localization and RNA localization during stress. Combinations of these in vitro and in vivo approaches will likely help shed light on the elusive function of PBs and SGs and ultimately inform our understanding of their cellular function during stress, potentially offering insight into disease states linked to aberrant stress response and granule assembly.

3.6 Figures

Figure 3.1: Protein composition of stress granules and p-bodies.

(A) Properties of yeast and mammalian SG and PB proteomes. Upper: Summary of protein activities of SG and PB proteomes. Lower: Overlap of SG and PB proteome components identified in both granule types for yeast and mammalian systems. Yeast and human SG proteomes and yeast PB proteome are from (Jain et al., 2016). The human PB proteome is from (Hubstenberger et al., 2017). Prion-like domains were predicted by PrionScan (Angarica et al., 2014) and PLAAC (Lancaster et al., 2014). The RNA-binding proteomes are from (Beckmann et al., 2015). ATPase activity annotations are from SGD and NCBI. (B) Representative functional, gene ontology (GO) classification of PB and SG proteomes. Yeast homologs are shown in parentheses. Components that are essential for PB/SG assembly and maintenance are highlighted in bold. GO analysis was performed by GO consortium (Ashburner et al., 2000; Carbon et al., 2017). Citations showing the presence and functions of listed components and those used to generate GO data include Serman et al., 2007; Luo et al., 2018; Andrei et al., 2005; Sheth & Parker, 2003; Hubstenberger et al., 2017; Franks & Lykke-Andersen, 2008; Eulalio et al., 2007; Marnef et al., 2010; Decker et al., 2007; Gilks, 2004; Kedersha et al., 2016; Yang et al., 2014; Buchan & Parker, 2009; Tourriere et al., 2003; Jain et al., 2016; & Markmiller et al., 2018.

A

Features	Yeast SG (159)	Human SG (411)	Yeast PB (52)	Human PB (109)
RNA-binding proteins (RBPs)	39	224	36	70
Prion-like domains	23	32	21	24
RBP & prion-like domains	18	30	11	13
ATPase activity	10	37	5	19

SG and PB overlap	Yeast	Human
Number	5	28
Components	Dhh1, Sbp1, Eap1, Dcp1, Scd6	ACTBL2, AGO2, DCP1A, DDX21, DDX50, DDX6, DHX30, EDC4, ELAVL1, ELAVL2, FAM120A, HSPB1, IGF2BP1, IGF2BP2, IGF2BP3, KIF23, LSM14A, LSM14B, MCM7, MEX3A, MOV10, MSI1, NOP58, PUM1, S100A9, STAU2, UPF1, ZC3HAV1

B

Processing Body (P-body/PB)

Translation repression	**CPEB1**, **EIF4E-T**
RNA decay and stabilization	**LSM14A**/B (**Scd6**), **DDX6** (**Dhh1**), IGF2BP2
miRNA pathway	**Ge-1**, GW182, AGO1/2, MOV10, ZCCHC3, PUM1
Nonsense-mediated mRNA decay (NMD)	UPF1, SMG7
Decapping complex components	**DCP1A/1B/2**, **EDC3/4**, **PATL1**
Deadenylation complex components	**LSM1-7**, **CCR4-NOT**

Stress Granule (SG)

Translation repression	**TIA-1/TIAR (Pub1/Ngr1)**, **Caprin-1**, FMRP/FXR1, Ataxin-2
Translation initiation	EIF2A, EIF3, EIF4A/B, EIF4G (Tif4631/**Tif4632**)
RNA decay and stabilization	**TDP-43**, **PAB1**, ELAVL1, IGF2BP1, TTP
Ribonuclease activity	**G3BP**, SND1, XRN1, DDX1, CCR-NOT
miRNA pathway	TNRC6B, AGO2, EIF3A
ATPase activity	**DDX6 (Ded1)**, **MCM**, **CCT**, **RUVBL1/2 (Rvb1/2)**

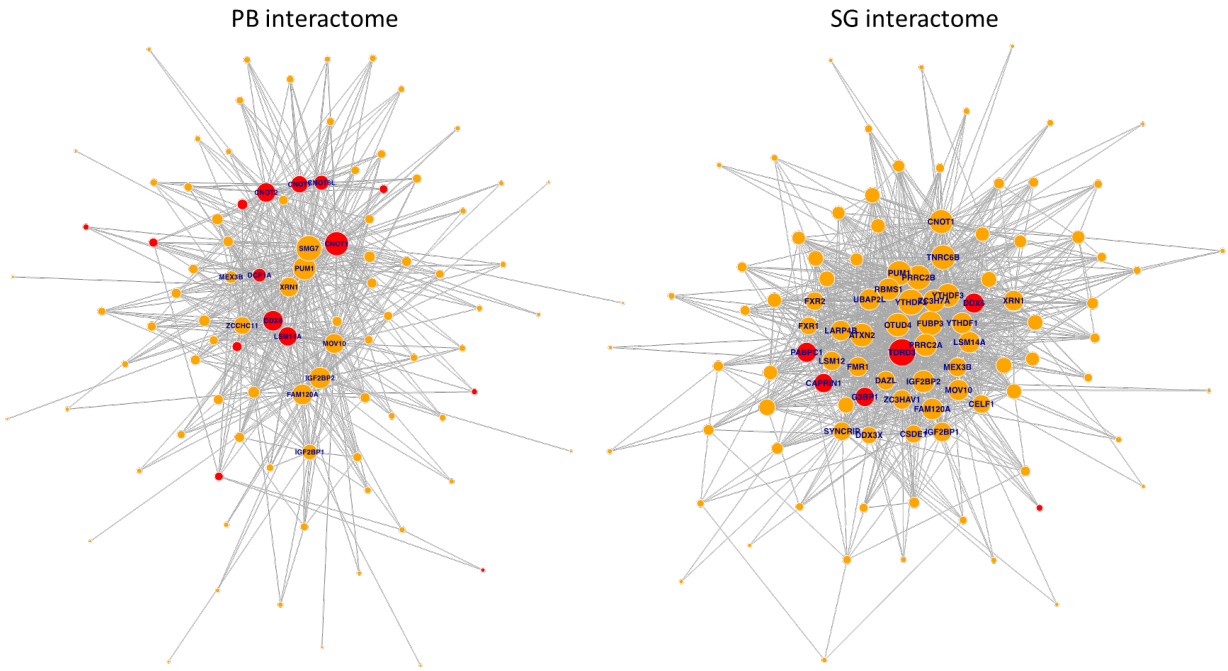

Figure 3.2: Interactions between mammalian PB and SG protein components.

Gene names of proteins with more than 15 interacting protein components in PBs are shown (left network) while those with more than 30 interacting protein components in SGs are shown (right network). Proteins that were identified as essential components for PB or SG assembly are highlighted in red; these tend to have increased numbers of interacting partners. Mammalian interactome datasets of PB and SG components are from Young et al., 2016. The mammalian SG proteome is from Jain et al., 2016 and the PB proteome is from Hubstenberger et al., 2017.

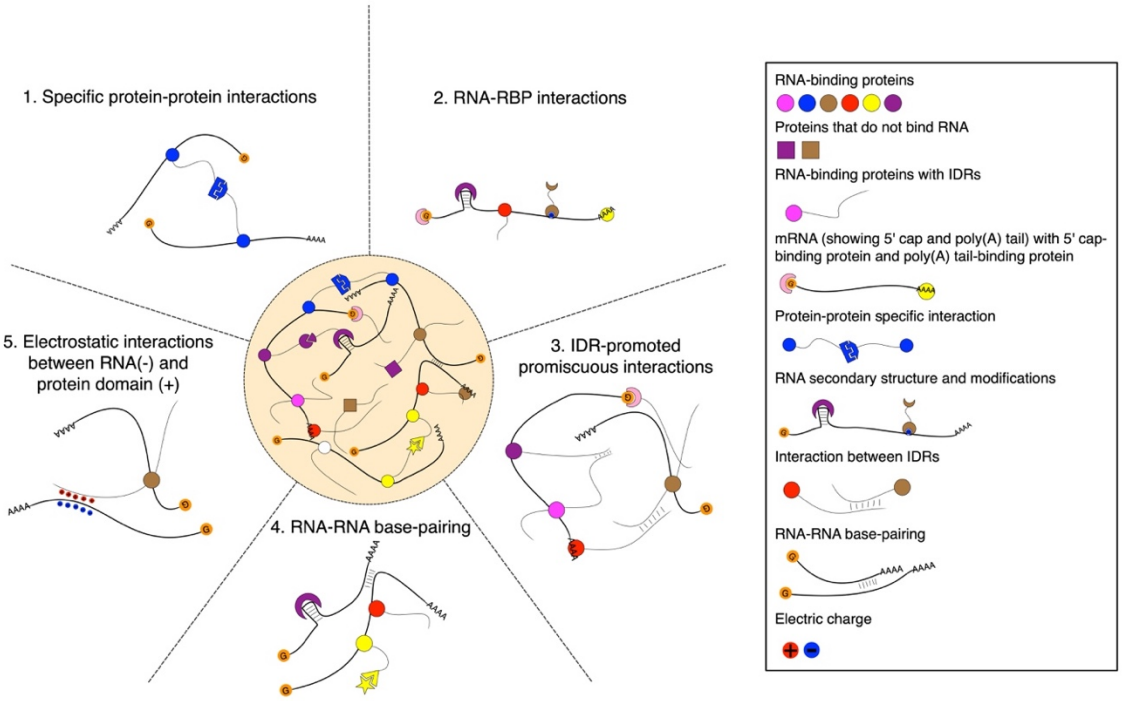

Figure 3.3: Diverse sets of interactions drive mRNP granule assembly and LLPS. Five classes of interactions that contribute to SG and PB formation are modeled. Different protein-protein, protein-RNA, and RNA-RNA interactions contribute to phase separation and drive the formation of stress-induced mRNP granules.

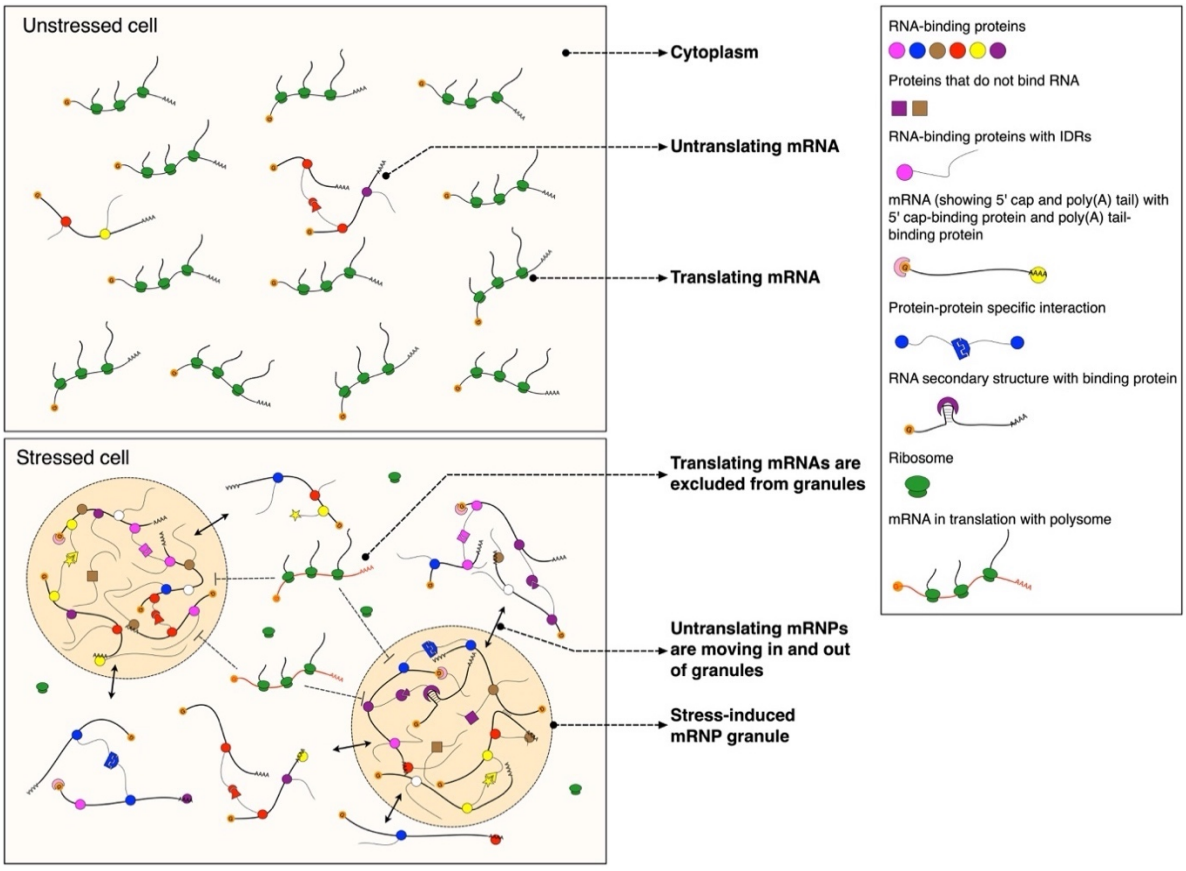

Figure 3.4: Model for composition dynamics and potential function of stress-induced mRNP granules.

Lines with double arrows show that mRNAs associated with RBPs move in and out of stress-induced mRNP granules. Dashed lines with inhibitory arrows show that mRNAs engaged in translation are excluded from stress-induced mRNP granules.

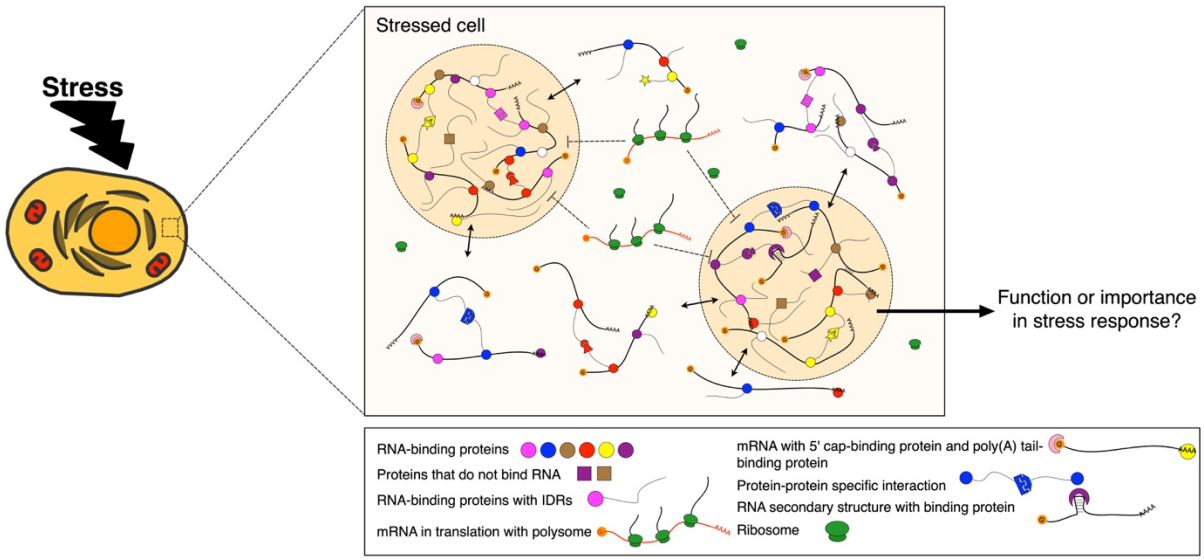

Figure 3.5: A graphic abstract

Diverse macromolecular interactions lead to the phase separation of protein and RNA during stress. While the identities of many proteins and RNAs contained in these granules (tan spheres) have been elucidated recently, the function of this conserved compartmentalization of the cytoplasm during stress response is still an open question.

3.7 Acknowledgement

We acknowledge support by the Zid lab startup funds from UCSD and MIRA grant from the National Institutes of Health R35GM128798 (to B.M.Z).

Chapter 3, in full, is a reformatted published material as it appears as: Guzikowski, Anna R.*; Chen, Yang S.*; Zid, Brian M. 2019. Stress-induced mRNP granules: form and function of processing bodies and stress granules. Wiley Interdisciplinary Reviews: RNA, 10(3), e1524. The dissertation author was the co-first author of this paper.

3.8 References

Adivarahan, S., Livingston, N., Nicholson, B., Rahman, S., Wu, B., Rissland, O.S., Zenklusen, D., 2018. Spatial Organization of Single mRNPs at Different Stages of the Gene Expression Pathway. Mol. Cell 72, 727-738.e5.

Alberti, S., 2018. Guilty by Association: Mapping Out the Molecular Sociology of Droplet Compartments. Mol Cell 69, 349–351.

Andrei, M.A., Ingelfinger, D., Heintzmann, R., Achsel, T., Rivera-Pomar, R., Lührmann, R., 2005. A role for eIF4E and eIF4E-transporter in targeting mRNPs to mammalian processing bodies. RNA 11, 717–727.

Archer, S.K., Shirokikh, N.E., Beilharz, T.H., Preiss, T., 2016. Dynamics of ribosome scanning and recycling revealed by translation complex profiling. Nature 535, 570–574.

Ashburner, M., Ball, C.A., Blake, J.A., Botstein, D., Butler, H., Cherry, J.M., Davis, A.P., Dolinski, K., Dwight, S.S., Eppig, J.T., Harris, M.A., Hill, D.P., Issel-Tarver, L., Kasarskis, A., Lewis, S., Matese, J.C., Richardson, J.E., Ringwald, M., Rubin, G.M., Sherlock, G., 2000. Gene Ontology: tool for the unification of biology. Nat. Genet. 25, 25–29.

Aumiller, W.M., Keating, C.D., 2015. Phosphorylation-mediated RNA/peptide complex coacervation as a model for intracellular liquid organelles. Nat. Chem. 8, 129–137.

Ayache, J., Bénard, M., Ernoult-Lange, M., Minshall, N., Standart, N., Kress, M., Weil, D., 2015. P-body assembly requires DDX6 repression complexes rather than decay or Ataxin2/2L complexes. Mol. Biol. Cell 26, 2579–2595.

Banani, S.F., Lee, H.O., Hyman, A.A., Rosen, M.K., 2017. Biomolecular condensates: organizers of cellular biochemistry. Nat Rev Mol Cell Biol 18, 285–298.

Banani, S.F., Rice, A.M., Peeples, W.B., Lin, Y., Jain, S., Parker, R., Rosen, M.K., 2016. Compositional Control of Phase-Separated Cellular Bodies. Cell 166, 651–663.

Bashkirov, V.I., Scherthan, H., Solinger, J.A., Buerstedde, J.M., Heyer, W.D., 1997. A mouse cytoplasmic exoribonuclease (mXRN1p) with preference for G4 tetraplex substrates. J. Cell Biol.

Beckmann, B.M., Horos, R., Fischer, B., Castello, A., Eichelbaum, K., Alleaume, A.M., Schwarzl, T., Curk, T., Foehr, S., Huber, W., Krijgsveld, J., Hentze, M.W., 2015. The RNA-binding proteomes from yeast to man harbour conserved enigmRBPs. Nat. Commun. 6, 10127.

Bley, N., Lederer, M., Pfalz, B., Reinke, C., Fuchs, T., Glaß, M., Möller, B., Hüttelmaier, S., 2015. Stress granules are dispensable for mRNA stabilization during cellular

stress. Nucleic Acids Res. 43, e26–e26.

Brangwynne, C.P., Eckmann, C.R., Courson, D.S., Rybarska, A., Hoege, C., Gharakhani, J., Jülicher, F., Hyman, A.A., 2009. Germline P granules are liquid droplets that localize by controlled dissolution/condensation. Science (80-.). 324, 1729–1732.

Brengues, M., Teixeira, D., Parker, R., 2005. Movement of eukaryotic mRNAs between polysomes and cytoplasmic processing bodies. Science (80-.). 310, 486–8075.

Buchan, J.R., Muhlrad, D., Parker, R., 2008. P bodies promote stress granule assembly in Saccharomyces cerevisiae. J Cell Biol 183, 441–455.

Buchan, J.R., Parker, R., 2009. Eukaryotic Stress Granules: The Ins and Outs of Translation. Mol. Cell 36, 932–941.

Carbon, S., Dietze, H., Lewis, S.E., Mungall, C.J., Munoz-Torres, M.C., Basu, S., Chisholm, R.L., Dodson, R.J., Fey, P., Thomas, P.D., Mi, H., Muruganujan, A., Huang, X., Poudel, S., Hu, J.C., Aleksander, S.A., McIntosh, B.K., Renfro, D.P., Siegele, D.A., Antonazzo, G., Attrill, H., Brown, N.H., Marygold, S.J., Mc-Quilton, P., Ponting, L., Millburn, G.H., Rey, A.J., Stefancsik, R., Tweedie, S., Falls, K., Schroeder, A.J., Courtot, M., Osumi-Sutherland, D., Parkinson, H., Roncaglia, P., Lovering, R.C., Foulger, R.E., Huntley, R.P., Denny, P., Campbell, N.H., Kramarz, B., Patel, S., Buxton, J.L., Umrao, Z., Deng, A.T., Alrohaif, H., Mitchell, K., Ratnaraj, F., Omer, W., Rodríguez-López, M., C. Chibucos, M., Giglio, M., Nadendla, S., Duesbury, M.J., Koch, M., Meldal, B.H.M., Melidoni, A., Porras, P., Orchard, S., Shrivastava, A., Chang, H.Y., Finn, R.D., Fraser, M., Mitchell, A.L., Nuka, G., Potter, S., Rawlings, N.D., Richardson, L., Sangrador-Vegas, A., Young, S.Y., Blake, J.A., Christie, K.R., Dolan, M.E., Drabkin, H.J., Hill, D.P., Ni, L., Sitnikov, D., Harris, M.A., Hayles, J., Oliver, S.G., Rutherford, K., Wood, V., Bahler, J., Lock, A., De Pons, J., Dwinell, M., Shimoyama, M., Laulederkind, S., Hayman, G.T., Tutaj, M., Wang, S.J., D'Eustachio, P., Matthews, L., Balhoff, J.P., Balakrishnan, R., Binkley, G., Cherry, J.M., Costanzo, M.C., Engel, S.R., Miyasato, S.R., Nash, R.S., Simison, M., Skrzypek, M.S., Weng, S., Wong, E.D., Feuermann, M., Gaudet, P., Berardini, T.Z., Li, D., Muller, B., Reiser, L., Huala, E., Argasinska, J., Arighi, C., Auchincloss, A., Axelsen, K., Argoud-Puy, G., Bateman, A., Bely, B., Blatter, M.C., Bonilla, C., Bougueleret, L., Boutet, E., Breuza, L., Bridge, A., Britto, R., Hye- A-Bye, H., Casals, C., Cibrian-Uhalte, E., Coudert, E., Cusin, I., Duek-Roggli, P., Estreicher, A., Famiglietti, L., Gane, P., Garmiri, P., Georghiou, G., Gos, A., Gruaz-Gumowski, N., Hatton-Ellis, E., Hinz, U., Holmes, A., Hulo, C., Jungo, F., Keller, G., Laiho, K., Lemercier, P., Lieberherr, D., Mac- Dougall, A., Magrane, M., Martin, M.J., Masson, P., Natale, D.A., O'Donovan, C., Pedruzzi, I., Pichler, K., Poggioli, D., Poux, S., Rivoire, C., Roechert, B., Sawford, T., Schneider, M., Speretta, E., Shypitsyna, A., Stutz, A., Sundaram, S., Tognolli, M., Wu, C., Xenarios, I., Yeh, L.S., Chan, J., Gao, S., Howe, K., Kishore, R., Lee, R., Li, Y., Lomax, J., Muller, H.M., Raciti, D., Van Auken, K., Berriman, M., Stein, Paul Kersey, L., W. Sternberg, P., Howe, D., Westerfield, M., 2017. Expansion of the gene ontology knowledgebase and resources: The gene ontology consortium. Nucleic Acids Res. 45, D331–D338.

Damgaard, C.K., Lykke-Andersen, J., 2011. Translational coregulation of 5'TOP mRNAs by TIA-1 and TIAR. Genes Dev.

Dang, Y., Kedersha, N., Low, W.K., Romo, D., Gorospe, M., Kaufman, R., Anderson, P., Liu, J.O., 2006. Eukaryotic initiation factor 2alpha-independent pathway of stress granule induction by the natural product pateamine A. J. Biol. Chem.

De Leeuw, F., Zhang, T., Wauquier, C., Huez, G., Kruys, V., Gueydan, C., 2007. The cold-inducible RNA-binding protein migrates from the nucleus to cytoplasmic stress granules by a methylation-dependent mechanism and acts as a translational repressor. Exp. Cell Res.

Decker, C.J., Teixeira, D., Parker, R., 2007. Edc3p and a glutamine/asparagine-rich domain of Lsm4p function in processing body assembly in Saccharomyces cerevisiae. J Cell Biol 179, 437–449.

Ditlev, J.A., Case, L.B., Rosen, M.K., 2018. Who's In and Who's Out-Compositional Control of Biomolecular Condensates. J Mol Biol.

Eisinger-Mathason, T.S.K., Andrade, J., Groehler, A.L., Clark, D.E., Muratore-Schroeder, T.L., Pasic, L., Smith, J.A., Shabanowitz, J., Hunt, D.F., Macara, I.G., Lannigan, D.A., 2008. Codependent Functions of RSK2 and the Apoptosis-Promoting Factor TIA-1 in Stress Granule Assembly and Cell Survival. Mol. Cell.

Espinosa Angarica, V., Ventura, S., Sancho, J., 2013. Discovering putative prion sequences in complete proteomes using probabilistic representations of Q/N-rich domains. BMC Genomics 14, 1–17.

Eulalio, A., Behm-Ansmant, I., Schweizer, D., Izaurralde, E., 2007. P-body formation is a consequence, not the cause, of RNA-mediated gene silencing. Mol Cell Biol 27, 3970–3981.

Fazal, F.M., Han, S., Parker, K.R., Kaewsapsak, P., Xu, J., Boettiger, A.N., Chang, H.Y., Ting, A.Y., 2019. Atlas of Subcellular RNA Localization Revealed by APEX-Seq. Cell 178, 473-490.e26.

Franks, T.M., Lykke-Andersen, J., 2008. The control of mRNA decapping and P-body formation. Mol Cell 32, 605–615.

Fromm, S.A., Kamenz, J., Noldeke, E.R., Neu, A., Zocher, G., Sprangers, R., 2014. In vitro reconstitution of a cellular phase-transition process that involves the mRNA decapping machinery. Angew Chem Int Ed Engl 53, 7354–7359.

Gilks, N., 2004. Stress Granule Assembly Is Mediated by Prion-like Aggregation of TIA-1. Mol. Biol. Cell.

Goulet, I., Boisvenue, S., Mokas, S., Mazroui, R., Cote, J., 2008. TDRD3, a novel Tudor domain-containing protein, localizes to cytoplasmic stress granules. Hum Mol Genet 17, 3055–3074.

Gowrishankar, G., Winzen, R., Dittrich-Breiholz, O., Redich, N., Kracht, M., Holtmann, H., 2006. Inhibition of mRNA deadenylation and degradation by different types of cell stress. Biol. Chem.

Han, T.W., Kato, M., Xie, S., Wu, L.C., Mirzaei, H., Pei, J., Chen, M., Xie, Y., Allen, J., Xiao, G., McKnight, S.L., 2012. Cell-free formation of RNA granules: Bound RNAs identify features and components of cellular assemblies. Cell.

Helder, S., Blythe, A.J., Bond, C.S., Mackay, J.P., 2016. Determinants of affinity and specificity in RNA-binding proteins. Curr. Opin. Struct. Biol. 38, 83–91.

Hilgers, V., Teixeira, D., Parker, R., 2006. Translation-independent inhibition of mRNA deadenylation during stress in Saccharomyces cerevisiae. RNA.

Horvathova, I., Voigt, F., Kotrys, A. V, Zhan, Y., Artus-Revel, C.G., Eglinger, J., Stadler, M.B., Giorgetti, L., Chao, J.A., 2017. The Dynamics of mRNA Turnover Revealed by Single-Molecule Imaging in Single Cells. Mol Cell.

Hubstenberger, A., Courel, M., Benard, M., Souquere, S., Ernoult-Lange, M., Chouaib, R., Yi, Z., Morlot, J.B., Munier, A., Fradet, M., Daunesse, M., Bertrand, E., Pierron, G., Mozziconacci, J., Kress, M., Weil, D., 2017. P-Body Purification Reveals the Condensation of Repressed mRNA Regulons. Mol Cell 68, 144-157 e5.

Ingolia, N.T., Ghaemmaghami, S., Newman, J.R., Weissman, J.S., 2009. Genome-wide analysis in vivo of translation with nucleotide resolution using ribosome profiling. Science (80-.). 324, 218–223.

Ishigaki, S., Masuda, A., Fujioka, Y., Iguchi, Y., Katsuno, M., Shibata, A., Urano, F., Sobue, G., Ohno, K., 2012. Position-dependent FUS-RNA interactions regulate alternative splicing events and transcriptions. Sci. Rep.

Jain, A., Vale, R.D., 2017. RNA phase transitions in repeat expansion disorders. Nature.

Jain, S., Wheeler, J.R., Walters, R.W., Agrawal, A., Barsic, A., Parker, R., 2016. ATPase-Modulated Stress Granules Contain a Diverse Proteome and Substructure. Cell 164, 487–498.

Jayabalan, A.K., Sanchez, A., Park, R.Y., Yoon, S.P., Kang, G.Y., Baek, J.H., Anderson, P., Kee, Y., Ohn, T., 2016. NEDDylation promotes stress granule assembly. Nat Commun 7, 12125.

Kedersha, N., Anderson, P., 2002. Stress granules: sites of mRNA triage that regulate mRNA stability and translatability. Biochem. Soc. Trans.

Kedersha, N., Cho, M.R., Li, W., Yacono, P.W., Chen, S., Gilks, N., Golan, D.E., Anderson, P., 2000. Dynamic Shuttling of Tia-1 Accompanies the Recruitment of mRNA to Mammalian Stress Granules. J Cell Biol 151, 1257–1268.

Kedersha, N., Panas, M.D., Achorn, C.A., Lyons, S., Tisdale, S., Hickman, T., Thomas, M., Lieberman, J., McInerney, G.M., Ivanov, P., Anderson, P., 2016. G3BP-Caprin1-

USP10 complexes mediate stress granule condensation and associate with 40S subunits. J Cell Biol 212, 845–860.

Kedersha, N., Stoecklin, G., Ayodele, M., Yacono, P., Lykke-Andersen, J., Fitzler, M.J., Scheuner, D., Kaufman, R.J., Golan, D.E., Anderson, P., 2005. Stress granules and processing bodies are dynamically linked sites of mRNP remodeling. J. Cell Biol.

Kedersha, N.L., Gupta, M., Li, W., Miller, I., Anderson, P., 1999. RNA-binding proteins TIA-1 and TIAR link the phosphorylation of eIF-2α to the assembly of mammalian stress granules. J. Cell Biol.

Kershaw, C.J., Ashe, M.P., 2017. Untangling P-Bodies: Dissecting the Complex Web of Interactions that Enable Tiered Control of Gene Expression. Mol Cell 68, 3–4.

Khong, A., Matheny, T., Jain, S., Mitchell, S.F., Wheeler, J.R., Parker, R., 2017. The Stress Granule Transcriptome Reveals Principles of mRNA Accumulation in Stress Granules. Mol. Cell.

Khong, A., Parker, R., 2018. MRNP architecture in translating and stress conditions reveals an ordered pathway of mRNP compaction. J. Cell Biol. 217, 4124–4140.

Kim, Y., Myong, S., 2016. RNA Remodeling Activity of DEAD Box Proteins Tuned by Protein Concentration, RNA Length, and ATP. Mol. Cell 63, 865–876.

Kroschwald, S., Maharana, S., Mateju, D., Malinovska, L., Nuske, E., Poser, I., Richter, D., Alberti, S., 2015. Promiscuous interactions and protein disaggregases determine the material state of stress-inducible RNP granules. Elife 4, e06807.

Kroschwald, S., Munder, M.C., Maharana, S., Franzmann, T.M., Richter, D., Ruer, M., Hyman, A.A., Alberti, S., 2018. Different Material States of Pub1 Condensates Define Distinct Modes of Stress Adaptation and Recovery. Cell Rep. 23, 3327–3339.

Kwon, S., Zhang, Y., Matthias, P., 2007. The deacetylase HDAC6 is a novel critical component of stress granules involved in the stress response. Genes Dev.

Lancaster, A.K., Nutter-Upham, A., Lindquist, S., King, O.D., 2014. PLAAC: A web and command-line application to identify proteins with prion-like amino acid composition. Bioinformatics 30, 2501–2502.

Langdon, E.M., Qiu, Y., Niaki, A.G., McLaughlin, G.A., Weidmann, C., Gerbich, T.M., Smith, J.A., Crutchley, J.M., Termini, C.M., Weeks, K.M., 2018. mRNA structure determines specificity of a polyQ-driven phase separation. Science (80-.). eaar7432.

Lavut, A., Raveh, D., 2012. Sequestration of highly expressed mrnas in cytoplasmic granules, p-bodies, and stress granules enhances cell viability. PLoS Genet.

Li, P., Banjade, S., Cheng, H.C., Kim, S., Chen, B., Guo, L., Llaguno, M., Hollingsworth, J. V, King, D.S., Banani, S.F., Russo, P.S., Jiang, Q.X., Nixon, B.T., Rosen, M.K., 2012. Phase transitions in the assembly of multivalent signalling proteins. Nature 483, 336–340.

Li, X.H., Chavali, P.L., Pancsa, R., Chavali, S., Babu, M.M., 2018. Function and Regulation of Phase-Separated Biological Condensates. Biochemistry.

Luo, Y., Na, Z., Slavoff, S.A., 2018. P-Bodies: Composition, Properties, and Functions. Biochemistry 57, 2424–2431.

Markmiller, S., Soltanieh, S., Server, K.L., Mak, R., Jin, W., Fang, M.Y., Luo, E.-C., Krach, F., Yang, D., Sen, A., Fulzele, A., Wozniak, J.M., Gonzalez, D.J., Kankel, M.W., Gao, F.-B., Bennett, E.J., Lécuyer, E., Yeo, G.W., 2018. Context-Dependent and Disease-Specific Diversity in Protein Interactions within Stress Granules. Cell 172, 590-604.e13.

Marnef, A., Maldonado, M., Bugaut, A., Balasubramanian, S., Kress, M., Weil, D., Standart, N., 2010. Distinct functions of maternal and somatic Pat1 protein paralogs. RNA 16, 2094–2107.

Mateju, D., Franzmann, T.M., Patel, A., Kopach, A., Boczek, E.E., Maharana, S., Lee, H.O., Carra, S., Hyman, A.A., Alberti, S., 2017. An aberrant phase transition of stress granules triggered by misfolded protein and prevented by chaperone function. EMBO J. 36, 1669–1687.

Mazroui, R., Di Marco, S., Kaufman, R.J., Gallouzi, I.-E., 2007. Inhibition of the Ubiquitin-Proteasome System Induces Stress Granule Formation. Mol. Biol. Cell.

Mazroui, R., Sukarieh, R., Bordeleau, M.-E., Kaufman, R.J., Northcote, P., Tanaka, J., Gallouzi, I., Pelletier, J., 2006. Inhibition of Ribosome Recruitment Induces Stress Granule Formation Independently of Eukaryotic Initiation Factor 2α Phosphorylation. Mol. Biol. Cell.

Mitchell, S.F., Jain, S., She, M., Parker, R., 2013. Global analysis of yeast mRNPs. Nat Struct Mol Biol 20, 127–133.

Moeller, B.J., Cao, Y., Li, C.Y., Dewhirst, M.W., 2004. Radiation activates HIF-1 to regulate vascular radiosensitivity in tumors: Role of reoxygenation, free radicals, and stress granules. Cancer Cell.

Mokas, S., Mills, J.R., Garreau, C., Fournier, M.-J., Robert, F., Arya, P., Kaufman, R.J., Pelletier, J., Mazroui, R., 2009. Uncoupling Stress Granule Assembly and Translation Initiation Inhibition. Mol. Biol. Cell.

Mollet, S., Cougot, N., Wilczynska, A., Dautry, F., Kress, M., Bertrand, E., Weil, D., 2008. Translationally Repressed mRNA Transiently Cycles through Stress Granules during Stress. Mol. Biol. Cell.

Molliex, A., Temirov, J., Lee, J., Coughlin, M., Kanagaraj, A.P., Kim, H.J., Mittag, T., Taylor, J.P., 2015. Phase separation by low complexity domains promotes stress granule assembly and drives pathological fibrillization. Cell 163, 123–133.

Moon, S.L., Morisaki, T., Khong, A., Lyon, K., Parker, R., Stasevich, T.J., 2018. Imaging of single mRNA translation repression reveals diverse interactions with mRNP

granules. bioRxiv.

Mugler, C.F., Hondele, M., Heinrich, S., Sachdev, R., Vallotton, P., Koek, A.Y., Chan, L.Y., Weis, K., 2016. ATPase activity of the DEAD-box protein Dhh1 controls processing body formation. Elife 5.

Namkoong, S., Ho, A., Woo, Y.M., Kwak, H., Lee, J.H., 2018. Systematic Characterization of Stress-Induced RNA Granulation. Mol Cell.

Ohn, T., Kedersha, N., Hickman, T., Tisdale, S., Anderson, P., 2008. A functional RNAi screen links O-GlcNAc modification of ribosomal proteins to stress granule and processing body assembly. Nat Cell Biol 10, 1224–1231.

Padrón, A., Iwasaki, S., Ingolia, N.T., 2019. Proximity RNA Labeling by APEX-Seq Reveals the Organization of Translation Initiation Complexes and Repressive RNA Granules. Mol. Cell 75, 875-887.e5.

Parker, R., Sheth, U., 2007. P bodies and the control of mRNA translation and degradation. Mol Cell 25, 635–646.

Patel, A., Malinovska, L., Saha, S., Wang, J., Alberti, S., Krishnan, Y., Hyman, A.A., 2017. Biochemistry: ATP as a biological hydrotrope. Science (80-.).

Pitchiaya, S., Mourao, M.D.A., Jalihal, A.P., Xiao, L., Jiang, X., Chinnaiyan, A.M., Schnell, S., Walter, N.G., 2018. Dynamic recruitment of single RNAs to processing bodies depends on RNA functionality. bioRxiv.

Protter, D.S.W., Rao, B.S., Van Treeck, B., Lin, Y., Mizoue, L., Rosen, M.K., Parker, R., 2018. Intrinsically Disordered Regions Can Contribute Promiscuous Interactions to RNP Granule Assembly. Cell Rep 22, 1401–1412.

Rao, B.S., Parker, R., 2017. Numerous interactions act redundantly to assemble a tunable size of P bodies in Saccharomyces cerevisiae. Proc Natl Acad Sci U S A.

Riback, J.A., Katanski, C.D., Kear-Scott, J.L., Pilipenko, E. V, Rojek, A.E., Sosnick, T.R., Drummond, D.A., 2017. Stress-Triggered Phase Separation Is an Adaptive, Evolutionarily Tuned Response. Cell 168, 1028-1040 e19.

Rogelj, B., Easton, L.E., Bogu, G.K., Stanton, L.W., Rot, G., Curk, T., Zupan, B., Sugimoto, Y., Modic, M., Haberman, N., Tollervey, J., Fujii, R., Takumi, T., Shaw, C.E., Ule, J., 2012. Widespread binding of FUS along nascent RNA regulates alternative splicing in the brain. Sci. Rep.

Saad, S., Cereghetti, G., Feng, Y., Picotti, P., Peter, M., Dechant, R., 2017. Reversible protein aggregation is a protective mechanism to ensure cell cycle restart after stress. Nat. Cell Biol.

Schütz, S., Nöldeke, E.R., Sprangers, R., 2017. A synergistic network of interactions promotes the formation of in vitro processing bodies and protects mRNA against decapping. Nucleic Acids Res. 45, 6911–6922.

Serman, A., Le Roy, F., Aigueperse, C., Kress, M., Dautry, F., Weil, D., 2007. GW body disassembly triggered by siRNAs independently of their silencing activity. Nucleic Acids Res. 35, 4715–4727.

Shah, K.H., Zhang, B., Ramachandran, V., Herman, P.K., 2013. Processing body and stress granule assembly occur by independent and Differentially regulated pathways in Saccharomyces cerevisiae. Genetics 193, 109–123.

Sheth, U., Parker, R., 2003. Decapping and decay of messenger RNA occur in cytoplasmic processing bodies. Science (80-.). 300, 805–8075.

Shin, Y., Berry, J., Pannucci, N., Haataja, M.P., Toettcher, J.E., Brangwynne, C.P., 2017. Spatiotemporal Control of Intracellular Phase Transitions Using Light-Activated optoDroplets. Cell 168, 159-171 e14.

Stöhr, N., Lederer, M., Reinke, C., Meyer, S., Hatzfeld, M., Singer, R.H., Hüttelmaier, S., 2006. ZBP1 regulates mRNA stability during cellular stress. J. Cell Biol.

Taylor, J.P., Zhang, P., Fan, B., Yang, P., Temirov, J., Messing, J., Kim, H.J., 2018. OptoGranules reveal the evolution of stress granules to ALS-FTD pathology. bioRxiv.

Teixeira, D., Sheth, U., Valencia-Sanchez, M.A., Brengues, M., Parker, R., 2005. Processing bodies require RNA for assembly and contain nontranslating mRNAs. RNA 11, 371–382.

Tourriere, H., Chebli, K., Zekri, L., Courselaud, B., Blanchard, J.M., Bertrand, E., Tazi, J., 2003. The RasGAP-associated endoribonuclease G3BP assembles stress granules. J Cell Biol 160, 823–831.

Tsai, N.P., Ho, P.C., Wei, L.N., 2008. Regulation of stress granule dynamics by Grb7 and FAK signalling pathway. EMBO J.

Van Treeck, B., Parker, R., 2018. Emerging Roles for Intermolecular RNA-RNA Interactions in RNP Assemblies. Cell 174, 791–802.

Wang, C., Schmich, F., Srivatsa, S., Weidner, J., Beerenwinkel, N., Spang, A., 2018. Context-dependent deposition and regulation of mRNAs in P-bodies. Elife 7.

Wang, X., Lu, Z., Gomez, A., Hon, G.C., Yue, Y., Han, D., Fu, Y., Parisien, M., Dai, Q., Jia, G., Ren, B., Pan, T., He, C., 2013. N6-methyladenosine-dependent regulation of messenger RNA stability. Nature 505, 117–120.

Wilbertz, J.H., Voigt, F., Horvathova, I., Roth, G., Zhan, Y., Chao, J.A., 2018. Single-molecule imaging of mRNA localization and regulation during the integrated stress response. bioRxiv.

Wilczynska, A., 2005. The translational regulator CPEB1 provides a link between dcp1 bodies and stress granules. J. Cell Sci.

Xing, W., Muhlrad, D., Parker, R., Rosen, M.K., 2020. A quantitative inventory of yeast P

body proteins reveals principles of composition and specificity. Elife 9, 1–63.

Yang, X., Shen, Y., Garre, E., Hao, X., Krumlinde, D., Cvijovic, M., Arens, C., Nystrom, T., Liu, B., Sunnerhagen, P., 2014. Stress granule-defective mutants deregulate stress responsive transcripts. PLoS Genet 10, e1004763.

Youn, J.Y., Dunham, W.H., Hong, S.J., Knight, J.D.R., Bashkurov, M., Chen, G.I., Bagci, H., Rathod, B., MacLeod, G., Eng, S.W.M., Angers, S., Morris, Q., Fabian, M., Cote, J.F., Gingras, A.C., 2018. High-Density Proximity Mapping Reveals the Subcellular Organization of mRNA-Associated Granules and Bodies. Mol Cell 69, 517-532 e11.

Zhang, H., Elbaum-Garfinkle, S., Langdon, E.M., Taylor, N., Occhipinti, P., Bridges, A.A., Brangwynne, C.P., Gladfelter, A.S., 2015. RNA Controls PolyQ Protein Phase Transitions. Mol Cell 60, 220–230.

Zid, B.M., O'Shea, E.K., 2014. Promoter sequences direct cytoplasmic localization and translation of mRNAs during starvation in yeast. Nature 514, 117–121.

Chapter 4: Further investigations on the promoter-driven mRNA localization and translational control

4.1 Abstract

During times of unpredictable stress, organisms must adapt their gene expression to maximize survival. Along with changes in transcription, one conserved means of gene regulation during conditions that quickly represses translation is the formation of cytoplasmic phase-separated mRNP (messenger ribonucleoprotein) granules such as processing bodies (P-bodies) and stress granules. Previously, we identified that distinct steps in gene expression can be coupled during glucose starvation as promoter sequences in the nucleus are able to direct the subcellular localization and translatability of mRNAs in the cytosol. In chapter 2, we reported a mechanism mediated by Rvb1/Rvb2 that they couple transcription, mRNA localization, and translatability of select mRNAs during glucose starvation. Here, in chapter 4, we talk about 3 more studies on understanding how promoter drives mRNA cytoplasmic fates from other perspectives. First, from an interesting loss-of-function mutant of Rvb1, we found that disruption of Rvb1's function suppresses the expression of stress-response genes. Second, we found that timing of transcription is a critical factor to determine mRNA cytoplasmic localization that mRNAs formed pre-stress go to P-bodies and mRNAs formed in stress go to assumed stress granules during glucose starvation. Third, after investigating on *HSP30* promoter, we found that there may be sequence elements residing between -300 bp and -500 bp on *HSP30* promoter that directs the mRNA's cytoplasmic fate. Overall, the

preliminary results from these 3 studies suggest hints on further mechanisms of how events in nucleus have an influence on the mRNAs in the cytosol.

4.2 Results

4.2.1 The disruption of Rvb1's function suppresses the expression of stress-response genes.

In chapter 2, AAA+ ATPase Rvb1/Rvb2 was found that they couple the transcription, mRNA cytoplasmic localization and translation of Class II alternative glucose metabolism genes during glucose starvation. To understand the necessity of Rvb proteins, a loss-of-function mutant of Rvb1 was made. Given *RVB1* is an essential gene and cannot be deleted from genome (SGD), we sought to deplete the Rvb1 protein in a timely manner using auxin-inducible degradation (AID) system (Morawska & Ulrich, 2013; Nishimura, Fukagawa, Takisawa, Kakimoto, & Kanemaki, 2009; Tanaka, Miyazawa-Onami, Iida, & Araki, 2015). To fast deplete Rvb1 using AID, Rvb1 was C-terminally fused with an AID tag derived from IAA17 proteins in *Arabidopsis thaliana*. The plant-origin auxin receptor Tir1 was then introduced in the cell. Upon adding auxin molecule indole-3-acetic acid (IAA), Rvb1-AID will be recognized by Tir1 and subjected to degradation through the ubiquitination pathway (Figure 4.1A). Western results showed that after 4 hours of IAA treatment, around 80% of Rvb1 was depleted (Figure 4.1B).

Then we tested if Rvb1 was depleted, how would the expression of Class I heat shock genes (e.g., *HSP30, HSP26*) and Class II (e.g., *GSY1*, *GLC3*) alternative glucose metabolism genes change (Figure supplement 2.4). According to our hypothesis, because Rvb1 plays a role in directing interacting mRNAs into assumed stress granules (Chapter 2), the Class II promoter-driven mRNAs are supposed to increase the translation and diffuse localization if Rvb1 is depleted. However, to our surprise, when Rvb1 was

partially depleted by AID system, the protein synthesis of *GSY1* promoter-driven reporter was significantly repressed (Figure 4.1C). Similarly, the protein synthesis of *HSP30* promoter-driven reporter was also significantly repressed. More surprisingly, when Rvb1 was fused with AID tag, even without treating the cell with IAA and Rvb1 was not depleted (Figure 4.1B), the protein synthesis of both *GSY1* and *HSP30* promoter-driven reporter was significantly repressed (Figure 4.1C), indicating that AID tag itself largely disrupts Rvb1's function. Since Rvb1 was reported to have multiple functions in the nucleus such as chromatin remodeling, it pointed that the AID system disrupts the Rvb1's function and may represses the following transcription activation of genes (Gnatovskiy, Mita, & Levy, 2013; Jha & Dutta, 2009; Paci et al., 2012). Then we tested the mRNA abundance of genes in Class I (*HSP30*), Class II (*GSY1*, *GLC3*), Class III (*PAB1*, *TUB1*), and a *GSY1* promoter-driven reporter mRNA during glucose starvation. Interestingly, when Rvb1 is disrupted, the mRNA abundance of both Class I and Class II genes significantly decreases. While the mRNA levels of Class III genes, that are highly expressed pre-stress but repressed during stress, do not change much when Rvb1 is disrupted (Figure 4.1D). It indicates that Rvb1 may be important for activating the transcription of stress-response genes (Class I and Class II) upon glucose starvation. Consistently, when Rvb1 is disrupted, the formation of *GLC3/GSY1* promoter-driven reporter containing granules was reduced during glucose starvation (Figure 4.1E). It points to 2 possibilities: maybe the mRNAs are too few in the cell to observe, or Rvb1 is required for these mRNAs to locate into the granules during glucose starvation.

As a separate finding, interestingly, we found that when Rvb1 is disrupted, the formation of Pab1 and Pub1 containing granules significantly increases during glucose

starvation (Figure supplement 4.1). Since Pab1 and Pub1 are reported as core stress granule components in mammalian cells (Brambilla, Martani, & Branduardi, 2017; Guzikowski, Chen, & Zid, 2019; Jain et al., 2016), and they were found in granules that are not colocalized with P-bodies in 60 minutes of glucose starvation in yeasts (data not shown), it is sound to assume that Pab1/Pub1 containing granules are stress granules. This result is consistent with published findings stating that Rvb proteins are important to keep the dynamics and size of stress granules (Jain et al., 2016; Narayanan et al., 2019; Zaarur et al., 2015; Zhou et al., 2017).

4.2.2 mRNAs formed pre-stress go to P-bodies and mRNAs formed in stress go to assumed stress granules during glucose starvation.

To investigate whether the timing of the transcription has an impact on mRNA's cytoplasmic localization during glucose starvation, we separated the transcription happened pre-stress and post-stress using a transcription inhibitor drug 1,10-phenanthroline (PNT). Surprisingly, when the cells were treated with PNT upon glucose starvation, which means no more mRNAs generated during the stress, the assumed stress granules that are not colocalized with P-bodies largely disappeared (Figure 4.2). While the similar levels of P-bodies were still formed during glucose starvation. It highly indicates that timing of mRNA's generation is critical to mRNA's localization in the cytosol when stress happens. mRNAs formed pre-stress go to P-bodies and mRNAs formed during stress go to assumed stress granules. This result is supported by the findings in (Zid & O'Shea, 2014), where they made a reporter that consisted of the doxycycline-inducible Tet-On promoter to control the timing of transcription. They found that if they

turn on the transcription only in glucose-rich log phase, the reporter mRNAs go to P-bodies. If they turn on the transcription only in glucose starvation phase, the reporter mRNAs go to assumed stress granules. If doxycycline was added the whole time, the mRNAs go to both granules.

4.2.3 There may be elements residing between -300 bp and -500 bp of *HSP30* promoter that directs the mRNA's cytoplasmic fate.

To further understand how promoter sequence might leave an impact on mRNA's cytoplasmic fates, we investigated the potential sequence elements that reside in the promoter. Previously, we found that heat shock element (HSE) plays an important role in driving mRNA excluded from phase-separated granules (Figure 4.3A), where an synthetic promoter that contains 3 HSEs makes mRNAs stay diffuse in the cytosol (Zid & O'Shea, 2014). However, there are exceptions: *HSP30* promoter does not have any HSE (Figure 4.3A). To look for more comprehensive understanding on the promoter sequence, the potential motifs and binding factors of Class I and Class II promoters were predicted *in silico* using an online motif finder MEME-ChIP (Figure 4.3B). Especially we were curious about the elements in *HSP30* promoter, so a prediction of motifs in *HSP30* promoter was performed (Figure 4.3C). From the predictions, motifs that are recognized by Mcm1, Tec1, Stp1/2, Aft1/2 are top hits that may play a role in keeping the mRNA transcribed diffuse in the cytosol during stress.

Since *HSP30* promoter do not have an HSE, we then asked what regions may play a role in dictating its mRNA's cytoplasmic localization. To narrow the regions down experimentally, we made a series of constructs consisting of 7 varied lengths of *HSP30*

promoter (1kb, 900, 800, 700, 500, 300, 180 bp), respectively, driving a nanoluciferase reporter (Figure 4.3D). Interestingly, during glucose starvation, 900 bp-long *HSP30* promoter drives the highest protein induction, while the shorter the promoter is, the lower the protein induction will be (Figure 4.3E). More interestingly, there is a deep reduction when *HSP30* promoter is shorten from 500 bp to 300 bp, indicating that there might be an important motif residing in this 200 bp region. Consistently, when we observed the mRNA subcellular localization, 300 bp-long *HSP30* promoter drove a significant higher granular localization of the reporter mRNA, indicating that there might be an important motif sitting between -500 bp and -300 bp that makes mRNA excluded from the granules (Figure 4.3G). What's more, even though we observed a huge reduction in protein synthesis between -300 bp and -180 bp of *HSP30* promoter, we did not observe an increase in the granular localization, indicating that maybe 180 bp-long *HSP30* promoter is too short to sufficiently drive a transcription (Figure 4.3E, 4.3G). Then we did a prediction of motifs within the range of -500 bp to -300 bp on *HSP30* promoter, Mcm1 is again a top hit (Figure 4.3F). As a future direction, it is worthwhile to further study on Mcm1 and test whether the Mcm1-binding motif is necessary for *HSP30* promoter to dictate the mRNA's cytoplasmic fate.

4.4 Conclusions

In this chapter, we reported and discussed 3 different projects that aim to understand the coupling of transcription, mRNA localization and translation during stress from different perspectives. First, from the study on an interesting loss-of-function mutant of Rvb1, we found that disruption of Rvb1's function suppresses the expression of stress-response genes (Class I and Class II). Combing with the findings about Rvb1/Rvb2 in chapter 2, it further indicated that Rvb proteins have multiple roles on both DNA and RNA, in both nucleus and cytoplasm, and couple the transcription and translation. Second, we found that the timing of transcription is a critical factor to determine mRNA's cytoplasmic localization that mRNAs formed pre-stress go to P-bodies and mRNAs formed in stress go to assumed stress granules during glucose starvation. It's interesting to further understand through what mechanism, the timing of mRNA generation could leave an effect on their localization in the cytoplasm. And what would be the biological meaning of it? Given the functions of stress granules and P-bodies are still unclear, understanding the mRNA components would help understanding the potential roles of these granules. Third, after studying *HSP30* promoter sequence, we found that there may be elements residing between -300 bp and -500 bp of *HSP30* promoter that directs the mRNA's cytoplasmic fate. What's more, Mcm1-binding motif may be a worthwhile hit to study further.

4.5 Availability of data and materials

Further information and requests for data, resources, scripts, and reagents should be directed to and will be fulfilled by the corresponding contact, B.M.Z. (zid@ucsd.edu).

4.6 Figures

Figure 4.1: The disruption of Rvb1's function suppresses the expression of stress-response genes.

(A) A schematic view of auxin-inducible degradation (AID) strategy on Rvb1. AID was used to fast-deplete Rvb1, thus test Rvb1's necessity. Rvb1 was C-terminally fused with auxin-inducible degron (AID) tag. When auxin is added, Rvb1's AID tag will be recognized by Tir1, a component of E3 ubiquitin ligase. Rvb1 will be degraded mediated by the ubiquitination pathway. (B) A quantitative analysis on the depletion of Rvb1 upon adding auxin. 1mM IAA: 1 mM indole-3-acetic acid (IAA), a classical auxin molecule. Ctrl: the cells were not treated with IAA. 1hr, 2hr, 3hr, 4hr: time of cells were treated by IAA before harvested. Rvb1-AID has a molecular weight around 75 kD. Depletion: percentage of Rvb1's depletion compared to control. (C) Protein synthesis of *GLC3/GSY1* promoter-driven nanoluciferase reporter in log phase and 25-minute glucose starvation. Y-axis: nanoluciferase synthesized within 5-minute time frame. Nanoluciferase reading was subtracted by the nanoluciferase reading of cycloheximide added 5 minutes earlier. No-AID: Rvb1 was not tagged by AID. None: Rvb1 was fused with AID tag, but no IAA was added. 90min, 180min: time after IAA treatment on cells. Error bars are from 2 biological replicates. (D) mRNA levels of endogenous genes and *GSY1*-promoter driven nanoluciderase reporter mRNA in log-phase and 15-minute glucose starvation. Y-axis: Ct values of reporter mRNAs were normalized by the internal control *ACT1*. Each facet represents each gene. No-AID: Rvb1 was not tagged by AID. None: Rvb1 was fused with AID tag, but no IAA was added. 90-min-IAA: 90 minutes of IAA treatment. Error bars are from 2 technical replicates. (E) Live imaging showing the subcellular localization of the *HSP30/GLC3/GSY1* promoter-driven reporter mRNA in log phase and 15-minute glucose starvation. Reporter mRNA was labeled by the MS2 imaging system. Rvb1-AID: Rvb1 was fused with AID tag, but no IAA was added. 1hr/3hr +IAA: time after IAA treatment on cells. WT: Rvb1 was not tagged by AID. In WT microscopy, reporter mRNA was labeled by GFP and Dcp2 (a P-body marker) was labeled by mRFP.

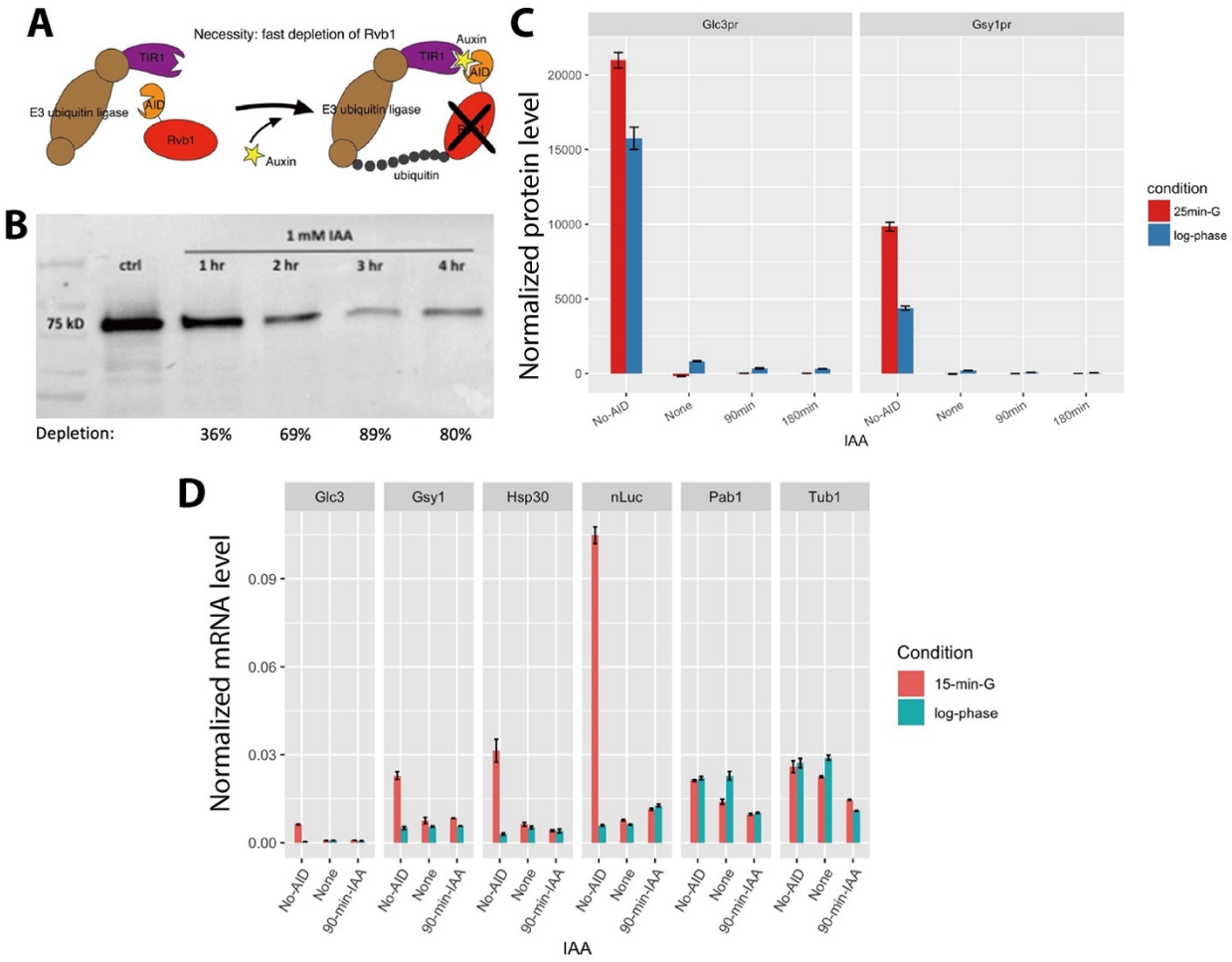
A
Necessity: fast depletion of Rvb1
TIR1
AID
E3 ubiquitin ligase
Rvb1
Auxin
ubiquitin
B
1 mM IAA
ctrl
1 hr
2 hr
3 hr
4 hr
75 kD
Depletion:
36%
69%
89%
80%
C
Glc3pr
Gsy1pr
Normalized protein level
20000
15000
10000
5000
0
No-AID
None
90min
180min
IAA
condition
25min-G
log-phase
D
Glc3
Gsy1
Hsp30
nLuc
Pab1
Tub1
Normalized mRNA level
0.09
0.06
0.03
0.00
No-AID
None
90-min-IAA
IAA
Condition
15-min-G
log-phase
E
Rvb1-AID
Rvb1-AID 1hr +IAA
Rvb1-AID 3h +IAA
WT
15 min-G
Log phase
15 min -G
HSP30pr
GLC3pr
GSY1pr

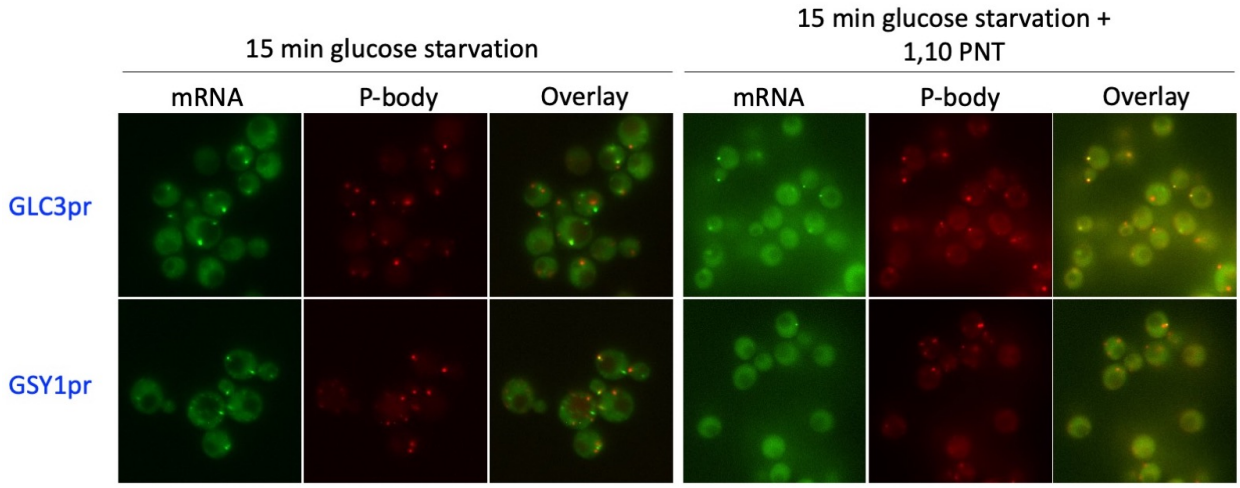

Figure 4.2: mRNAs formed pre-stress go to P-bodies and mRNAs formed in stress go to assumed stress granules during glucose starvation.

Live imaging showing the subcellular localization of the *GLC3/GSY1* promoter-driven reporter mRNA in 15-minute glucose starvation, and 15-minute glucose starvation and transcription stop. Reporter mRNA was labeled by the MS2 imaging system. P-body was labeled by marker protein Dcp2. Transcription was stop by adding 1,10-phenanthroline (PNT).

Figure 4.3: There may be elements residing between -300 bp and -500 bp of HSP30 promoter that directs the mRNA's cytoplasmic fate.

(A) A summary of numbers of HSE and STRE elements in promoters. HSE: heat shock elements. STRE: stress response elements. (B) A prediction of the occurrences of motifs in Class I and Class II promoters. Binding factors recognize certain motifs. (C) A summary of the occurrences of *HSP30*-promoter predicted motifs in Class I and Class II promoter. (D) A schematic view of the *HSP30* promoter truncation study. We studied 1000, 900, 800, 700, 500, 300, 180 bp of *HSP30* promoter driven nanoluciferase's expression. (E) Fold change of protein synthesis in 25-minute glucose starvation vs log phase of varied-length *HSP30* promoter-driven nanoluciferase. Y-axis: Fold change of nanoluciferase synthesized within 5-minute time frame in glucose starvation vs log phase. Nanoluciferase reading was subtracted by the nanoluciferase reading of cycloheximide added 5 minutes earlier. GLC3: *GLC3* promoter driven nanoluciferase reporter, as a control. HSP30-Xbp: varied-length *HSP30*-promoter driven nanoluciferase reporter. Error bars are from 2 technical replicates. (F) A prediction of the occurrences of motifs in -500 bp to -300 bp of *HSP30* promoter. (G) A quantification of subcellular localization of *HSP30* promoter-driven reporter mRNAs in log phase and 15-minute glucose starvation. Reporter mRNA was labeled by the MS2 imaging system. Y-axis: percentage of cells that have the reporter mRNA-containing granule foci. The 300 bp-long *HSP30* promoter is highlighted in square. N = 200.

A

Promoter	HSE	STRE
GLC3	1	3
GSY1	0	2
HXK1	1	2
GPH1	0	3
HSP42	3	3
HSP26	3	4
HSP30	0	0
TMA10	0	3
HSP12	1	7
HSP104	4	0

B

Summary of motif occurrences in Class 1/Class 2 promoters

	Binding factors	Class 1	Class 2
Class 2 dominant	Ste12	0	5
	Hac1	2	4
Tie	Hsf1	3	3
	Gis1, Msn2, Msn4	4	5
	Fkh1, Fkh2	5	5
	Gcr1	5	5
	Stb5	5	5
Class 1 dominant	Nrg1	4	0
	Mcm1	4	1
	Stp1, Stp2	3	0

C

HSP30 motifs occurrences in Class 1/Class 2 promoters

Binding factors	Class 1	Class 2
Fkh1, Fkh2	5	5
Gcr1	5	5
Stb5	5	5
Mcm1	4	1
Tec1	5	2
Stp1, Stp2	3	0
Aft2p, Aft1	2	0

D

E

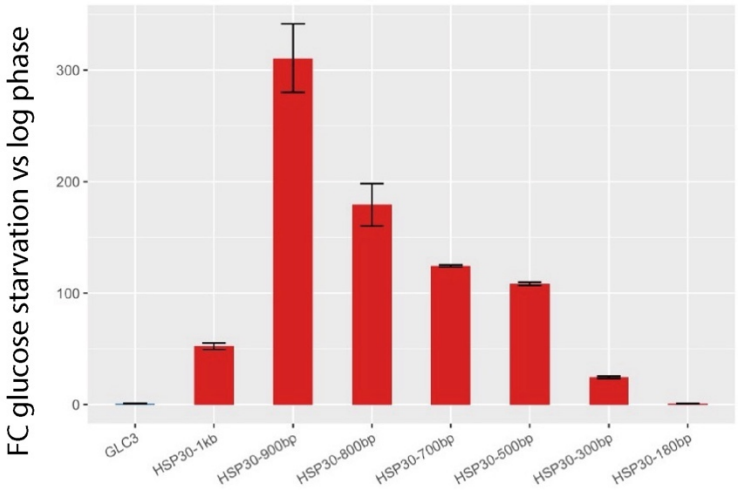

F

Motifs between -300 and -500

Binding factors	Location -300 ~ -500	Total occurrences
Fkh1, Fkh2	-387/R	5
Gcr1	-412/F,-403/F,-352/F	7
Mcm1	-291/F,-290/F	2
Mot3	-415/R, -344/R,-409/R	7
Rgt1	-416/R	1
Yap1	-480/R	2
Gsm1	-416/R,-428/R	2

G

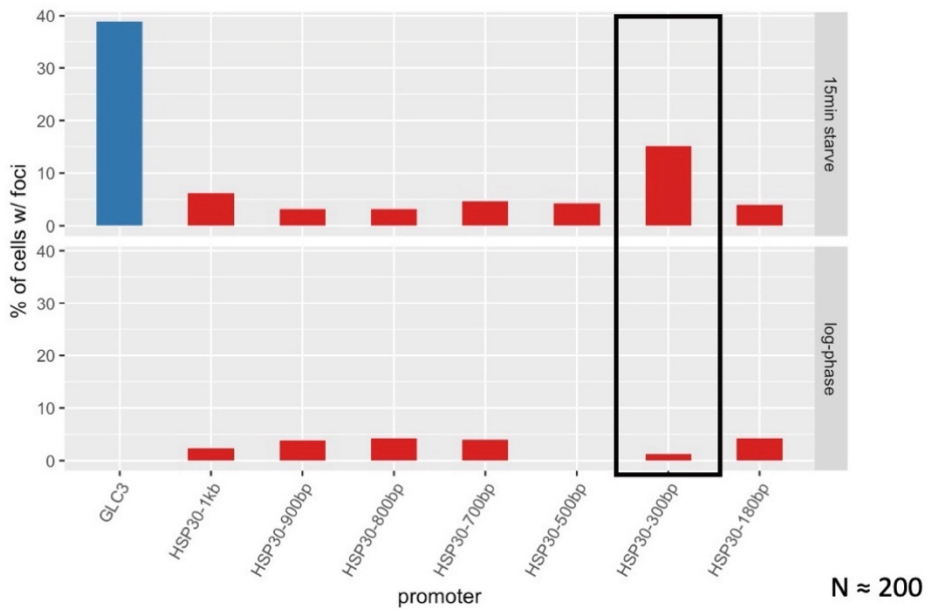

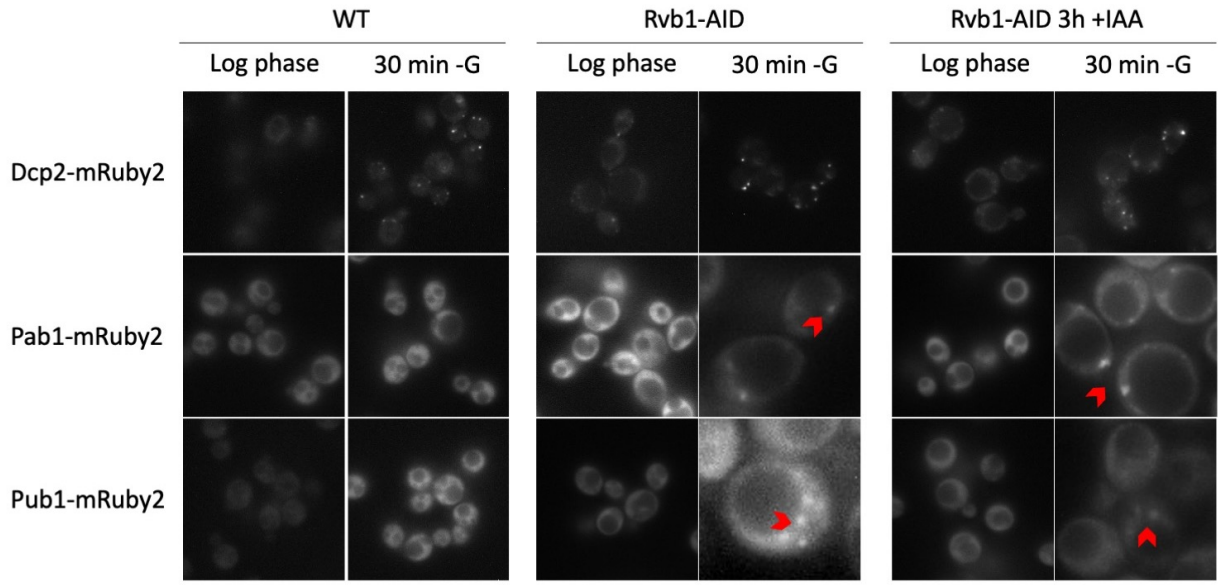

Figure supplement 4.1: Disruption of Rvb1 increases the formation of assumed stress granules.

Live imaging showing the subcellular localization of Dcp2, Pab1 and Pub1 proteins in log phase and 30-minute glucose starvation. Proteins of interest were fused with mRuby2. Dcp2 are considered as a P-body marker. Pab1 and Pub1 are considered as markers for stress granules in mammalian cells. WT: Rvb1 was not fused with AID tag. Rvb1-AID: Rvb1 was fused with AID tag but cells were not IAA treated. Rvb1-AID 3h +IAA: cells were treated with IAA for 3 hours. Arrows are used to highlight the Pab1/Pub1-containing granules.

4.7 Methods

4.7.1 Yeast strains and plasmids:

The yeast strains and plasmids used in this study are listed in Supplementary file 3 and the oligonucleotides used for the plasmid construction, yeast cloning and RT-qPCR are described in Supplementary file 4. The strains were created through genomic integration of a linear PCR product, or a plasmid linearized through restriction digest. The background strain used was W303 (EY0690), one laboratory strain that is closely related to S288C. In yeast cloning for the C-terminal fusion on the endogenous proteins (e.g. Pab1-mRuby2, Pub1-mRuby2 etc.), we used plasmids of Pringle pFA6a and pKT system (Lee, Lim, & Thorn, 2013; Longtine et al., 1998; Zid & O'Shea, 2014), gifts from the E. K. O'Shea laboratory and the K. Thorn laboratory. We modified the pFA6a and pKT plasmids by inserting in the peptides of interest into the plasmids. The primers used to amplify the fragments from these plasmids contain 2 parts from 3' to 5': a uniform homolog sequence to amplify the plasmid and a homolog sequence to direct inserting the fragments to the genomic loci of interest. The fragments were transformed into the yeasts and integrated to the genome by homologous recombination. The integrations were confirmed by genomic DNA PCR (Yeast DNA Extraction Kit from Thermo Fisher). In the cloning of the reporter strains, we used a strain ZY18 that was derived from W303 and has one-copied genomic insertion of MYOpr-MS2CP-2XGFP and an endogenous fusion Dcp2-mRFP (Zid & O'Shea, 2014), as the background strain. Further we transformed the linearized MS2-loop-containing reporter plasmids into the strain by restriction digest and genomic integration. RT-qPCR was performed to verify the one-copied genomic integration. To

generate the MS2-loop-containing reporter plasmids (e.g., ZP315 pRS305-GSY1prUTR-nLuc-PEST-12XMS2-tADH1), we started from the plasmid ZP15 pRS305-12XMS2-tAdh1 (Zid & O'Shea, 2014). ZP15 was linearized by the restriction enzymes SacII and NotI (NEB). Promoter fragments, nanoluciferase-pest CDS fragments were inserted into linearized ZP15 using Gibson Assembly. Promoter sequences were amplified by PCR from the W303 genomic DNA. Nanoluciferase-pest CDS was amplified by PCR from the geneblock (Masser, Kandasamy, Kaimal, & Andreasson, 2016). In the cloning of the auxin-inducible degradation experiments, detailed procedures were described in the "Auxin-inducible degradation".

4.7.2 Yeast growth, media and conditions:

The background yeast strain w303 (EY0690) was used for all experiments. For cells cultured in the functional experiments, cells were streaked out on the yeast extract peptone dextrose (YPD) agarose plate (BD) from the frozen stocks and grew at 30 °C for 2 days. Single colony was selected to start the over-night culture for each biological replicate. Cells were grown at 30°C in batch culture with shaking at 200 r.p.m. in synthetic complete glucose medium (SCD medium: yeast nitrogen base from RPI, glucose from Sigma-Aldrich, SC from Sunrise Science). When the OD_{660} of cells reached 0.4, half of the culture was harvested as the pre-starved sample. The other half of the culture was transferred to the prewarmed synthetic complete medium lacking glucose (SC -G medium) by centrifugation method. Cells are centrifuged at 3000 xg, washed once by SC medium and resuspended in the same volume as the pre-starvation medium of SC medium. Glucose starvation was performed in the same 200 r.p.m shaking speed and 30°C. The

length of the glucose starvation time varies from 10 minutes to 30 minutes depending on the experiments. For 1,10-phenanthroline treatment, a stock solution of 100 mg/mL of 1,10-phenanthroline (PNT) in isopropanol was made(stored in 4°C, good for 2 weeks) (Tsuboi et al., 2020). Then PNT was added in the culture with a final concentration of 0.25 mg/mL.

4.7.3 Auxin-inducible degradation (AID):

The Auxin-inducible degradation protocol was adapted from (Morawska & Ulrich, 2013; Nishimura et al., 2009; Tanaka et al., 2015). The background yeast strain w303 (EY0690) was used. Primers were designed to amplify the fragments containing an AID tag, a 9Xmyc tag and a URA selection ORF from the plasmid, a gift from the Ulrich lab. PCR fragments were later integrated into the genomic DNA at C-terminus of endogenous *RVB1* using standard yeast transformation protocol. The insertion was verified by genomic DNA PCR. Then one copy of plasmid containing a yeast optimized Tir1 was transformed into the cell by restriction digestion and yeast transformation. The copy number of the insertion was checked by genomic DNA qPCR. The depletion of Rvb1 was detected by Western. To induce the depletion, 1 mM of IAA as the final concentration was used.

4.7.4 Live cell imaging and analysis:

Cells were grown to an OD_{660} to ~0.4 in SCD medium at 30°C and glucose-starved in SC -G medium for 15 and 30 minutes. 100 µL of cell culture was loaded onto a 96-well glass-bottom microplate (Cellvis). Cells were imaged using an Eclipse Ti-E microscope

(Nikon) with an oil-immersion 63X objective. Imaging was controlled using NIS-Elements software (Nikon). Imaging analysis was performed on Fiji software.

4.7.5 Nanoluciferase assay and analysis:

The nanoluciferase assay was adapted from methods previously described by (Masser et al., 2016). Cells were grown to an OD_{660} to ~0.4 in SCD medium at 30°C and glucose-starved in SC -G medium for 20 minutes. 90 µL of cell culture was loaded onto a Cellstar non-transparent white 96-well flat-bottom plate (Sigma-Aldrich). OD_{660} of cells was taken for each sample. For cells treated with cycloheximide (CHX), CHX was added to a final concentration of 100 µg/mL to stop the translation for 5 minutes. To measure the nanoluciferase signal, 11 µL of substrate mix (10 µL of Promega Nano-Glo® Luciferase Assay Buffer, 0.1 µL of Promega NanoLuc® luciferase substrate and 1 µL of 10 mg/mL CHX) was added and mixed with the samples by pipetting. Measurements were taken immediately after addition of substrate mix by Tecan Infinite Lumi plate reader. To analyze the data, the luciferase level of samples was firstly divided by the OD_{660} level of the samples. Then the normalized luciferase level of non-CHX-treated sample was further normalized by subtracting the luciferase level of CHX-treated sample.

4.7.6 Western blotting:

The RT-qPCR protocol was adapted from (Tsuboi et al., 2020). RNA was extracted using the MasterPure Yeast RNA Purification Kit (Epicentre). cDNA was prepared using ProtoScript II Reverse Transcriptase (NEB #M0368X) with a 1:1 combination of oligodT 18 primers and random hexamers (NEB) according to the manufacturer's instructions.

mRNA abundance was determined by qPCR using a home-brew recipe with SYBR Green at a final concentration of 0.5X (Thermo Fisher #S7564). Primers specific for each transcript were described in Supplementary file 2. The mRNA levels were normalized to *ACT1* abundance, and the fold change between samples was calculated by a standard ΔΔCt analysis.

4.7.7 Real-time quantitative PCR (RT-qPCR):

The RT-qPCR protocol was adapted from (Tsuboi et al., 2020). RNA was extracted using the MasterPure Yeast RNA Purification Kit (Epicentre). cDNA was prepared using ProtoScript II Reverse Transcriptase (NEB #M0368X) with a 1:1 combination of oligodT 18 primers and random hexamers (NEB) according to the manufacturer's instructions. mRNA abundance was determined by qPCR using a home-brew recipe with SYBR Green at a final concentration of 0.5X (Thermo Fisher #S7564). Primers specific for each transcript were described in Supplementary file 2. The mRNA levels were normalized to *ACT1* abundance, and the fold change between samples was calculated by a standard ΔΔCt analysis.

4.7.8 Motif prediction:

The motif prediction was performed using the MEME-ChIP online data analysis software (https://meme-suite.org/meme/tools/meme-chip) (Machanick & Bailey, 2011).

4.8 Acknowledgements

We acknowledge support by the Zid lab startup funds from UCSD and MIRA grant from the National Institutes of Health R35GM128798 (to B.M.Z).

4.9 References

Brambilla, M., Martani, F., Branduardi, P., 2017. The recruitment of the Saccharomyces cerevisiae poly(A)-binding protein into stress granules: new insights into the contribution of the different protein domains. FEMS Yeast Res 17.

Gnatovskiy, L., Mita, P., Levy, D.E., 2013. The Human RVB Complex Is Required for Efficient Transcription of Type I Interferon-Stimulated Genes. Mol. Cell. Biol. 33, 3817–3825.

Guzikowski, A.R., Chen, Y.S., Zid, B.M., 2019. Stress-induced mRNP granules: Form and function of processing bodies and stress granules. Wiley Interdiscip. Rev. RNA 10, e1524.

Jain, S., Wheeler, J.R., Walters, R.W., Agrawal, A., Barsic, A., Parker, R., 2016. ATPase-Modulated Stress Granules Contain a Diverse Proteome and Substructure. Cell 164, 487–498.

Jha, S., Dutta, A., 2009. RVB1/RVB2: running rings around molecular biology. Mol Cell 34, 521–533.

Lee, S., Lim, W.A., Thorn, K.S., 2013. Improved Blue, Green, and Red Fluorescent Protein Tagging Vectors for S. cerevisiae. PLoS One 8, e67902.

Longtine, M.S., McKenzie III, A., Demarini, D.J., Shah, N.G., Wach, A., Brachat, A., Philippsen, P., Pringle, J.R., 1998. Additional modules for versatile and economical PCR-based gene deletion and modification in Saccharomyces cerevisiae. Yeast 14, 953–961.

Machanick, P., Bailey, T.L., 2011. MEME-ChIP: Motif analysis of large DNA datasets. Bioinformatics 27, 1696–1697.

Masser, A.E., Kandasamy, G., Kaimal, J.M., Andreasson, C., 2016. Luciferase NanoLuc as a reporter for gene expression and protein levels in Saccharomyces cerevisiae. Yeast 33, 191–200.

Morawska, M., Ulrich, H.D., 2013. An expanded tool kit for the auxin-inducible degron system in budding yeast. Yeast 30, 341–351.

Narayanan, A., Meriin, A., Andrews, J.O., Spille, J.-H., Sherman, M.Y., Cisse, I.I., 2019. A first order phase transition mechanism underlies protein aggregation in mammalian cells. Elife 8.

Nishimura, K., Fukagawa, T., Takisawa, H., Kakimoto, T., Kanemaki, M., 2009. An auxin-based degron system for the rapid depletion of proteins in nonplant cells. Nat

Methods 6, 917–922.

Paci, A., Liu, X.H., Huang, H., Lim, A., Houry, W.A., Zhao, R., 2012. The stability of the small nucleolar ribonucleoprotein (snoRNP) assembly protein Pih1 in Saccharomyces cerevisiae is modulated by its C terminus. J. Biol. Chem. 287, 43205–43214.

Tanaka, S., Miyazawa-Onami, M., Iida, T., Araki, H., 2015. iAID: an improved auxin-inducible degron system for the construction of a “tight” conditional mutant in the budding yeast Saccharomyces cerevisiae. Yeast 32, 567–581.

Tsuboi, T., Viana, M.P., Xu, F., Yu, J., Chanchani, R., Arceo, X.G., Tutucci, E., Choi, J., Chen, Y.S., Singer, R.H., Rafelski, S.M., Zid, B.M., 2020. Mitochondrial volume fraction and translation duration impact mitochondrial mRNA localization and protein synthesis. Elife 9, 1–24.

Zaarur, N., Xu, X., Lestienne, P., Meriin, A.B., McComb, M., Costello, C.E., Newnam, G.P., Ganti, R., Romanova, N. V, Shanmugasundaram, M., Silva, S.T., Bandeiras, T.M., Matias, P.M., Lobachev, K.S., Lednev, I.K., Chernoff, Y.O., Sherman, M.Y., 2015. RuvbL1 and RuvbL2 enhance aggresome formation and disaggregate amyloid fibrils. EMBO J. 34, 2363–2382.

Zhou, C.Y., Stoddard, C.I., Johnston, J.B., Trnka, M.J., Echeverria, I., Palovcak, E., Sali, A., Burlingame, A.L., Cheng, Y., Narlikar, G.J., 2017. Regulation of Rvb1/Rvb2 by a Domain within the INO80 Chromatin Remodeling Complex Implicates the Yeast Rvbs as Protein Assembly Chaperones. Cell Rep. 19, 2033–2044.

Zid, B.M., O’Shea, E.K., 2014. Promoter sequences direct cytoplasmic localization and translation of mRNAs during starvation in yeast. Nature 514, 117–121.

Chapter 5: Insights and future directions

In fluctuating environments, cells must quickly adjust the expression of different genes dependent upon cellular needs. The coupling of transcription and translation of specific genes may be an important adaptation for cells to survive during stress conditions. In the previous findings, during glucose starvation in yeast, promoter sequences play an important role in determining the cytoplasmic fate of mRNAs such as mRNA localization regarding to phase-separated granules and translation (Zid & O'Shea, 2014). In my PhD, I investigated the potential mechanisms behind this interesting phenomenon from different perspectives:

In chapter 2, our results demonstrate a novel function of the AAA+ proteins Rvb1/Rvb2 in the cytoplasm, and a novel mechanism of Rvb1/Rvb2 in coupling the transcription, mRNA cytoplasmic localization, and translation of specific genes. The biological meaning of this coupling process may reside in the cell needs to fast adjust its expression profile during stress. From the perspective of cell needs, the special coupling of increased transcription but repressed translation mediated by Rvb1/Rvb2 may serve as an emergency but prospective mechanism for cells to precisely repress the translation of the alternative glucose metabolism mRNAs during stress but be able to quickly translate these pre-stored mRNAs once the cells are no longer starved (Jiang, AkhavanAghdam, Li, Zid, & Hao, 2020). Since the genes regulated by Rvb1/Rvb2 are highly dependent on the type of stresses. We observed this interesting mechanism on the alternative glucose metabolism genes during glucose starvation stress. It will be interesting to test if there is similar regulation on different sets of genes that are related

to other types of stresses, such as heat shock and osmotic stress responses. Rvb1/Rvb2 may regulate different sets of genes according to the different stresses or maybe different protein factors play a role in the mechanism. With our methodology, it is promising to generalize the mechanism toward various stress conditions.

In chapter 4, we reported and discussed 3 different projects that aim to understand the coupling of transcription, mRNA localization and translation during stress from different perspectives.

First, from the study on an interesting loss-of-function mutant of Rvb1, we found that disruption of Rvb1's function suppresses the expression of stress-response genes (Class I and Class II). Given that Rvb1/Rvb2 have effects on both DNA and RNA, it's worthwhile to find a strategy to decouple the steps when studying Rvb proteins. Also finding a less leaky and milder way to deplete Rvb1/Rvb2 such as anchor-away or heat shock sensitive mutant would provide a clearer findings in Rvb proteins' necessity in regulating the binding mRNA's cytoplasmic fates (Haruki, Nishikawa, & Laemmli, 2008; Solís et al., 2016).

Second, we found that the timing of transcription is a critical factor to determine mRNA's cytoplasmic localization that mRNAs formed pre-stress go to P-bodies and mRNAs formed in stress go to assumed stress granules during glucose starvation. It's interesting to further understand through what mechanism, the timing of mRNA generation could leave an effect on their localization in the cytoplasm. And what would be the biological meaning of it? What are the differences for mRNAs going to P-bodies from mRNAs going to stress granules? Given the functions of stress granules and P-

bodies are still unclear, understanding the mRNA components would help understanding the potential roles of these granules.

Third, after studying *HSP30* promoter sequence, we found that there may be elements residing between -300 bp and -500 bp of *HSP30* promoter that directs the mRNA's cytoplasmic fate. What's more, after the motif prediction on -300 bp - -500 bp of *HSP30* promoter, Mcm1-binding motif seems like an overrepresented hit in the region. Mcm1 is predominantly considered as transcription factor but localizes to the cytosol in response to hypoxia (Dastidar et al., 2012; Passmore, Elble, & Tye, 1989). For the next step, Mcm1-binding motif may be a worthwhile hit to study further.

5.1 References

Dastidar, R.G., Hooda, J., Shah, A., Cao, T.M., Henke, R.M., Zhang, L., 2012. The nuclear localization of SWI/SNF proteins is subjected to oxygen regulation. Cell Biosci. 2, 1–13.

Haruki, H., Nishikawa, J., Laemmli, U.K., 2008. The Anchor-Away Technique: Rapid, Conditional Establishment of Yeast Mutant Phenotypes. Mol. Cell 31, 925–932.

Jiang, Y., AkhavanAghdam, Z., Li, Y., Zid, B.M., Hao, N., 2020. A protein kinase A–regulated network encodes short- And long-lived cellular memories. Sci. Signal. 13.

Passmore, S., Elble, R., Tye, B.K., 1989. A protein involved in minichromosome maintenance in yeast binds a transcriptional enhancer conserved in eukaryotes. Genes Dev. 3, 921–935.

Solís, E.J., Pandey, J.P., Zheng, X., Jin, D.X., Gupta, P.B., Airoldi, E.M., Pincus, D., Denic, V., Solis, E.J., Pandey, J.P., Zheng, X., Jin, D.X., Gupta, P.B., Airoldi, E.M., Pincus, D., Denic, V., 2016. Defining the Essential Function of Yeast Hsf1 Reveals a Compact Transcriptional Program for Maintaining Eukaryotic Proteostasis. Mol Cell 63, 60–71.

Zid, B.M., O'Shea, E.K., 2014. Promoter sequences direct cytoplasmic localization and translation of mRNAs during starvation in yeast. Nature 514, 117–121.